3

91

08158

Order Number 9108158

Nuclear magnetic resonances studies of polymer electrolytes

Pak, Yiu Sun, Ph.D.

City University of New York, 1990

U·M·I
300 N. Zeeb Rd.
Ann Arbor, MI 48106

A

NUCLEAR MAGNETIC RESONANCES STUDIES OF POLYMER ELECTROLYTES

by

Yiu Sun Pak

A dissertation submitted to the Graduate Faculty in Physics in partial fulfillment of the requirements for the degree of Doctor of Philosophy, The City University of New York.

1990

This manuscript has been read and accepted for the Graduate Faculty in Physics in satisfaction of the dissertation requirement for the degree of Doctor of Philosophy.

5/24/90 Professor Steve G. Greenbaum
Date Chair of Examining Committee

5/24/90 Professor Joel I. Gersten
Date Executive Officer

Professor Marten L. denBoer

Professor John J. Fontanella

Professor Robert A. Marino

Professor Ruth E. Stark
Supervisory Committee

The City University of New York

ABSTRACT

NUCLEAR MAGNETIC RESONANCE STUDIES OF POLYMER ELECTROLYTES

by

Yiu Sun Pak

Adviser: Professor Steve G. Greenbaum

^{23}Na NMR studies have been made on a variety of polymer electrolytes. Remarkably, the measurements reveal features that are common to nearly all types of material studied, including the presence of mobile and bound (aggregates) of sodium. T_1's of the mobile and bound sodium are in the range of milliseconds and seconds respectively. The bound Na has a relatively temperature insensitive linewidth of about 5 kHz. The linewidth of mobile Na is typically 5 kHz below the glass transition temperature (T_g), and undergoes motional narrowing above T_g (evidence of the importance of polymer segmental motion in the ion transport process) to a minimum of about 0.5 kHz at around 45-55 K above T_g, and then broadens somewhat. The broadening is due to the relatively fast spin-lattice relaxation time ($T_1 \approx 300\ \mu s$), i.e. lifetime-broadening.

The temperature dependence of the ratio of mobile to bound Na (M/B) indicates the process of ion dissociation and a minor role of thermal "carrier

generation". A study of a series of poly(propylene-oxide) (PPO) NaI complexes of different salt concentration suggests that PPO_8NaI is the only stable amorphous phase in the complexes. Both T_1 and linewidth of the bound Na measurements show that bound Na is likely to be an ion-aggregate (~ 10 or more ions). The drop of M/B above 353 K indicates the occurrence of salt precipitation (SP).

Ion-ion and ion-polymer interactions in polymer complexes are further investigated by measurement of a series of PPO complexes with different sodium salts. Satisfactory correlation between SP temperature and melting point of pure salt has been found. ^{23}Na chemical shifts due to mobile Na^+ ions exhibit a strong dependence on anion and temperature. Moreover, ^{13}C NMR data show differences in ion-polymer interaction for Li- and Na- PPO complexes.

High pressure NMR of several PPO and siloxane complexes exhibit a systematic decrease in M/B with increasing pressure. In addition, the linewidth increases or decreases with the application of pressure, depending on the value of $T - T_g$. The results are consistent with collaborative high pressure conductivity measurements, which also indicate that T_g increases with increasing pressure. In multi-frequency ^{23}Na NMR of PPO and siloxane-based complexes, the linewidth of the mobile Na^+ ion is inversely proportional to the resonance frequency, implying second order quadrupole broadening.

ACKNOWLEDGEMENTS

I would like to thank Professor Steven G. Greenbaum, my advisor, for his support of this work, his knowledge, guidance, and for his reading of this manuscript. Professor Kresimir Adamic is greatly thanked for his expertise and preparation of samples throughout this work. Special thanks are due to Mr. Richard Krumm for his technical assistance, including designing and building the high pressure probe, and the probe for low resonance frequency experiments. Professor Robert A. Marino, my NMR "uncle", Mr Shi Zhe Li, and Armando Howard are gratefully acknowledged for their friendship, encouragement, and helpful discussion. Other members of the group to be acknowledged include, Ms Meng Chiao, Ms Gillian Reynolds and Ms Sandra Brown.

Professor Ruth E. Stark of College of Staten Island is thanked for kindly allowing me to do ^{13}C NMR experiments in her laboratory, as well as for her guidance throughout the course of the work. Special thanks are also due to Mr Abraham Malz for his technical assistance in the work.

Professor John J. Fontanella of Naval Academy is gratefully acknowledged for his collaborative DSC and conductivity measurements, and his useful discussions. Of course, thanks are due to his group members. Our NMR results have been more fruitful due to their collaborative measurements.

Professor Y. Okamoto of Polytechnic University is gratefully thanked for his supply of (PMPS-EO) siloxane based and cationic conducting complexes, as well as

Professor A. V. Chadwick of University of Kent (UK) for his preparation of amorphous poly(ethylene oxide) complexes.

I am grateful to the other thesis committee members, Professor Marten DenBoer, Professor John Fontanella, Professor Robert Marino and Professor Ruth Stark, for their support and supervision. Finally, I wish to thank my mother and other family members for their support and encouragement.

This research was supported by grants from the Office of Naval Research and PSC-CUNY Research Award Program.

TABLE OF CONTENTS

LIST OF TABLES

LIST OF FIGURES

Page

Page

Page

INTRODUCTION

Much interest has been focused on the high ionic conductivity of certain kinds of polymers, in terms of fundamental understanding of fast ion-transport mechanisms as well as their potential application as solid electrolytes. Study of ionic motion in polymer electrolytes is thus of current and significant interest in materials science and technology.

Nuclear magnetic resonance (NMR) spectroscopy is a well established and powerful technique which can be used to probe molecular structure and mobility. The advantages of NMR are nuclear specificity, sensitivity to the microscopic environment of the diffusing ion, and ability to study materials over a wide temperature range and as a function of applied pressure. ^{23}Na is chosen as the probe ion in most of this work because of its relatively high sensitivity and large quadrupole moment. This will give us more information about the microscopic environment of the ion in the complexes. Of equal importance is the fact that the preparation of highly conducting polymer-Na salt complexes is straightforward. The most widely used NMR techniques for the study of ionic transport are relaxation time studies. For instance, the ionic motion in the frequency range of tens of MHz (the Larmor frequency) is probed by T_1 measurements, and kHz motions can be deduced from linewidth measurements. It is well known that ionic motion in the material is through the coordination of the ether oxygen in the polymer chain and the cation coupled with segmental motion of the polymer.

Over the past few years, NMR studies on polymer electrolytes were conducted in this laboratory. The experiments were carried out on various kinds of polymer

complexes. As the Na^+ species in the complexes are generally distinguishable, efforts have been made to get a quantitative measurement of their separate contributions to the NMR lineshape as a function of temperature or pressure. With the combination of spin-lattice relaxation (T_1), linewidth measurement, ^{13}C NMR experiments and multi-frequency ^{23}Na NMR measurements, this thesis constitutes a comprehensive NMR investigation of the material. Of course, collaborative work with other institutions, such as DSC and conductivity measurements performed at the Naval Academy, provide us a better understanding of ionic behavior in the material. Moreover, NMR studies of some new synthetic materials, for example an exclusively cationic conducting electrolyte, was made possible through collaboration with the polymer chemistry department of Polytechnic University.

The general organization of this thesis is as follows: Chapter 1 gives a general review of the theoretical background of NMR, including BPP theory, quadrupole interaction of spin 3/2 in solids, and a brief discussion of high resolution solid state NMR techniques. Chapter 2 presents experimental methods and instrumental specifications. Technical information on the high pressure NMR probe built in this laboratory is also included. In addition, a general discussion of magneto-acoustic noise in low frequency NMR work is provided. Chapter 3 starts with a general review of polymer electrolytes. Experimental results are then presented for different host polymers and then discussed. This chapter closes with a summary of our results. Finally, a program utilized in the laboratory microcomputer, involving interfacing with the LeCroy 9400 digital oscilloscope, is included in the appendix.

Chapter 1

THEORETICAL BACKGROUND

(1.1) Basic Theory of NMR [1]

A basic problem in nuclear magnetism is the description of the behaviour of a spin system (nucleus or electron spin) in a uniform magnetic field. For simplicity, let us consider a nuclear spin possessing an angular momentum $\vec{I}\hbar$ and a magnetic moment $\vec{\mu}$, where the two quantities are related as:

$$\vec{\mu} = \gamma \vec{I}\hbar \qquad (1.1)$$

where γ is the magnetogyric ratio, a characteristic property of the nucleus.

$\hbar$ is Planck's constant divided by 2π.

In the presence of a static magnetic field $\vec{H}_o$, the Hamiltonian of the Zeeman interaction is given by

$$\mathcal{H}_o = -\vec{\mu} \bullet \vec{H}_o \qquad (1.2a)$$

with the field H_0 along the z direction,

$$\mathcal{H}_o = -\gamma \hbar H_o I_z \qquad (1.2b)$$

As I_z can take any of the 2I+1 discrete values I, I-1, ..., -I, the eigenvalues for the Hamiltonian $\mathcal{H}_0$ are

$$E_m = -\gamma \hbar H_o m \qquad m = I, I-1, \ldots\ldots, -I \qquad (I.3)$$

In general, the equation of time evolution of the spins can be shown (classically or quantum mechanically) to be

$$\frac{d\langle \vec{\mu} \rangle}{dt} = \langle \vec{\mu} \rangle \times \vec{H} \qquad (1.4)$$

where $\langle\vec{\mu}\rangle = \sum_i \langle\vec{\mu}_i\rangle$, $\langle\vec{\mu}_i\rangle$ = expectation value of $\vec{\mu}_i$, and

$\vec{H}$ = external magnetic field (may depend on time)

Magnetic dipole transitions are allowed between adjacent levels. According to equation (1.3), the energy required for the transition is $\gamma\hbar H_o$. In order to study the spin system spectroscopically by NMR, one induces a resonance by applying, in addition to the large static magnetic field $\vec{H}_o$, a small sinusoidal rf field $\vec{H}_1$ normal to $\vec{H}_o$ and of frequency ω. The Hamiltonian of a spin is then :

$$\begin{aligned}\mathcal{H} &= -\gamma\hbar\vec{I}\cdot\vec{H}_o - \gamma\hbar\vec{I}\cdot\vec{H}_1 \\ &= -\gamma\hbar H_o I_z - \gamma\hbar I_x(2H_1\cos\omega t) \\ &= \hbar\omega_o I_z + 2\hbar\omega_1 I_x\cos\omega t\end{aligned} \qquad (1.5a)$$

where we have used the notations:

$$\omega_o = -\gamma H_o \quad , \quad \omega_1 = -\gamma H_1$$
$$\vec{H}_1 = 2H_1\cos\omega t\ \hat{i} \quad , \quad \vec{H}_o = H_o\ \hat{k} \qquad (1.5b)$$

Instead of the fixed laboratory frame, it is easier to examine the spin system in the rotating frame of frequency ω. As shown elsewhere [1], the effective Hamiltonian in the rotating frame is

$$\mathcal{H}_{eff} = \hbar(\omega_o - \omega) I_z + 2\hbar\omega_1 I_x \qquad (1.6a)$$

which is time independent as all components of the magnetic field are stationary in that frame.

The components of the effective field are then:

$$H_x = 2H_1, \quad H_y = 0, \quad H_z = -\frac{(\omega_o - \omega)}{\gamma} = -H_o + \frac{\omega}{\gamma} \qquad (1.6b)$$

At the resonance condition ($\omega = \gamma H_o$) and with the magnetization vector lying along the z-axis at time t=0,

$$\langle \mu_z(t) \rangle = \langle \mu_z(0) \rangle \cos\gamma H_1 t \qquad (1.7)$$

The condition $\gamma H_1 t_w = \frac{1}{2}\pi$ defines the so called "90°" pulse (t_w is the pulse width); it rotates the magnetic moment from the z-axis to the y-axis. With the detection coil axis in the x-y plane, an induced emf may be observed. Once the rf field is turned off, the transverse magnetization undergoes a damped rotatiHx in the laboratory frame, whereas the longitudinal component relaxes back to its equilibrium value. The signal following the "90°" pulse is commonly called the "Free Induction Decay" (FID), and it decays exponentially with a time constant T_2^*. In the frequency domain, the linewidths at half maximum for the Gaussian and the Lorentzian are $3.34/2\pi T_2^*$ and $1/\pi T_2^*$, respectively. The relaxation of the longitudinal component is characterized by the time constant T_1, known as the spin-lattice relaxation time constant. T_1 measures how fast the nuclei attain thermal equilibrium with the "lattice" (i.e. all the other non-spin degrees of freedom). Besides spin-lattice relaxation, the other relaxation process is spin-spin relaxation which is marked by the time constant T_2. T_2 is the time constant associated with the dephasing of the transverse magnetization due to the homonuclear dipolar interaction.

The pulse technique facilitates the measurement of the relaxation times T_1 and T_2. T_2 can be determined by the spin echo amplitude as a function of τ, the separation between the "90°" and the "180°" pulses [2]. In practice, it is found that T_2 can be fit by the equation:

$$A(2\tau) = A_o \exp\left(-\frac{2\tau}{T_2}\right) \qquad (1.8)$$

Other techniques are also used to measure T_2, such as Carr-Purcell pulse sequence and Meiboom-Gill modified Carr-Purcell sequence (CPMG) as described elsewhere [3,4].

The usual procedure for determining T_1 is to measure the amplitude of the FID as a function of τ', the time delay between "90°" pulses. In most cases, the recovery to the thermal equilibrium can be cast in an exponential form

$$A(\tau') = A_o\left(1 - \exp\left(-\frac{\tau'}{T_1}\right)\right) \qquad (1.9)$$

where $A(\tau')$ is the amplitude of the FID.

It should be noted that T_2^* is related to T_2 by

$$\frac{1}{T_2^*} = \frac{1}{T_2} + \gamma\Delta H + \text{"others"} \qquad (1.10)$$

where $\gamma\Delta H$ is the effect due to the field inhomogenity and "others" represents other inhomogeneous broadening mechanisms such as that associated with the quadrupole interaction for $I > \frac{1}{2}$.

The earliest model which related molecular motion to the relaxation times of spin ½ nuclei was due to Bloembergen, Purcell and Pound and is referred as the BPP theory [5]. Under the assumption that the fluctuation of the local field h(t) is an exponential time correlation function G(t) given by

$$G(t) \propto h(t)h(0) = G_o \exp\left(-\frac{t}{\tau_c}\right) \qquad (1.11)$$

where τ_c is the correlation time of the the motional process, the mean time elapsed before the nuclei experience any appreciable change in h(t). τ_c is related to the activation energy E_a by the Arrhenius relation τ_c = constant * $\exp(E_a/k_BT)$

For spin I=½, the relaxation rates are given by:

$$\frac{1}{T_1} \sim \frac{\omega_d^2 \tau_c}{1+\omega_o^2 \tau_c^2} + \frac{4\omega_d^2 \tau_c}{1+4\omega_o^2 \tau_c^2} \qquad (1.12a)$$

$$\frac{1}{T_2} \sim \omega_d^2 \tau_c \left(3 + \frac{5}{1+\omega_o^2 \tau_c^2} + \frac{2}{1+4\omega_o^2 \tau_c^2} \right) \qquad (1.12b)$$

where ω_d is the frequency corresponding to the typical dipolar coupling.

The above relationships lead to the temperature dependence shown in fig. 1. In the limit of $\omega_o \tau_c \ll 1$, these equations yield:

$$\frac{1}{T_1} \propto \frac{1}{T_2} \sim \omega_d^2 \tau_c \qquad (1.12c)$$

and T_1 and T_2 increase with increasing temperature. As the temperature decreases, the substance becomes more viscous and τ_c increases. The term that is independent of ω_o in equation (1.12b) then becomes important and this causes T_1 and T_2 to separate. At low temperature at which $\omega_o \tau_c \gg 1$,

$$\frac{1}{T_1} \sim \frac{1}{\omega_o^2 \tau_c} \sim \frac{1}{\tau_c} \quad , \quad \frac{1}{T_2} \sim \tau_c \qquad (1.12d)$$

hence T_1 increases and T_2 decreases with decreasing temperature. However, the BBP result predicts that the T_2 decrease ceases in the "rigid" temperature region at a constant, say τ_o, at which $T_2 \propto \tau_o$. T_2 is then temperature independent, and the line

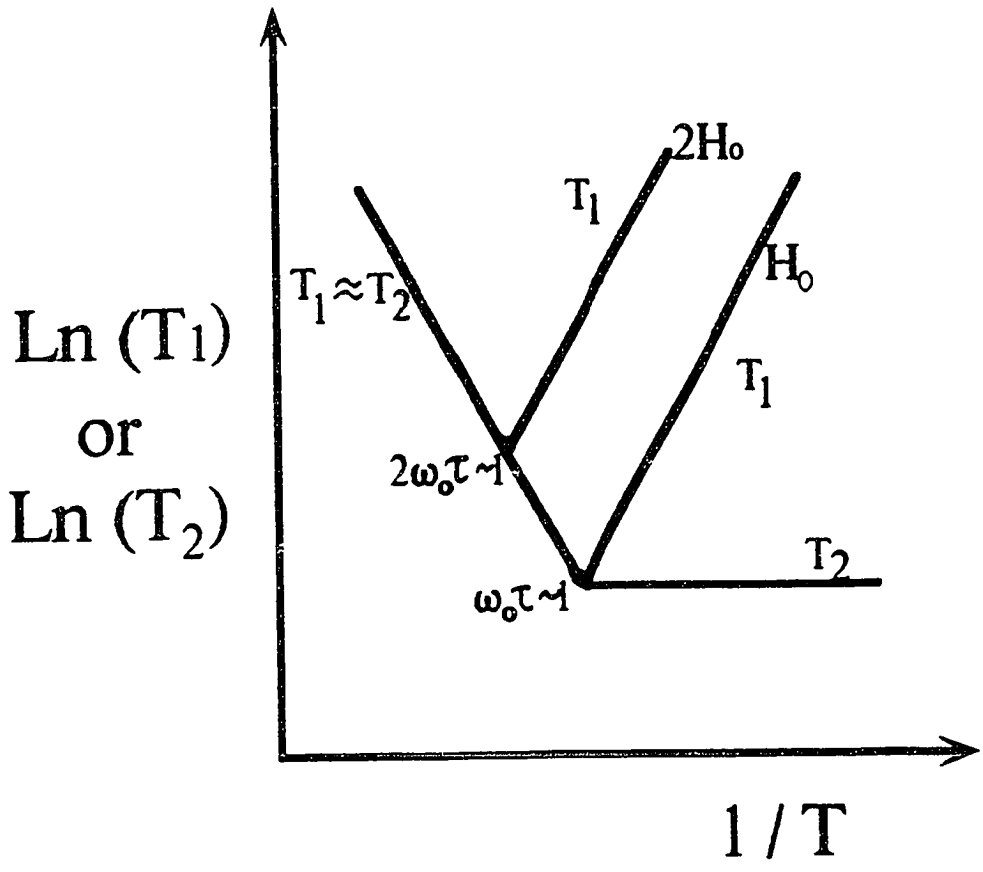

Figure 1.1 Arrhenius plot of spin-lattice relaxation time (T_1) and spin-spin relaxation time (T_2), BPP theory [5].

breadth is the rigid-lattice line breadth. As seen from equations (1.12c) and (1.12d), T_1 has two different temperature dependences in those limits, and there must exist a minimum in between. The T_1 minimum is important as it enables us to determine τ_c, i.e. where $\omega_0\tau_c \sim 1$, and τ_c can be treated as the correlation time of the nuclear motion.

(1.2) Quadrupole broadening for spin I=3/2

So far we have considered only the magnetic interaction of the nucleus with its surroundings. Besides this magnetic interaction, a nucleus possessing an electric quadrupole moment may have electrostatic interaction with its local environment. This interaction is called the nuclear quadrupole effect. Nuclear quadrupole effects in solids have been studied since the 1950's. There are several well presented monographs on this topic, such as Das & Hahn, and Cohen & Reif [6]. In this section, we will review quadrupole broadening effect in NMR studies as well as quadrupolar relaxation effects. Nuclei with I= ½ have a spherical charge distribution. This is not true for nuclei of spin, I > ½ and consequently such nuclei possess an electric quadrupole moment. As a result, the nuclei interact with the local electric field gradient (efg). Considering a nuclear charge density $\rho(\vec{x})$ at the point $\vec{x}$, the classical energy of interaction can be written as

$$W = \int \rho(\vec{x}) V(\vec{x}) d^3\vec{x} \qquad (1.13)$$

where $V(\vec{x})$ is the potential arising from all charges other than the nucleus under consideration.

By expanding $V(\vec{x})$ about the point at which the nucleus is located, denoted as the origin,

$$V(\vec{x}) = V(0) + \sum_j x_j \left(\frac{\partial V}{\partial x_j} \right)_0 + \frac{1}{2} \sum_{jk} x_j x_k \left(\frac{\partial^2 V}{\partial x_j \partial x_k} \right)_0 + \ldots . \qquad (1.14)$$

where x_j denotes the cartesian components of the coordinate system.

Thus one obtains the Hamiltonian $\mathcal{H}$,

$$\mathcal{H} = ZeV(0) + \sum_j p_j \left(\frac{\partial V}{\partial x_j} \right)_0 + \frac{1}{2} \sum_{jk} Q_{jk} \left(\frac{\partial^2 V}{\partial x_j \partial x_k} \right)_0 + \ldots . \qquad (1.15)$$

$$\int d^3x \rho(x) \equiv Ze - \text{nuclear charge}$$

$$\int d^3x \ \rho(x) x_j \equiv p_j \ - \ \text{electric dipole moment} = 0$$

$$\int d^3x \rho(x) x_j x_k \equiv Q_{jk} \ - \ \textit{electric quadrupole moment}$$

The quadrupole Hamiltonian in the above expression is then

$$\mathcal{H}_Q = \frac{1}{2} \sum_{j,k} Q_{jk} \left(\frac{\partial^2 V}{\partial x_j \partial x_k} \right)_0 = \frac{1}{2} \sum_{j,k} Q_{jk} (V_{jk})_0 \qquad (1.16)$$

Let us choose the axes of the coordinate system OXYZ as the principal axes of the symmetrical tensor V_{ij}, so that $V_{xz} = V_{yz} = V_{xy} = 0$, and $|V_{xx}| \leq |V_{yy}| \leq |V_{zz}|$. With the introduction of the following quantities:

$$Q_{jk} = 3Q_{jk} - \delta_{jk} \sum_i Q_{ii} \ , \ \eta = \frac{V_{xx} - V_{yy}}{V_{zz}}, \ eq = V_{zz}$$

η represents the departure of the efg from the axial symmetry. One can easily show that the Hamiltonian of a nuclear spin ($I > \frac{1}{2}$), in the presence of an applied field $\vec{H}_o$, is the following

$$\mathcal{H} = -\gamma h\vec{H}_o \bullet \vec{I} + \frac{e^2qQ}{4I(2I-1)}[3I_z^2 - I(I+1) + \frac{\eta}{2}(I_+^2 + I_-^2)] \qquad (1.17)$$
$$= \mathcal{H}_z + \mathcal{H}_Q$$

where eQ ≡ <I, m_I=I $|Q_{33}|$ m_I=I, I> and I_+ and I_- are the raising and lowering operators of spin I.

In a high magnetic field, the quadrupole Hamiltonian can be treated as a perturbation of the Zeeman Hamiltonian $\mathcal{H}_z$. From perturbation theory [7], the first order frequency shift for the m → m-1 NMR transition is

$$\omega_m^{(1)} = -\frac{\omega_Q}{4}[(3\cos^2\theta - 1) - \eta\sin^2\theta\cos 2\phi](2m-1) \qquad (1.18)$$

where m = magnetic quantum number.

$$\omega_Q = \frac{3e^2qQ}{2I\hbar(2I-1)}$$

θ and ϕ are the angles of the principal coordinate system of the efg tensor relative to $\vec{H}_o$. For a given orientation in a single crystal, 2I discrete resonance lines are observed. The transitions adjacent to the central one are called satellite lines. It can be easily seen that $\omega_m^{(1)}$ vanishes for m = ½. Thus, for half-integer spins, the frHxuency of the central transition ½ ↔ -½ is not shifted in first order by the quadrupole interaction. However in the case of η = 0 and the frequency shift for the central transition ½ ↔ -½ , the second order calculation yields the following

$$\omega_{1/2}^{(2)} = -\frac{\omega_Q^2}{16\omega_L}\left[I(I+1) - \frac{3}{4}\right](9\cos^2\theta - 1)(1 - \cos^2\theta) \qquad (1.19)$$

If the efg at the nucleus is sufficiently small, a first-order satellite splitting may be observed. As the quadrupole interaction increases, there can also be a shift and a splitting of the central line. A simple test for the second order quadrupole effect involves checking the inverse proportionality of the splitting to the applied field or frequency ω_L. In actual situations, there may be a distribution of splittings because the field gradient may differ slightly from nucleus to nucleus. In the first order effect, the central transition is unshifted and only dipolar broadened. In second order, the central resonance is strongly broadened asymmetrically. There are cases where the quadrupole interaction is so large as to cause even the central transition to be broadened beyond detection. Figure 1.2 shows the quadrupole splittings of the magnetic resonance of a nucleus of spin 3/2, e.g. ^{23}Na, and a sketch of the lines expected in a powder sample with the additional effect of the dipolar broadening.

As T_1 measures the interaction between the spin system and the lattice, it can give useful information about the fluctuating internal fields which exist in solids. For spins $I=\frac{1}{2}$ ($Q=0$), the fluctuating fields responsible for the relaxation are magnetic in origin. If a nucleus possesses an electric quadrupole moment, quadrupole interactions may become important in causing the nuclear relaxation. It can be shown that the Hamiltonian $\mathcal{H}_Q$ in equation (1.17) causes nuclear transitions for $\Delta m = \pm 1$ or $\Delta m = \pm 2$. If the equilibrium populations of the nuclear energy levels are perturbed, the nuclear spins return to their equilibrium magnetization will not be described by a simple exponential law when quadrupole interactions are involved. This means that a unique T_1 cannot, in general, be defined. In most cases, the longest time constant may then be designated as a measure of a characteristic

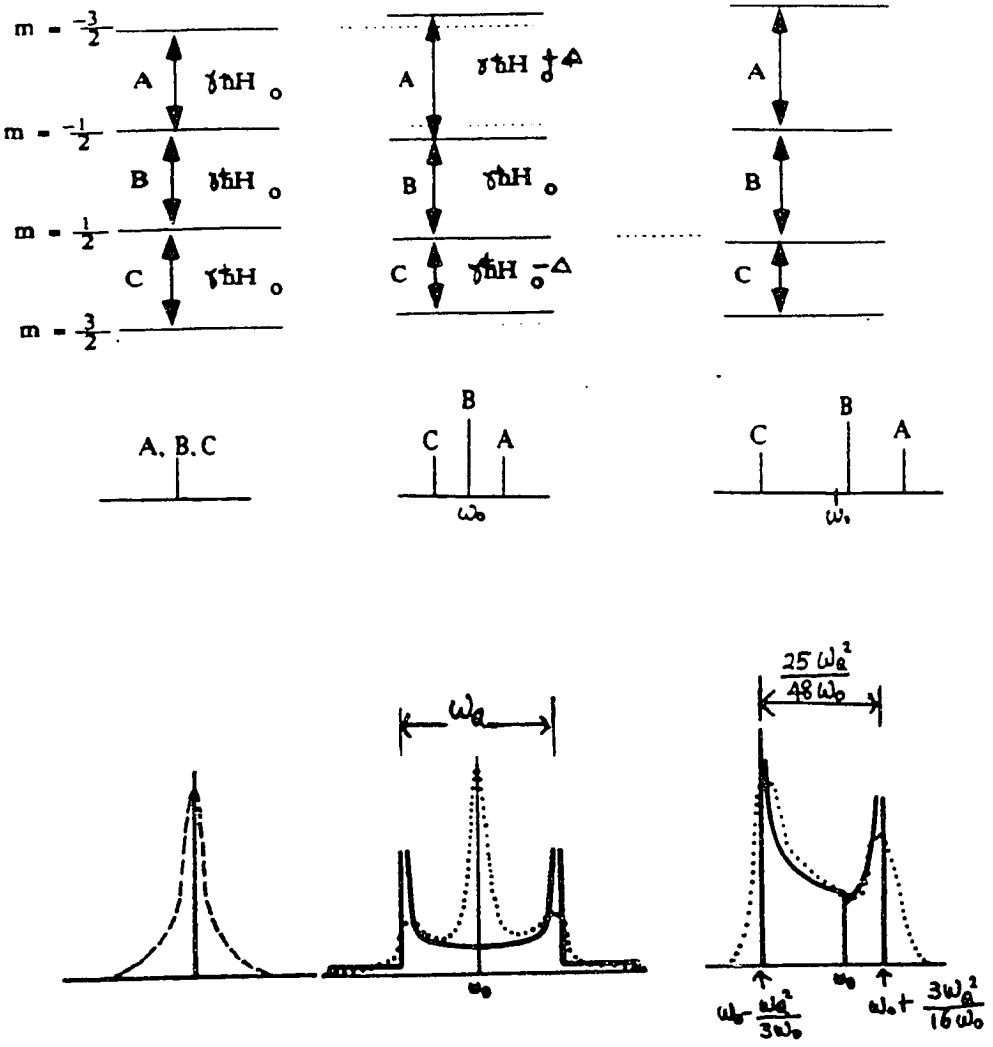

$$\omega_0 = \gamma H_0 \qquad \omega_Q = \frac{e^2qQ}{2\hbar} \qquad \Delta = \frac{\omega_Q(3\cos^2\theta - 1)}{2}$$

Figure 1.2 Quadrupole splitting of the magnetic resonance of a nucleus of spin 3/2.
Left: no quadrupople interaction.
Center: first order splitting of satellite.
Right: second order shifting of the central component.
Top: energy spectrum
Middle: spectrum of a single nucleus without dipolar broadening.
Bottom: spectrum of a powdered sample with axially symmetric field gradients.
With the dipolar broadening superimposed, the dotted curves result.

relaxation time. However, non-exponential T_1 observed in heterogenous material may not be due to exclusively to quadrupole interactions. The non-exponential behavior can also be a result of T_1 contributions from two different spin species in the material. The latter interpretation is easily verified if individual resonance spectra can be distinguished from each other, or if their characteristic T_1's differ by more than one order of magnitude. In fact, the latter scenario has most often been the case in this work.

(1.3) High resolution NMR of solids[8]

In solids, the NMR line is broadened because of the dipolar interaction between the nuclei and the chemical shift anisotropy (CSA). Of course,the above mentioned quadrupole interaction is an additional broadening for $I>\frac{1}{2}$. The chemical shift effect is due to the "shielding" of the nucleus from the applied field H_o as a result of induced orbital motion (diamagnetism) of the electrons in the molecule. The effective magnetic field can be written as

$$\vec{H}_{eff}=\vec{H}_o(1-\sigma) \tag{1.20}$$

where σ - chemical shift factor

$\vec{H}_{eff}$ - effective field as seen by the nucleus.

The effect depends on the orientation of the molecules in the magnetic field, as well as the neighboring nuclei and electrons. Therefore, σ is usually a tensor. In liquids we typically have rapid tumbling and can observe only the result of a random average of the principal axes with respect to the magnetic field. When the chemical shift of a nucleus depends upon the orientation of the molecule within the applied

magnetic field, the chemical shift is said to be anisotropic. In principle, one can measure the full chemical shift tensor in a solid. However, the lack of motional narrowing in solids results in the dipolar broadened lines and the anisotropic shift is masked. One must overcome this masking in order to obtain more information about the local environment of the nucleus in the solid.

In order to study high resolution NMR in solids, certain barriers have to be overcome. The first one is the broadening of the NMR line due to CSA and the dipolar interaction. The technique called " Magic Angle Spinning " (MAS) is used to resolve the anisotropy. The sample is spun, at a frequency of several kHz, about an axis at 54.74° with respect to the magnetic field. The term "magic angle" refers to the fact that the average value of the term $(3\cos^2\theta - 1)$ in the CAS is equal to zero if $\theta = 54.74°$. It is noted that the heteronuclear dipolar coupling also contains a similar $(3\cos^2\theta - 1)$ term. Thus MAS also reduces the dipolar interaction. However, the heteronuclear dipolar interaction is mainly eliminated by the high power decoupling technique. Let us consider the ^{13}C solid state NMR experiment. The multiplet of ^{13}C lines, due to the dipolar interaction of the neighboring protons, is collapsed into a single line by applying a high power rf field at the proton Larmor frequency. Finally, the sensitivity of ^{13}C signal is enhanced by cross-polarization to transfer polarization from the proton nuclei provided that the Hartmann-Hahn condition

$$\gamma_c H_{1c} = \gamma_p H_{1p} \tag{1.21}$$

is fulfilled, where H_{1c}, H_{1p} denote the rf field of carbon and proton resonance respectively.

Figure 1.3 shows the pulse sequence for a typical ^{13}C NMR experiment. There is a vast literature on this type of measurement and readers can refer to the reference for details [9].

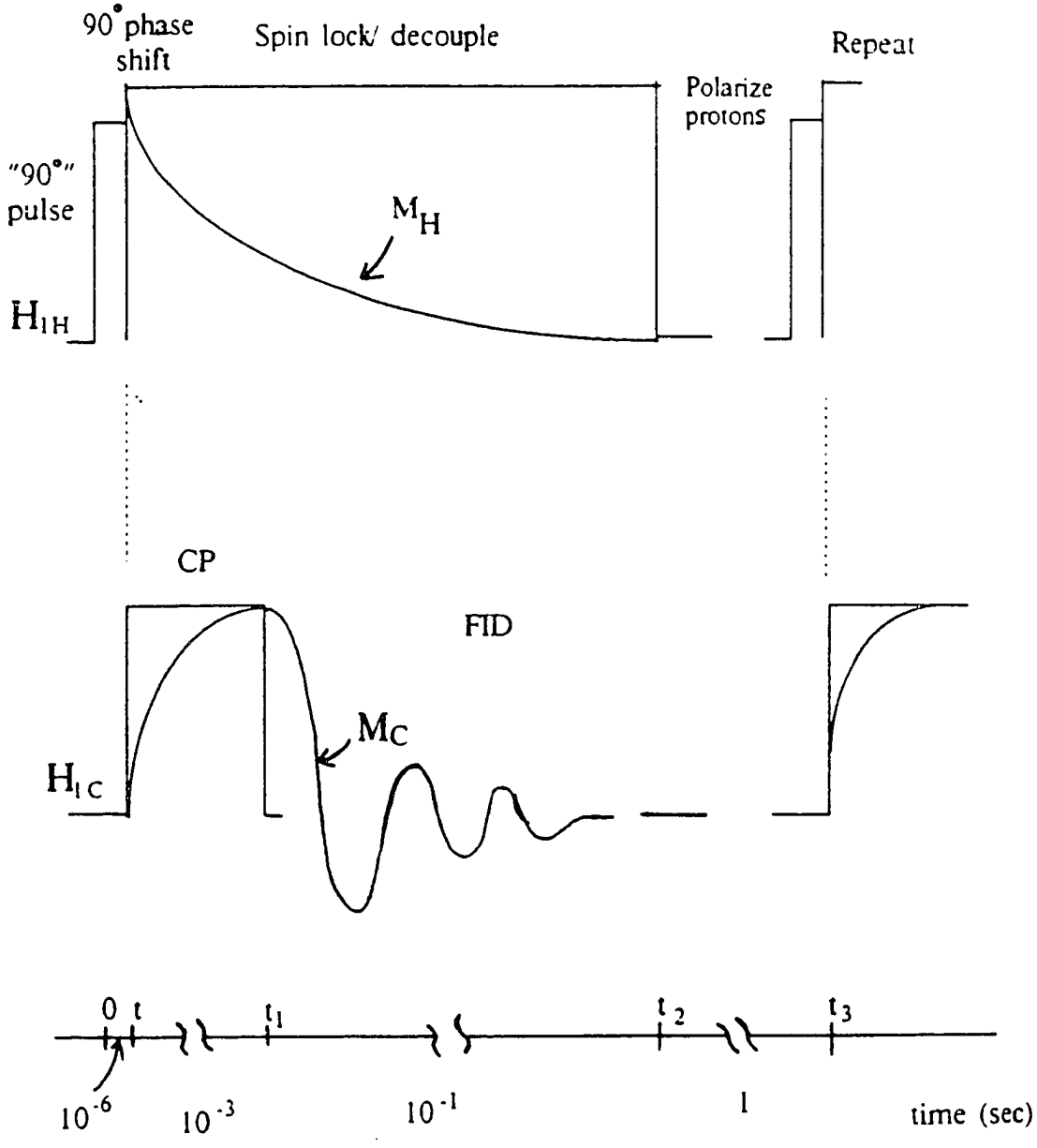

Figure 1.3 Single-contact spin-lock cross polarization (CP) rf pulse sequence, showing the time dependence of the carbon and proton magnetization.

Chapter 2

EXPERIMENTAL EQUIPMENT AND PROCEDURES

(2.1) Solid State Pulse NMR Spectrometer

(A) Spectrometer specification

Most of this thesis work was conducted with a Novex^{TM} NMR spectrometer, in conjunction with a Cryomagnet System superconductor magnet of field strength 7.16 T. The homogeneity of the field is about 1 ppm (part per million) for ^2H nuclei (liquid D_2O) at 45.0 MHz over a volume of $1cm^3$.

A block diagram of the spectrometer is shown in fig. 2.1. The low level (1 volt p-p) continuous wave (CW) signal provided by the frequency synthesizer is fed to the gate driver and receiver for phase detection. The appropriate pulse sequence is written in ASCII format by the computer [10] and generated by the Novex pulse programmer. Typical pulse sequence files are shown in fig. 2.2. Typically, 2 kW peak power of rf pulse is supplied by the power amplifier to the matching network and then the sample coil. The schematic diagram of the matching network is shown in fig. 2.3. There are two channels available with different frequency ranges. The range of tuning capacitance in channel 1 is 0.8 - 10 pf, suitable for work at high frequency (~ 80 MHz). The shunt capacitor furnishes the flexibility of tuning at some lower frequency, e.g. 45 MHz for ^2H, although channel 2 is also available for lower frequency work. It must be noted that the capacitors are physically as close to the sample coil as possible, avoiding the additional stray capacitance of the coaxial

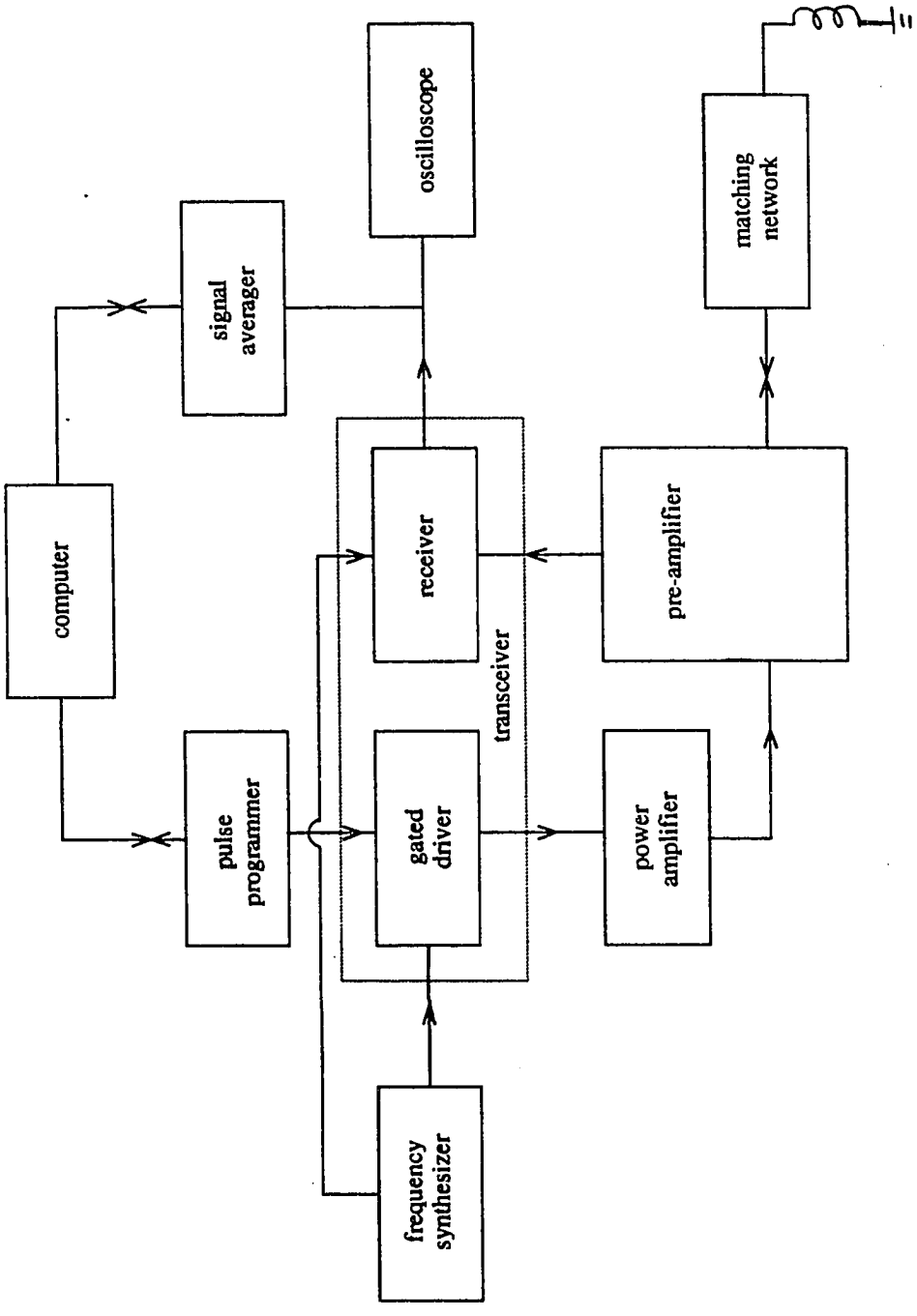

Figure 2.1 Block diagram Novex™ NMR spectrometer.

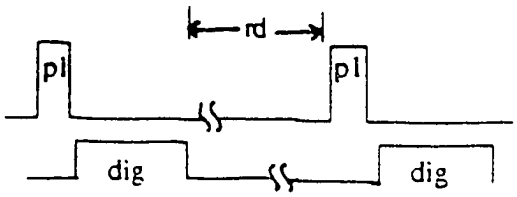

(a) One Pulse Sequence

```
;
; Sequence
- 1.0u          0       0       0       0       0       0       0
- p1            1       0       a       0       0       0       0
- 1.0u          0       0       0       0       0       0       0
- dig           2       0       0       0       0       0       0
b strobe 1
- rd            0       0       0       0       0       0       0
;
; tweak parameters
T p1
T a
;
; default parameter
P tau = 100u
```

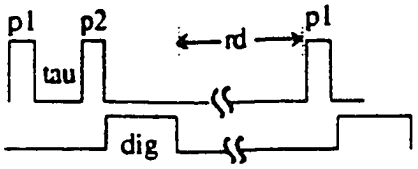

(b) Spin Echo Sequence:

```
;
; Sequence
- 1.0u          0       0       0       0       0       0       0
- p1            1       0       a       0       0       0       0
- 1t            0       0       0       0       0       0       0
- p2            1       ph      a       0       0       0       0
- 1.0u          0       0       0       0       0       0       0
- dig           2       0       0       0       0       0       0
b strobe 1
- rd            0       0       0       0       0       0       0
;
; tweak parameters
T tau
T a
T p1
T p2
```

Figure 2.2 Novex pulse sequence ASCII files.

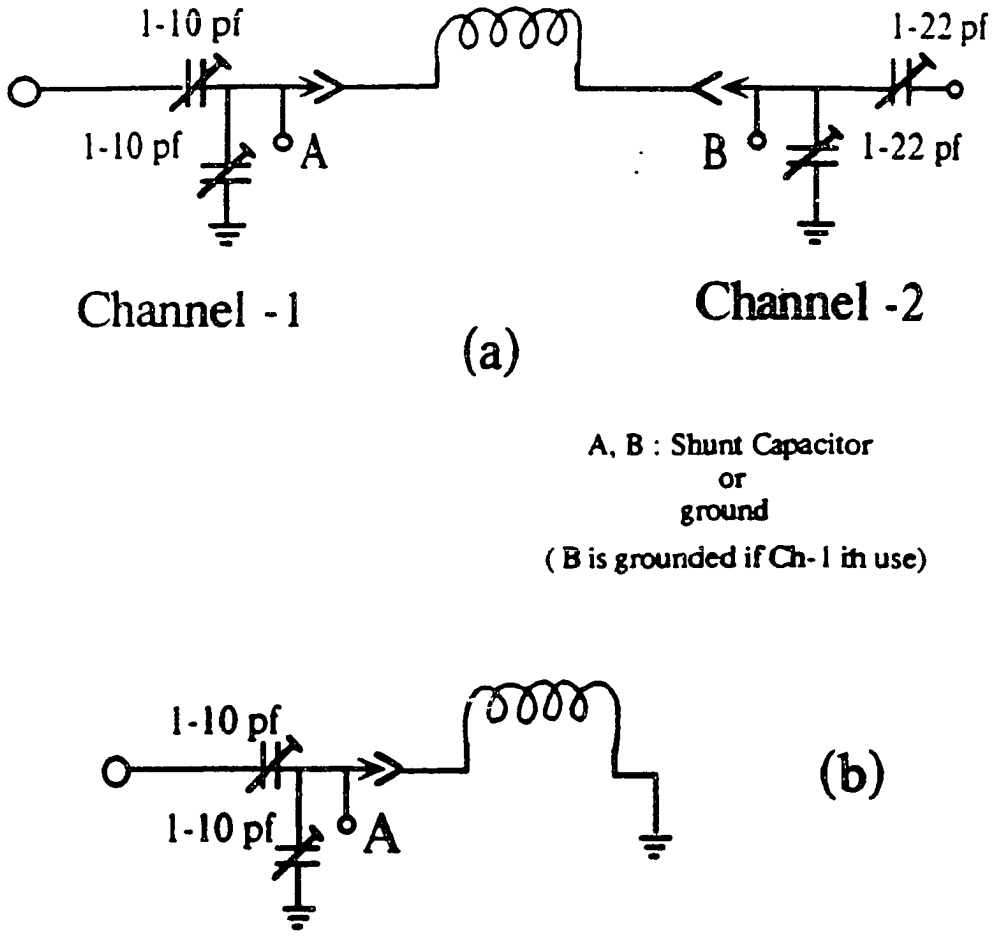

Figure 2.3 Schematic diagram of the matching network. (a) 2 channels for different frequency works. (b) Channel 1 configuration, with channel 2 grounded.

cable (≈20 pf per foot) [11]. For 81 MHz, a solenoidal sample coil of appropriate inductance, in the range of 0.3-0.35 μH, is placed inside an aluminum cylindrical cavity for shielding purpose. The matching network shown includes only the variable capacitors. The protective circuit elements, i.e. crossed diodes, are built into the Novex preamplifier. There is a great deal of literature describing this kind of circuit [12]. The blanking of the receiver during the pulse transmission facilitates the recovery (time of 1 μsec), and thus extraction of signals of short T_2^*. The video output of the receiver is either viewed directly on the oscilloscope or stored in the Nicolet 1170 signal averager or the LeCroy 9400 digital oscilloscope. The recorded data was stored in an IBM computer. The program used and details of the format of the LeCroy data are described in Appendix A for later reference.

Fast Fourier Transform (FFT) of the NMR signal is provided with the Novex NMR software, with features such as apodization, phase correction etc.. The details of how to operate the software are given in reference [12]. In additional, FFT can be performed by the LeCroy 9400 digital oscilloscope with the built in FFT option.

(B) Experimental procedure

The sample was packed into either a 5 mm or 10 mm diameter quartz tube, with the sample volume equal to 0.2 or 1 cm^3. An appropriate solenoidal coil was chosen to maximize the filling factor for a given inductance. As ^{23}Na is the nucleus of interest, the spectrometer frequency is tuned at 80.6 MHz at the 7.16 T magnetic field. Temperature regulation is achieved by the nitrogen gas flow regulation unit. The range is between 173 and 420 K, with stability over the measuring time (up to

1 hour) being about ± 1 K. The typical "90°" pulse width was 3 μsec or 7 μsec for the small and large coil respectively. Arcing inside the capacitors present at high power levels prevents us from using a higher amplitude pulse (i.e. H_1 amplitude), so that we have to use a wider pulse with a lower amplitude. A small pulse width is required to cover a suitable range of the frequency spectrum, especially for a broad resonance. A new type of cylindrical capacitor (CRANE Polyflon, New Rochelle, NY) was recently tested. Arcing seems to be ameliorated in preliminary tests. At the time of writing, a new probe is under construction and further testing of this probe is in progress.

Three basic sets of measurements were carried out:

(i) Temperature dependence of T_1

T_1 was measured by either the double pulse sequence (inversion recovery or saturation recovery) or the steady state single pulse sequence [13]. The pulse sequences are shown in fig. 2.4. All three sequences are very similar to each other, with the initial pulse initializing the spin system and then the next pulse monitoring the evolution of the magnetization (or FID).

The simplest one is the steady state sequence. It is an infinite train of "90°" pulses with a separation τ. The signal after each pulse, given by $M(\tau) = M_o[1-\exp(\tau/T_1)]$, was measured several hundred times and averaged. The measurement was repeated, using different τ values. T_1 was then calculated as the reciprocal of the negative slope in the semi-log plot of $[M_o - M(\tau)]$ vs τ. This sequence is very efficient but it has a drawback. A relatively heavy duty cycle is required from the

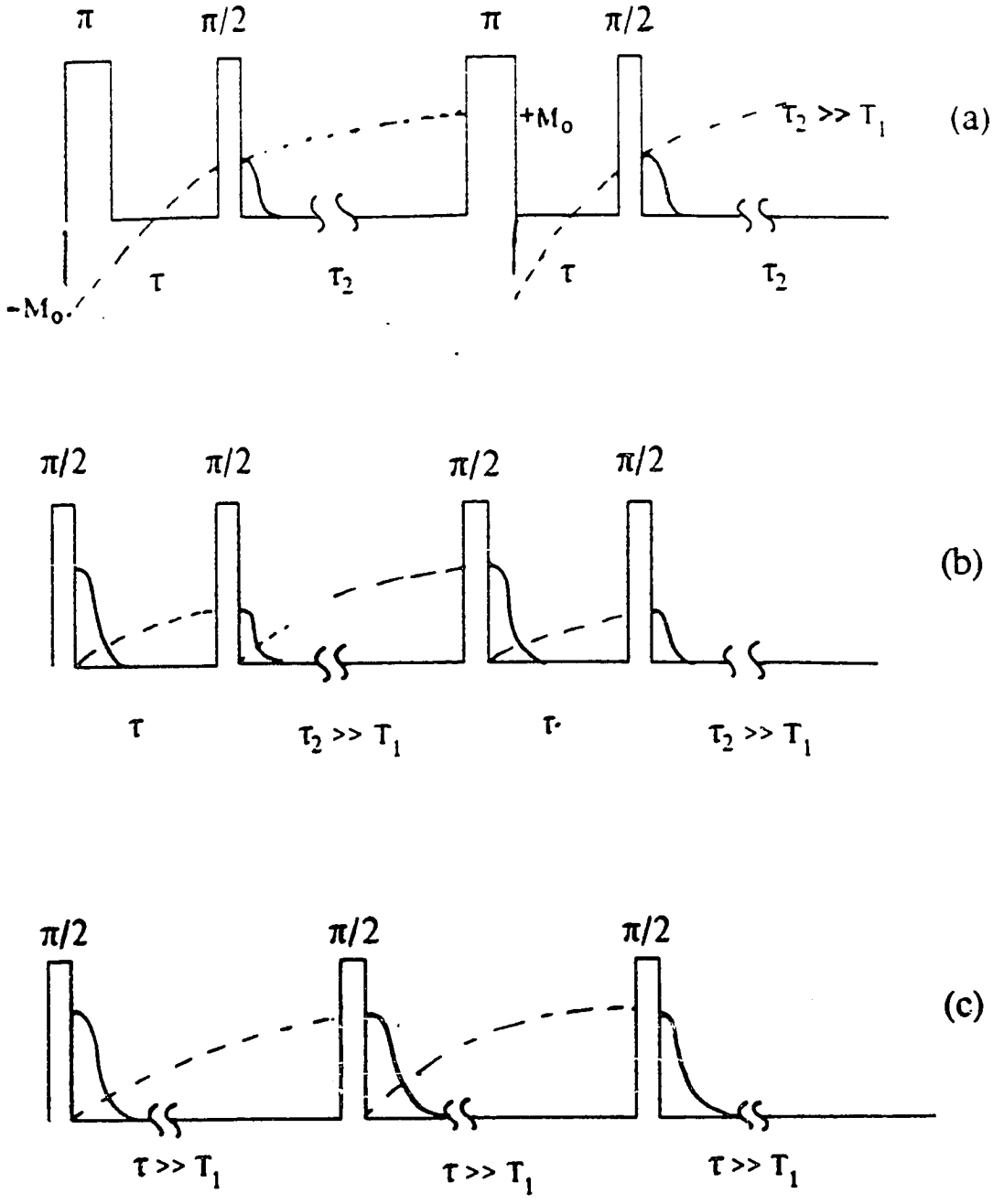

Figure 2.4 Pulse sequences for T_1 measurement.
(a) Inversion recovery.
(b) Saturation recovery.
(c) Steady state single pulse sequence.

output power transmitter for samples with short T_1. In the polymer samples studied, there are usually two ^{23}Na species with T_1 values differing by three orders of magnitude. They are on the order of milliseconds and seconds respectively. For short T_1 resonance signals, double pulse sequences were preferable.

The sequences 90-τ-90-rd, 180-τ-90-rd are called saturation and inversion recovery respectively. As seen in fig. 2.4, the first pulse prepares the spin system and the second pulse measures the magnetization after the waiting period τ. The time delay (rd) is a period long enough for the magnetization to relax back to its thermal equilibrium value M_o, usually greater than 5 times T_1. It is possible to perform the saturation recovery sequence with an arbitrarily short delay between the two pulse pairs. This is because the z-component of the magnetization is identically equal to zero after any "90°" pulse regardless of the magnetization before the pulse. This sequence does not require a full magnetization before any pulse. However, rd should be long enough to reduce the overall duty cycle. $M(\tau)$ is given by $M(\tau) = M_o[1 - 2*\exp(\tau/T_1)]$ or $M(\tau) = M_o[1 - \exp(\tau/T_1)]$ for the inversion and the saturation recovery sequence respectively. The method to calculate T_1 is the same as the one for the steady state sequence. T_1 was sometimes estimated in the inversion recovery sequence by finding the value of τ_o such that $M(\tau_o)=0$, in which case T_1 is equal to $\tau_o/\ln 2$.

In this work, T_1 was measured as a function of temperature. As mentioned in chapter 1, T_1 can provide information on the motion of the ^{23}Na nuclei. In general, it also shows Arrhenius behavior, from which the activation energy of the

motion can be determined. As NMR is a tool to probe nuclei motion on a microscopic scale, the activation energy determined is often smaller than the one deduced by macroscopic techniques, such as conductivity measurement.

(ii) Temperature variation of the reciprocal of T_2^*

As cited in chapter 1, T_2^* is the exponential decay time constant of the FID. The steady state sequence was utilized to signal average the FID off resonance and the amplitude of the peaks was measured as a function of the time. The amplitude, A(t), was fitted with the equation, $A(t) = A_o \exp(-t/T_2^*)$. Hence, the reciprocal of T_2^* was calculated from the semi-log plot of A(t) vs time t. As the reciprocal of T_2^* is proportional to the full width at half maximum (FWHM) in the corresponding frequency spectrum, some of the data presented in a later chapter used $(T_2^*)^{-1}$ as the equivalent linewidth. In addition, the linewidth was measured by utilizing the FFT program of the Novex or the LeCroy 9400. The temperature variation of linewidth provides information concerning Na^+ motion in the region of motional narrowing.

(iii) Temperature dependence of the ratio of the two different ^{23}Na nuclear species

In the samples studied, there are two nuclear species with T_1 differing by three orders of magnitude. It is thus feasible to obtain the spectrum of one by saturating the other one. Considering the steady state sequence, $M(\tau)$ is close to zero if the delay $\tau \ll T_1$. By setting τ to the order of milliseconds, the type of nuclei of long T_1 would be saturated. The signal obtained is the one of short T_1. If the value of τ is set to a few seconds, the signal would be a combination of the two. By subtracting the two signals, one can obtain the long T_1 signal. The area of the FID,

corresponding to the spectral intensity of the signal, was then calculated by either the built in integration feature of the Nicolet or a self-written program.

(2.2) High Pressure NMR Studies

Ionic conduction in the polymer complexes is a dynamic process that is closely coupled to the motion of the host polymer chains. Valuable information regarding this coupling may be obtained if pressure studies are carried out. The combination of pressure dependence and the probing technique of NMR is a novel approach for these studies. Hence, NMR experiments at high pressure were designed. Some preliminary work has been done so far. The measurements were done with the Novex^{TM} spectrometer, at a magnetic field of 7.16 T. In this section, the design of the pressure probe and experimental set-up are presented. The experimental set up is shown in fig. 2.5. It consists of three parts: the hydraulic pressure pump, the pressure cell and the electrical feedthrough assembly holding the solenoidal coil. The pressure pump is an ENERPAC 11-400 hand operated pump with a maximum pressure of 40000 psi (pounds per square in.) or 2.76 kbar. The tubing connecting the pump to the cylinder is from Harwood Engineering Co., Walpole, MA. The series number is 3M-025, with a working pressure of 200,000 psi. The pressure gauge is CM-50984, from Heise, Newtown, CT. The maximum operating pressure in this set up is 2.5 kbar. The pump fluid used is Fluorinet FC 77. Figure 2.6 shows the dimensions of the pressure cell. The outer dimension of the cell is constrained by that of the inner bore of our superconducting magnet. The ratio of the inner to the outer diameter of the cell must be in an appropriate ratio so as to sustain the

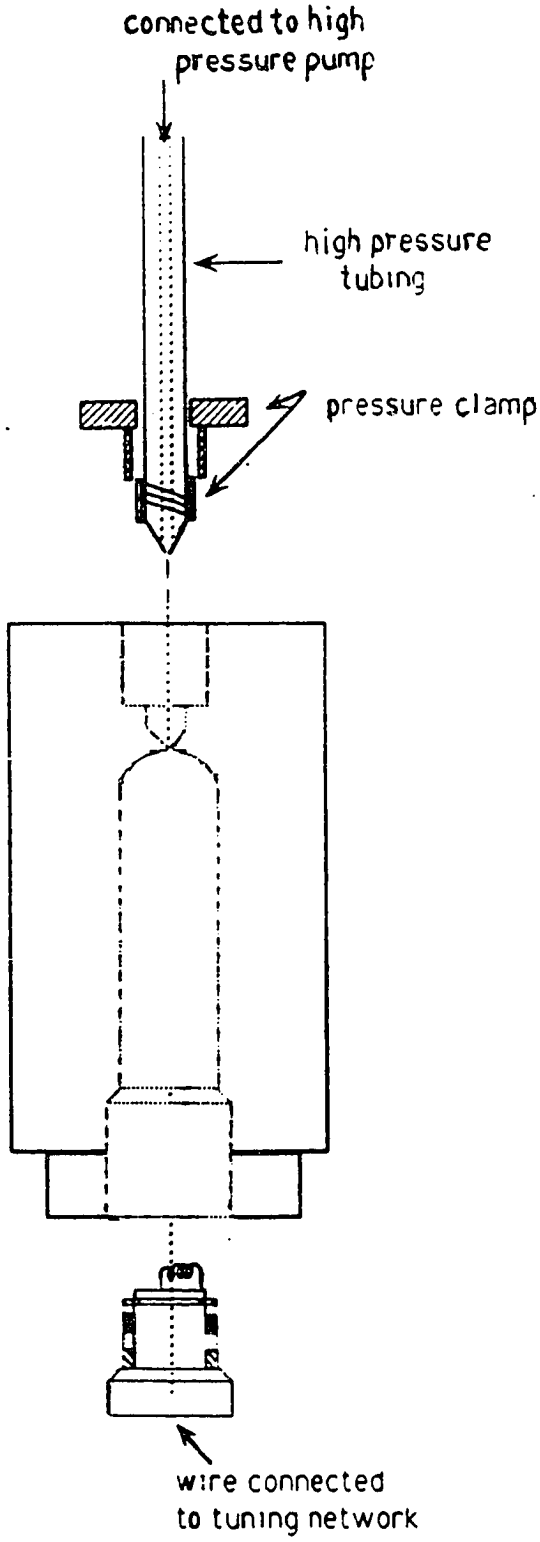

Figure 2.5 Set-up diagram for high pressure NMR experiment.

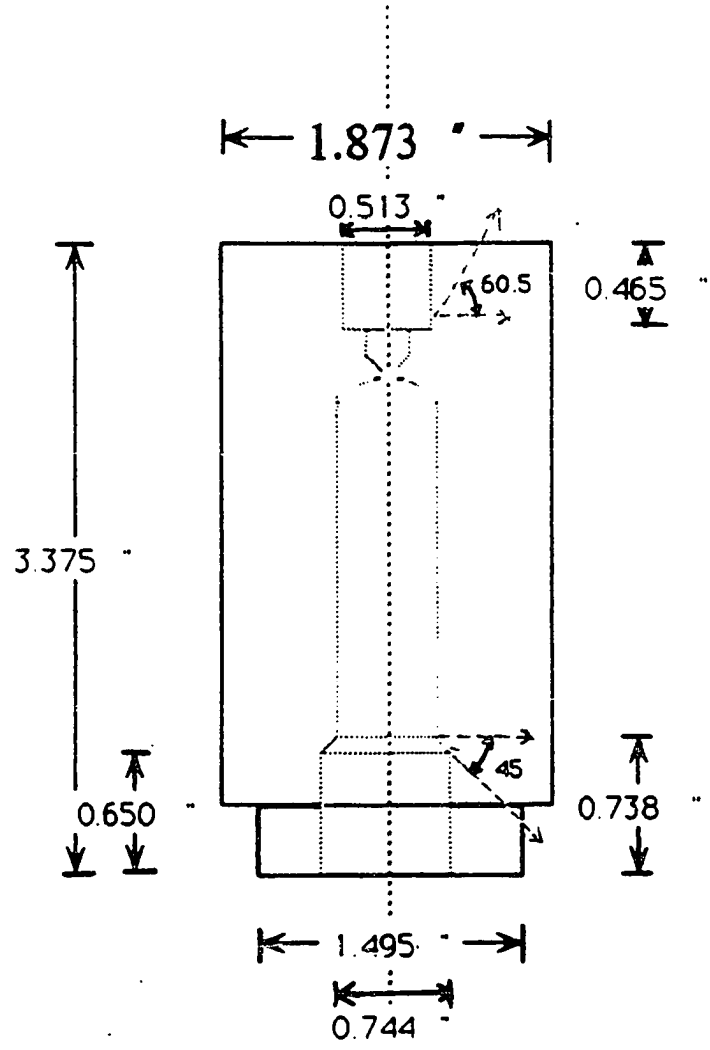

Figure 2.6 Dimension of the pressure cell, all measurements in inches.

pressure. The dimensions of the NMR assembly are shown in fig. 2.7. The linear scale in fig. 2.7 is four times the actual size of the assembly. The function of the assembly is to hold the solenoidal coil and the sample and to seal the pressure cell. The three washer rings are slightly press fitted to ensure good sealing. The inner part of the assembly, which constitutes the electrical feedthrough, is electrically insulated from the outer side with 50/50 aluminium oxide epoxy. The V shaped feature is designed so that the two separate parts are pressed tightly together whenever pressure is applied. The wire in the bottom of the assembly is connected to the matching network. The matching network is similar to the one shown in figure 2.3(b).

The sample was enclosed in a rubber finger cot in order to isolate it from the pressure transmitting fluid, and then loaded into the rf coil inside the pressure cell. To heat the sample, the entire cell was heated by a warm air stream and allowed to reach thermal equilibrium for about one hour prior to any measurement.

(2.3) ^{23}Na NMR Studies at different magnetic fields

Most of the work described in this thesis was done at a constant high field, 7.16 Tesla. However, NMR at different resonance frequencies will tell us more about the quadrupole interaction, for instance whether it is of first order or second order, of the ^{23}Na nuclei in the sample as well as the validity of using the BPP theory to describe dynamic processes in polymer electrolytes.

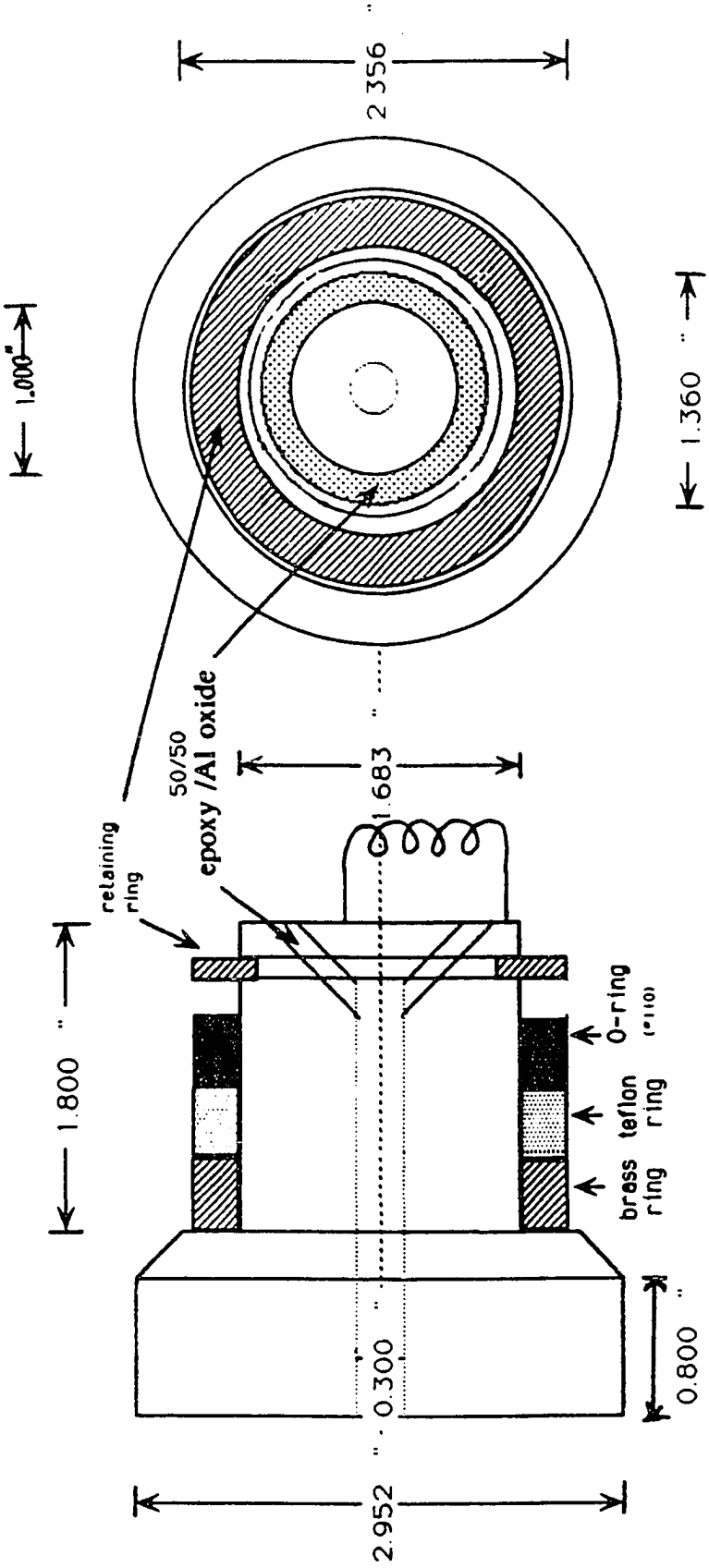

Figure 2.7 Dimension of the electrical feedthrough assembly. Linear scale is four times the actual size.

The NMR experiment at higher field (9.38 T) was done in the JEOL JNM-GX400 FT NMR spectrometer, Chemistry Department of Hunter College. The sample (about 1 c.c.) was packed into a 10 mm quartz tube. Inversion recovery pulse sequence was used to measure T_1. The experimental procedure is similar to the one described in the previous section. The low field work was done in the Novex^{TM} NMR spectrometer in conjunction with the Varian Fieldial^{TM} electromagnet system. The electromagnet and the power supply were cooled with water and a Hall-effect probe is used as the field regulation device. The electromagnet was turned on for at least five hours before any measurement was taken. A maximum magnetic field of 1.90 T corresponding to a current supply of 120 amp. could be obtained in this system. The work was done at 1.68 kgauss, or resonance frequency of 19.0 MHz for ^{23}Na. Throughout the experiment, the probe was tuned and fixed at about 19.0 MHz and the magnetic field was adjusted as the experimental condition required.

A variable temperature NMR probe was built for this project. The shielding box is made of brass with layers of epoxy inside for temperature insulation. A detailed drawing of the probe and the experimental setup is shown in fig. 2.8. The tuning capacitors could be placed outside the probe because the stray capacitance of the cable is not as crucial as in the high frequency probe, of course, the size of the capacitors and their values are much bigger than in the high field probe. The matching network is shown in fig. 2.9. In principle, the one shown in fig. 2.3, but with bigger capacitance, should work well. Judging from the ^{23}Na S/N in NaCl solution, the network in fig. 2.9 worked better, at least in our Novex system.

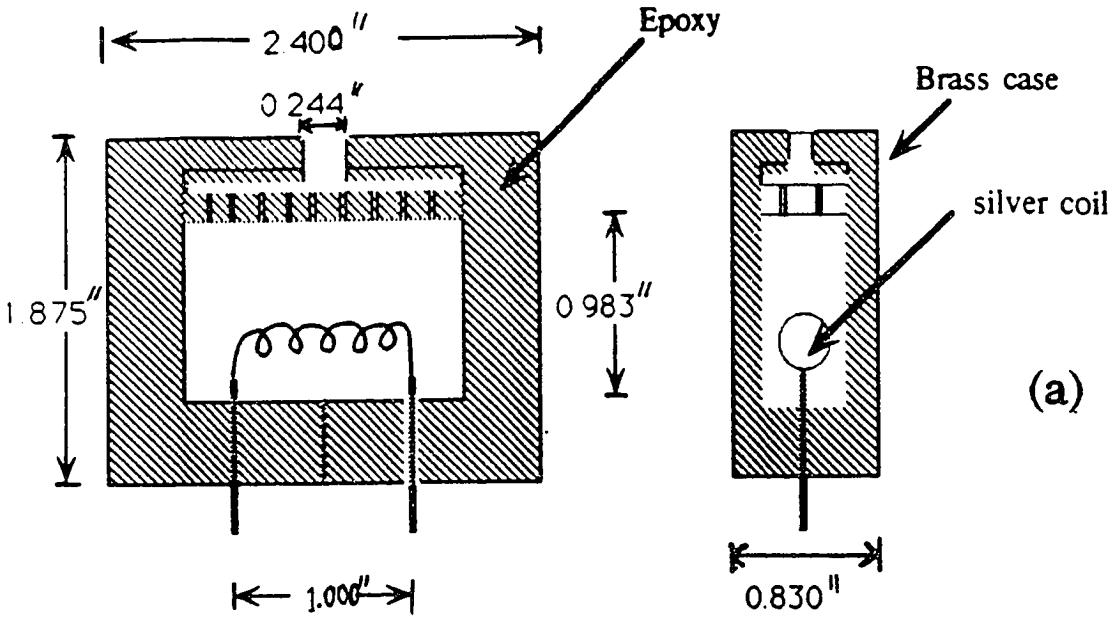

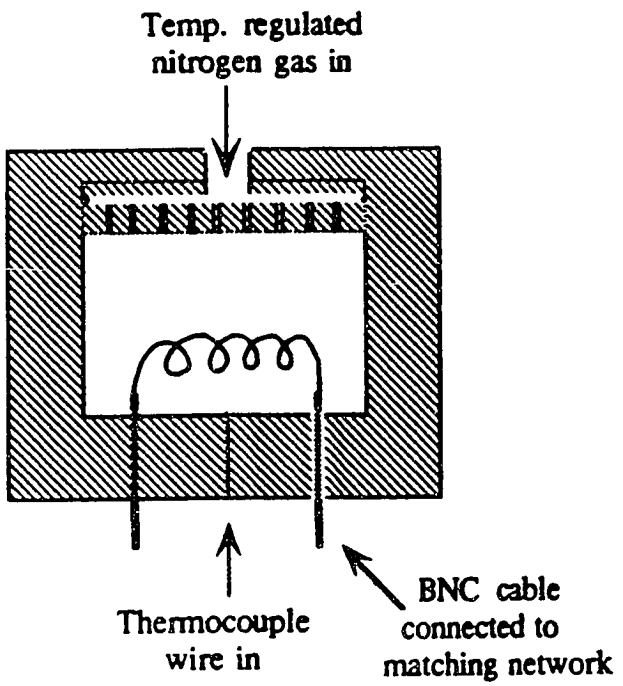

Figure 2.8 Low frequency NMR experiment:
(a) dimension of the probe,
(b) experimental set-up.

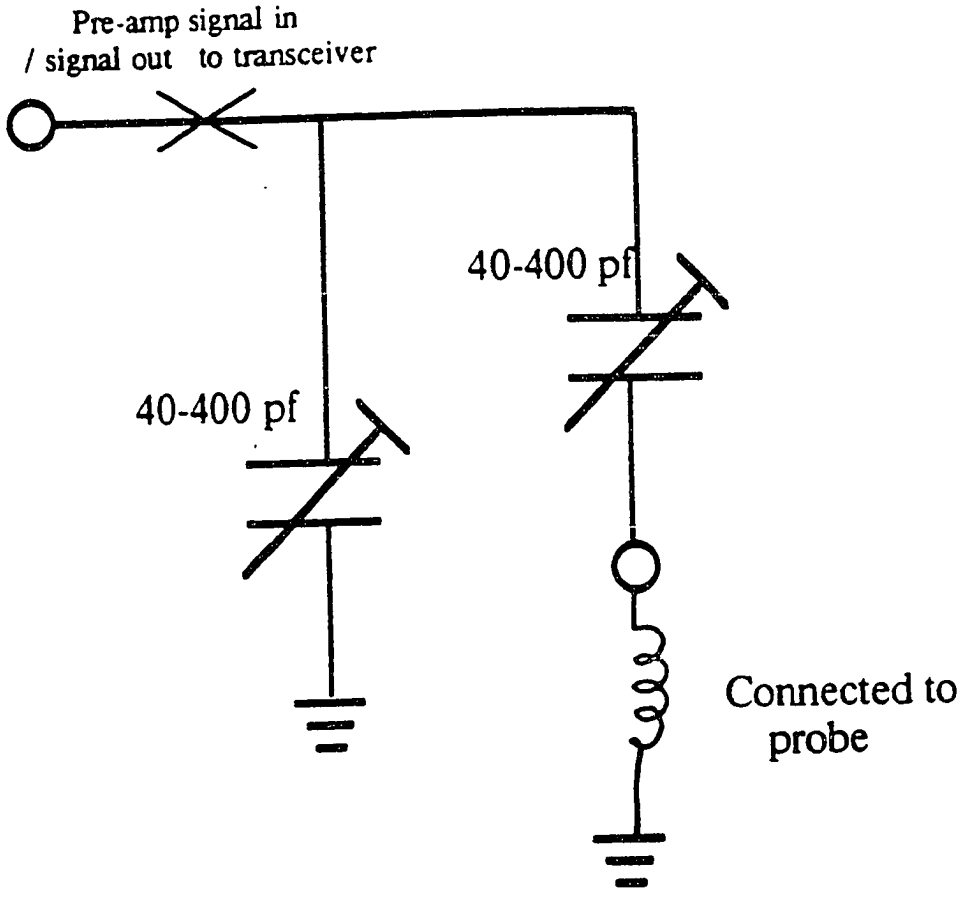

Figure 2.9 Matching network for low frequency NMR experiment.

The temperature control of the probe is through the nitrogen gas flow regulation unit, in the range of 173 K to 373 K.

The solenoidal coil, providing the rf field, is made of silver wire (99.9% purity). The inductance is about 0.8 μH with a high quality factor (Q factor) of 280. The choice of silver over copper for the low field work was made because the resonance frequency of ^{23}Na is very close to that of ^{63}Cu. For a magnetic field 1 T, the resonance frequency is 11.262 MHz and 11.285 MHz for ^{23}Na and ^{63}Cu respectively [14]. That is, their difference in resonance magnetic field is only 30 Gauss if the frequency is set to 19.0 MHz, leading to overlap of the ^{23}Na signal with that of copper nuclei in a "standard" coil; hence the coil is made of silver. The difference is of course larger in high field NMR, and thus a copper coil can be used in that situation.

Acoustic ringing in the pulsed NMR probe has been studied since 1974 [15, 16]. It is most commonly observed under high magnetic field, high pulse power, and low frequency. The problem is very severe in low frequency NMR experiment. An acoustic standing wave can be set up by an rf pulse in a conductor placed in the magnetic field. This acoustic wave is converted back into rf radiation and is then picked up by the receiver coil [15]. The noise amplitude is directly proportional to the H_1 field, the square of H_0 field and the pulse width. Fukushima et al. [16] considered the conversion efficiency factor E and stated that brass is about 2.4 times better than aluminum and stainless steel about 14 times better. Thus, the proper choice of probe material is one of the approaches for alleviating the problem. As

expected, the brass probe is much better than the aluminum one. Stainless steel was also tried and found to be similar to brass in suppressing the ringing. However, we found that a nominally non-magnetic stainless steel probe became magnetized inside a magnetic field, thus affecting the field homogeneity. This may be due to the presence of Ni in the stainless steel material.

In order to destroy the standing wave pattern in the probe wall, we drilled a lot of shallow holes on the inside surface of the wall. We found that it reduced the ringing time as well as the amplitude. Another solution to the problem is to dampen the acoustic wave. This can be accomplished by coating the probe surface with an acoustically lossy substance, such as silicone rubber compound RTV [15]. We didn't find much improvement from doing so. However, coating the solenoidal coil with silicone rubber helped a lot in alleviating the problem. In the end the best result we could get was to keep the acoustic noise within 50 μs after a pulse of 8μs.

Due to the broad resonance and the acoustic noise after pulses, the FID was averaged by either a solid echo sequence or the method of subtracting noise. The solid echo sequence is $(90)_x$-τ-$(90)_y$-rd, where the subscripts denote that there are 90° phase shifts between the two pulses. A half-echo similar to a FID was observed beginning at 2τ after the $(90)_x$ pulse. The τ value was in the range of 50-100 μs. In the method of subtracting noise, the difference between the FID near resonance and that 800 Gauss off resonance was measured. T_2^* was determined by an exponential curve fit.

(2.4) High Resolution ^{13}C NMR Experiments

This part of the work was done in the laboratory of Professor R. E. Stark, Chemistry Department of the College of Staten Island, CUNY, New York. Approximately 1 gram of polymer sample was powdered with a cryogenic grinder (Spex Industries). The sample was then packed into a 7 mm cylindrical Al_2O_3 rotor, inside a nitrogen glove bag. The ^{13}C NMR spectra were obtained on an IBM Instruments WP-200 spectrometer, with a Doty Scientific magic angle spinning probe. The experiments were run at the ^{13}C resonant frequency of 50.33 MHz. Cross Polarization Magic Angle Spinning (CPMAS) experiments were run at 291 K, with the sample spinning rate between 1.9 and 3.0 kHz. The heteronuclear decoupling was achieved with a high power ^{1}H decoupling field of 42 MHz. Delays of 1 second were inserted between acquisitions to have ^{1}H fully repolarized. According to experimental conditions, 1000 to 2000 scans were averaged for each measurement.

Chapter 3

EXPERIMENTAL RESULTS AND DISCUSSION

(3.1) Review of Polymer Electrolyte

Since the original description of solvent free polymer/salt complex electrolytes (herein called polymer electrolyte) by Wright et al [17], major advances in preparation, characterization, and understanding of the polymer system have been achieved during the past fifteen years [18, 19]. As it is not possible to present all details in a few pages, interested readers can refer to other literature, for example reference 20. Polymer electrolytes are complexes formed by dissolving alkali metal salts or alkaline earth metal salts in a particular kind of polymer. In general, ionic conductivities are in the range of 10^{-3} - 10^{-4} Scm^{-1} at 100 °C. The general principles governing polymer-salt complex formation are:[20]

(1) The polymer must have polar groups such as ether or ketonic oxygen, amine, sulphur etc.. These polar moieties coordinate to the cations of the salt.

(2) For a given cation, the salts having a low lattice energy are most likely to form polymer complexes, e.g., $CF_3SO_3^-$, I^-, ClO_4^-, and CF_3COO^-.

(3) Polymers with an optimal spacing of polar groups and high flexibility, have the greatest tendency to interact with salts.

The simplest way to make polymer electrolytes is usually carried out by dissolving both commercially available polymer and salt in a common solvent, such as methanol or acetonitrile, followed by evaporating the solvent completely.

However, methods for preparing other systems, such as crosslinked siloxane ethylene oxide copolymers or MEEP complexes, are considerably more complicated. In addition, a solvent-free method has been used with finely divided salt mixed in the molten polymer [20]. As salt-complexes are formed, there is a remarkable increase in the glass transition temperature (Tg). The polymer hosts studied mostly frequently are shown on table 3.1. Among these, poly(ethylene oxide) (PEO) and poly-(propylene oxide) (PPO) have received maximum attention. PEO is a linear polymer and the regularity of the units allows a high degree of crystallinity (about 80%). It has been shown that the segmental motion of the polymer chain and the interaction with the cation, through the ether oxygen, drives the ions through the complexes. Thus ion conduction is primarily through the amorphous region. This understanding led to the synthesis of amorphous polymers, such as network polyethers [21] and comb polymers [22], that form amorphous polymer-salt complexes. For the comb polymers, short polyether chains are attached to a highly flexible, low T_g, backbone (-P=N-, or -Si-O-) [23]. PPO has the same backbone structure as PEO. The ionic conductivity of PPO complexes is comparable to that of PEO in spite of its lower salt solvating power. As a matter of fact, PEO has the highest salt solvating power. As suggested by Armand [24], this is due to the optimal spacing of the heteroatoms in the chain unit.

In order to avoid charge polarization at the electrode/electrolyte interface, an ac technique is used to measure ionic conductivity. From the plot of the imaginary part vs the real part of the impedance, bulk resistance of the electrolyte and thus dc conductivity is deduced [25]. The temperature dependence of the

Name	Monomer Unit
Linear Polymer	
Poly(ethylene oxide)	$(CH_2CH_2O)_n$
Poly(propylene oxide)	$(CH_2\underset{\displaystyle CH_3}{\underset{\vert}{C}}HO)_n$
Poly(ethylenimine)	$(CH_2CH_2NH)_n$
Poly(ethylene succinate)	$(CH_2CH_2OCO_2CH_2CH_2CO_2)n$
Comblike and Branched Polymers	
Poly(bis(methoxyethoxyethoxy) phosphazene)	
$[NP(O(CH_2CH_2O)_xCH_3)_2]_n$ (x=1, 2, 7, 12 and 17)	
Poly(methoxypolyethylene oxide)methyl siloxane	
$[SiO(CH_3)(OCCH_2CH_2O)_2\ Me)]_n$	
Copolymer	
Poly(dimethyl siloxane-co-ethylene oxide)	
$(\text{-}\underset{\displaystyle CH_3}{\underset{\vert}{Si}}\text{-}O(CH_2CH_2O)_x\text{-})_n$	

Table 3.1 List of Polymer hosts studied most frequently.

conductivity of the electrolyte indicates a thermally activated process. The conductivity data can be fitted by the Vogel-Tamman-Fulcher, VTF equation.

$$\sigma(T) = AT^{-1/2}\exp\left(\frac{-E_a}{T-T_o}\right) \tag{3.1}$$

where σ, and E_a, are the conductivity and activation energy respectively. T_o is the fitting parameter and usually $T_o \approx T_g$- 50 K [26]. The conductivity data can also be fitted by the Williams-Landel-Ferry, WLF equation. It defines a shift factor, a_T, which is the ratio of any relaxation process (e.g. viscosity, conductivity, and diffusion etc.) at temperature T to its value at some reference temperature T_s. Through appropriate choice of T_s, a universal plot of $\log(a_T)$ verus $(T-T_s)$ can be obtained. The curve fits well in the region from T_g to about 100 K over T_g, with $T_s \approx T_g + 50K$. Rewriting the WLF equation in term of T_g instead of T_s, we obtain

$$\log a_T = \frac{-17.44(T-T_g)}{51.6+T-T_g} \tag{3.2}$$

Both WLF and VTF equations themselves are empirical generalizations, rather than the result of any theoretical approach. However, both equations are consistent with free volume theory [27]. Independent work by Angell's group [28] showed that the mechanical and electrical relaxation times are comparable to each other in polymer electrolytes. These interpretations, implying close relationship between the conductivity and the relaxation properties, indicate strongly that there is a relationship between the segmental motion of the polymer host and the ionic motion. Of course, there are results from others also supporting this point, such as the dielectric relaxation and "Arrhenius activation volume" work done by the Fontanella

group [26]. As our NMR results show, line narrowing also occurs at temperatures just above T_g. This idea will be discussed in more detail in a later part of this chapter. Previous NMR results on polymer electrolytes have been reported by Berthier and coworkers [29, 30]. Their work was based on the semicrystalline PEO complexes, such as $PEO_8LiCF_3SO_3$. By measurements of FID and spin echo, they were able to separate two components of proton (or Li) resonances in the crystalline and amorphous phases. The relative amount of crystalline and elastomeric phases at all temperatures, as well as the salt concentration in these various phases, was then determined. In addition, the pulse field gradient NMR method was also employed to determine the diffusion constant of the ion [31]. Our NMR results, e.g. low frequency ^{23}Na NMR studies, also show the presence of ion-ion interaction in the polymer complexes (to be discussed later).

On a more microscopic scale, Ratner et al. [32] have developed a dynamic percolation model to describe ionic motion as occurring in a dynamically disordered lattice. They introduced the idea that the available paths for ionic motion are constantly opening and closing at a certain renewal rate. The renewal process corresponds to the conformation changes in the polymer and thus leads to ionic transport. Another classical theory is the configurational entropy model [33], in which the parameter T_0 in the VTF equation is interpreted to be the temperature at which the probability of the configuration transitions tends to become zero.

One of the applications of polymer electrolytes concerns the solid state secondary battery. Up to date, most of the work is based on lithium polymer

electrolyte [34], although there has been some developmental work on sodium batteries [35]. The electrochemical cell consists of a Li^+ source and Li^+ sink separated by a Li-polymer electrolyte acting as ion carriers (typical thickness 100-200 μm). In practice, the lithium source can be a lithium foil, a low Li ion insertion structure (e.g. WO_2) or a lithium n-doped conjugated polymer (e.g. n-doped polyacetylene). The sink is any Li ion insertion structure (e.g. TiS_2, V_6O_{13} etc.), lithium reducible transition-metal compound such as FeS_2, Ni_2, or p-doped conjugated polymer. The main characteristics of the polymer battery are as follows: (1) It is possible to manufacture all solid state cells without the difficulties generally associated with the use of rigid or liquid electrolyte. The adhesion and elastomericity of the polymer electrolyte provide a better contact between the solid electrolyte and the electrode.

(2) A large surface area to thickness ratio is easily achieved with plastic material. This compensates for the limited ion mobility. This also leads to another advantage which is the acceptability of using low current density, because electrochemical processes become more reversible and energy efficient at low discharge rates.

(3) the electrolyte can be made very thin to improve the energy density. It is also a suitable mechanical interelectrode separator.

Finally, we summarize the technology of polymer battery by table 3.2, which shows the differences between the lithium polymer battery and two existing aqueous systems [35].

Lead-acid battery: $Pb/H_2SO_4 \cdot H_2O/PbO_2$

- Electrolyte participation in electrode reactions.
- Overall reaction:

$$Pb + PbO_2 + 2H_2SO_4 \rightleftharpoons 2PbSO_4 + 2H_2O$$

- Energy density (Wh/kg): 250 (theoretical), ~25-35 (practical, ~1/8).
- Secondary reaction: $H_2O \rightarrow H_2 + \frac{1}{2}H_2O$
- % Efficiency (Ah and Wh): 85 and 70-75%.
- Cycling characteristic (full discharges): short cycle life (300 cycles).
- Operating temperature range: -20 to 40 °C.

Nickel-cadmium battery: $Cd/KOH\text{-}H_2O/NiOOH$

- Water participation in electrode reactions.
- Overall reaction:

$$Cd + 2NiOOH + 2H_2O \rightleftharpoons 2Ni(OH)_2 + Cd(OH)_2$$

- Energy density (Wh/kg): 245 (theoretical), ~35 (practical, ~1/7).
- Secondary reaction: $H_2O \rightarrow H_2 + \frac{1}{2}O_2$.
- % Efficiency (Ah and Wh): 70 and 60-65%.
- Cycling characteristic: good cycle life (500-1000 cycles), memory effect.
- Operating temperature range: -40 to 50 °C.

Lithium polymer battery: Li/Li polymer electrolyte/TiS_2

- The electrolyte is simply a Li^+ ion carrier.
- Overall reaction:

$$TiS_2 + xLi \rightleftharpoons Li_xTiS_2$$

- Energy density (Wh/kg): 480 (theoretical), ~120(practical, ~1/4).
- No secondary reaction.
- % Efficiency (Ah and Wh): ~100 and 85-95%.
- Cycling characteristic: full discharge capability (600 cycles).
- Operating temperature range: -10 to 130 °C.

Table 3.2 Main differences between the Li polymer battery and existing aqueous systems.

As shown in table 3.2 , the lithium battery has certain advantages over the others. However, its success as a small scale electrochemical cell will remain a laboratory curiosity unless the corresponding processes and materials for large scale production exist or become price-competitive. Thin lithium foil (<100 μm) is difficult to manipulate and still expensive to produce. In addition, the reliability of a thin film multilayer cell developed over a large surface area is a critical issue for polymer electrolyte batteries. Therefore, there is a lot of technical challenge to be overcome before a large scale polymer battery is marketable.

(3.2) Experimental Results and Discussion

A variety of samples have been investigated in this work. The list is shown in table 3.3. Hereafter, the names of the samples will be referred to their molecular formulae. All polymer electrolytes studied are of high molecular weight, with mol. wt.> 10^5, so their physical state is solid-like (MEEP appearing in a form of viscous liquid as an exception). As a reference, table 3.4 lists the T_g values of the complexes as determined by differential scanning calorimetry (DSC). The presentation of the results will be divided into several sections with respect to the different host polymers investigated.

(A) Siloxane Copolymers

Siloxane copolymers complexed with alkali salts have received much attention as solid electrolytes because of their very low glass transition temperatures due to the flexibility of the siloxane backbone [36, 37]. It is well known that this feature

Siloxane Copolymer

(1) Dimethylsiloxane ethylene oxide copolymer (PDMS-EO)
(i) complexed with $NaCF_3COO$, EO/Na = 8:1
(ii) complexed with $NaCF_3SO_3$, EO/Na = 8:1

(2) Monophenylsiloxane ethylene oxide copolymer (PMPS-EO) complexed with $NaCF_3SO_3$, EO/Na = 8:1 and 12:1

Comb Branched Poly(ethylene oxide) Copolymer

(3) Poly(bis-methoxyethoxyethoxide) phosphazene (MEEP) complexed with $NaCF_3SO_3$: $MEEP_4NaCF_3SO_3$

Poly(propylene oxide) complexes $(PPO)_nNaX$

(4) $(PPO)_8NaI$; $(PPO)_{12}NaI$; $(PPO)_{16}NaI$

(5) $(PPO)_8NaClO_4$

(6) $(PPO)_8NaSCN$

(7) $(PPO)_8NaCF_3SO_3$

(8) $(PPO)_8(NaCF_3SO_3)_{½}(NaI)_{½}$

(9) $(PPO)_8NaB\phi_4$, where ϕ = phenyl group

Amorphous Poly(ethylene oxide) complexes $(PEO)_nNaX$

(10) $(PEO)_9NaCF_3SO_3$

(11) $(PEO)_9NaI$

Exclusive Cation Conducting Complexes

(12) Complex based on a Nylon-1 backbone, ethylene-oxide sides chains, and attached dibutyl phenolate anion (detail structure in fig. 3.23).

Table 3.3 List of Polymer complexes studied in this work

Complexes	Central glass transition temperature (K)
(PDMS-EO)-$NaCF_3COO$ (EO/Na=8:1)	216
(PMPS-EO)-$NaCF_3SO_3$ (EO/Na=12:1)	225
PPO_8NaClO_4	about 273
PPO_8NaI	about 273
PPO_8NaSCN	about 273
$PPO_8NaCF_3SO_3$	about 273
$PPO_8(NaCF_3SO_3)_{½}(NaI)_{½}$	about 273
$PPO_8NaB(C_6H_5)_4$	about 273
<u>amorphous PEO</u> $PEO_9NaCF_3SO_3$	251
PEO_9NaI	259
$MEEP_4NaCF_3SO_3$	219
cation-conducting complex	254

Table 3.4 List of T_g of the complexes (as determined by DSC)

enhances ionic conductivity. There are two different siloxane copolymers studied, poly(dimethylsiloxane-ethylene oxide) PDMS-EO and poly(monophenylsiloxane-ethylene oxide) PMPS-EO. PDMS-EO complexes were prepared in this laboratory [38]. The sample preparation consisted of three steps: polymerization (chain extension) ; complexing with sodium salt; and crosslinking. The prepolymers were ethylene-dimethyl-siloxane oxide ABA block copolymer (Petrarch; m.w.1120). Triacetoxy and triethoxy silane were used as crosslinking agents. Detailed description could be found in reference [38]. PMPS-EO complexes were prepared by the research group of Professor Y. Okamoto [39].

Results and Discussion

In (PDMS-EO) siloxane based complex, the ^{23}Na absorption lineshape consists of a relatively narrow (0.5-5 KHz) line superimposed on a broad line (20-30 kHz) (both FWHM), throughout the temperature range -100 to +100 °C. Figure 3.1 shows the absorption spectra for the sample PDMS-EO complexed with sodium trifluor-acetate ($NaCF_3COO$), with the dotted line indicating the narrow component. The "90°" pulse width of the ^{23}Na signal was measured to be one half of that of NaCl powder. The absorption line of the sample is thus associated with the $+\frac{1}{2}$ to $-\frac{1}{2}$ central transition [40]. T'_1s of the two components are different by 2 to 3 orders of magnitude. The temperature dependence of both T'_1s is plotted in fig. 3.2. T_1 of the narrow line has a more pronounced temperature dependence than that of the broad line, in addition to its substantially shorter time scale. Between the glass transition temperature (-50 °C) and room temperature, the relaxation of the narrow line is

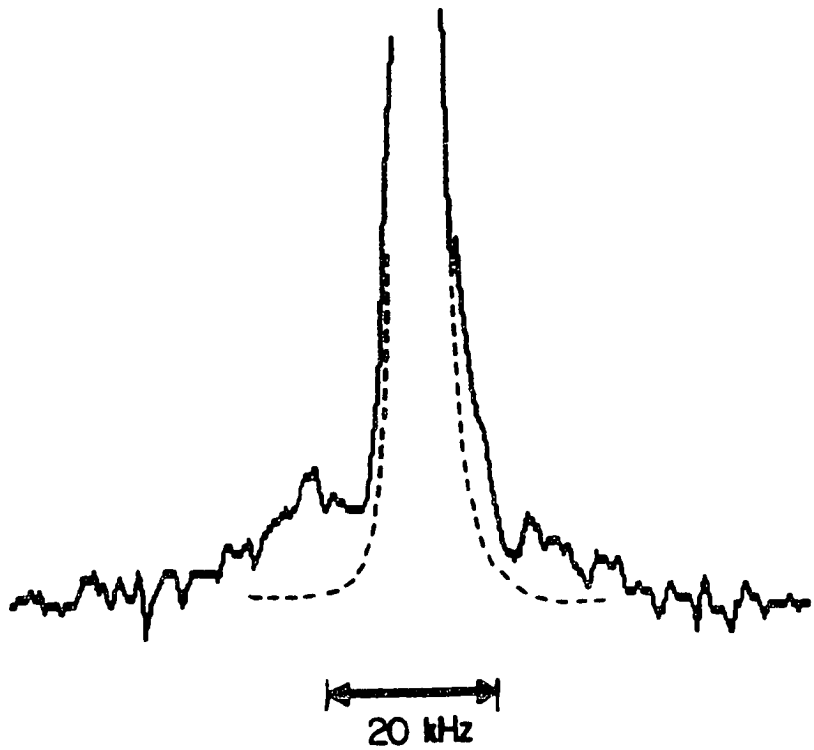

Figure 3.1 ^{23}Na NMR absorption spectra for PDMS-EO complexed with $NaCF_3SO_3$. The broken curve is spectrum obtained with a short sequence delay, in which the broad component is completely saturated.

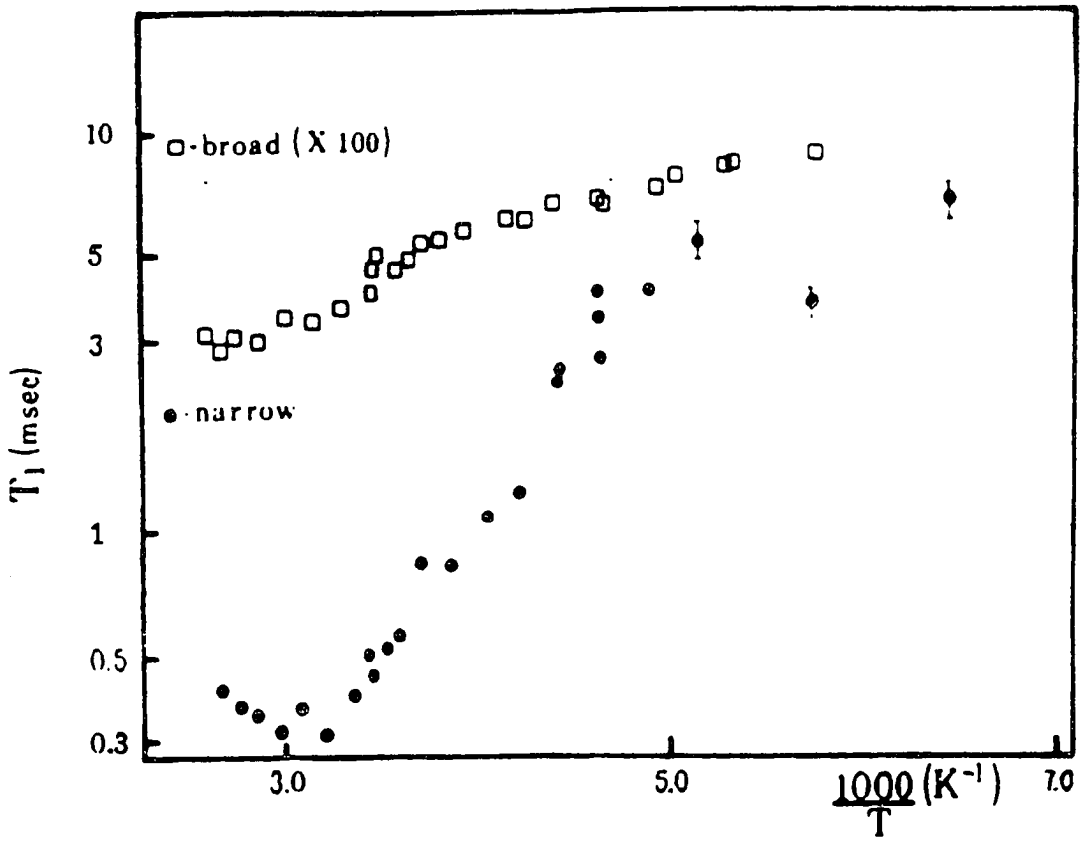

Figure 3.2 ^{23}Na T_1 vs reciprocal temperature for broad and narrow line-shape components.

approximately Arrhenius with an activation energy of roughly 0.1 eV. A T_1 minimum appears just above room temperature at which the ionic motion is probed to be in the timescale of 10^{-9} s.

The strength of the quadrupole interaction was estimated to be on the order of one to several MHz from the second order splitting. This suggests that the ^{23}Na nuclei reside at asymmetric sites for a time scale of at least 10^{-6} s. The broad line is possibly associated with the ions bonded strongly to the host polymer; or isolated cation-anion pairs [41, 42] ;or small clusters of ions. This assignment will be justified later, following discussion of the results for other samples. The narrow line is assigned as the mobile ion in the electrolyte. As determined from NMR experiments with different resonance fields (to be presented in a later section), the mobile ion resonance is also second order quadrupole broadened.

One of the parameters which affect ionic conductivity is the number of ions transported in the electrolyte. Hence, it is of interest to determine the temperature dependence of the mobile ion concentration, e.g., the conversion of bound ions to mobile ions as temperature increases. This can be represented as an ion-pair (or aggregate) dissociation process. As the T_1's of the two components differ by 2-3 orders of magnitude, it is possible to collect individual components by selective saturation and substraction. By integration of the FID of individual components, quantitative determination of the relative mobile/bound concentration (denoted as M/B) has been made. Figure 3.3 depicts the temperature dependence of M/B. The ratio increases by only a factor of ten from -100 °C to 100 °C, while the conductivity

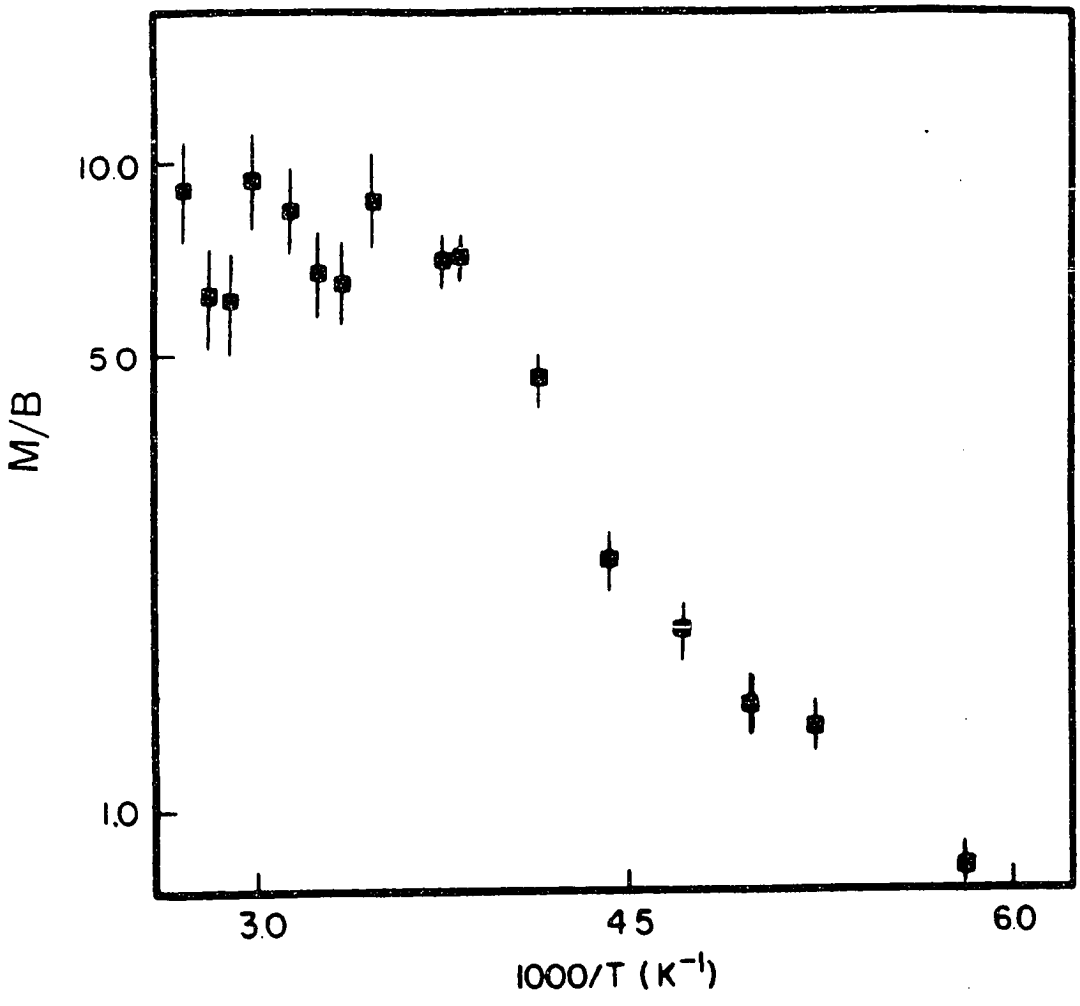

Figure 3.3 Reciprocal temperature plot of mobile (M)/ bound (B) line intensity ratios for PDMS-EO complexed with $NaCF_3COO$.

exhibits roughly a five-order of magnitude increase over the same range [43]. Thus, 'carrier generation' only plays a minor role in the transport process.

Figure 3.4 plots M/B for similar siloxane complexes but with two different anions, $CF_3SO_3^-$ and CF_3COO^-. At all temperature studied, the triflate compound has a greater mobile Na^+ concentration than the trifluoracetate sample. This result seems to be consistent with the relatively high dissociation energy of $NaCF_3COO$ as compared to the triflate salt.

Another siloxane based electrolyte has been studied, PMPS-EO complexes. These complexes have phenyl groups attached to the siloxane chain, with two different salt concentrations (EO/Na = 8:1 and 12:1). ^{23}Na FID of both lineshape components for 8:1 (at 273 K) are shown in fig. 3.5. The top FID corresponds to the mobile Na^+ ions and is motionally narrowed (in the frequency domain) with respect to the bound Na response (bottom). The plot of relative ratios vs temperature is shown in fig. 3.6. As expected, the 12:1 complexes (higher EO/Na ratio) shows higher degree of dissociation, more than 99% of the Na are mobile above 300 K.

The NMR linewidth is proportional to the reciprocal of the FID time constant $(T_2^*)^{-1}$, which is plotted as a function of temperature in fig. 3.7. $(T_2^*)^{-1}$ motionally narrows above T_g (233 K for 8:1 and 225 K for 12:1) and reaches a minimum at about 45-55 K above T_g and then broadens somewhat. The motional narrowing phenomenon [44] is due to large scale segmental motion of the polymer chain. The local field experienced by the nuclear spins is averaged out, resulting in a decrease in linewidth. The high temperature broadening is consistent with the extremely

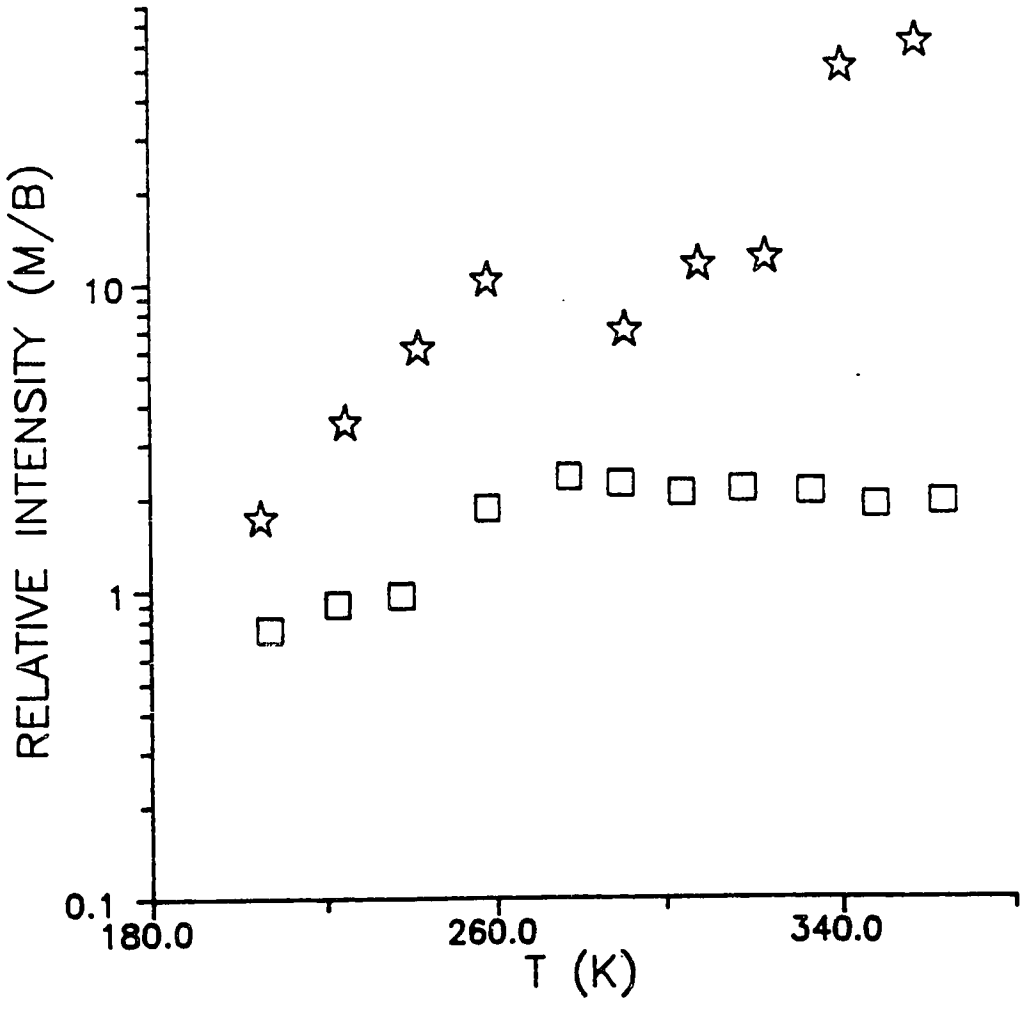

Figure 3.4 M/B vs temperature for PDMS-EO complexed with $NaCF_3SO_3$ (top) and $NaCF_3COO$ (bottom); ether oxygen/Na ratio is approximately 8.

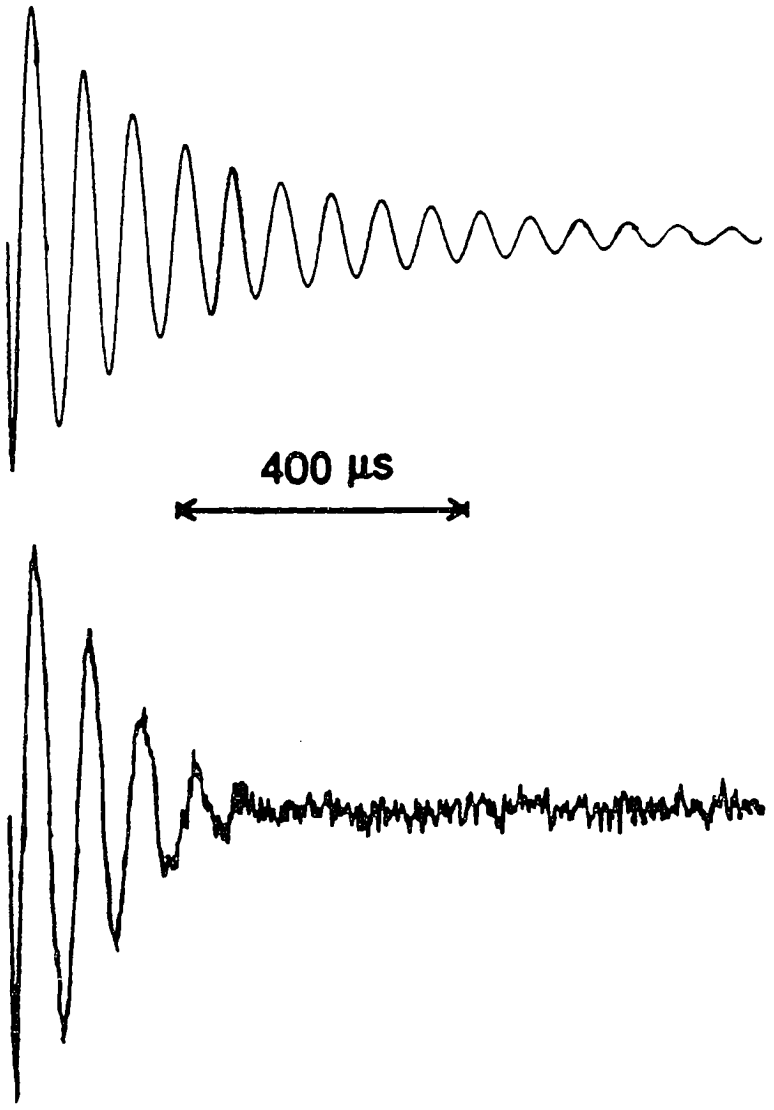

Figure 3.5 Free induction decays for the mobile (top) and bound (bottom) Na^+ in the 8:1 PMPS-EO complex at 273 K. The vertical gain in the bottom figure is a factor of ten higher than in the top.

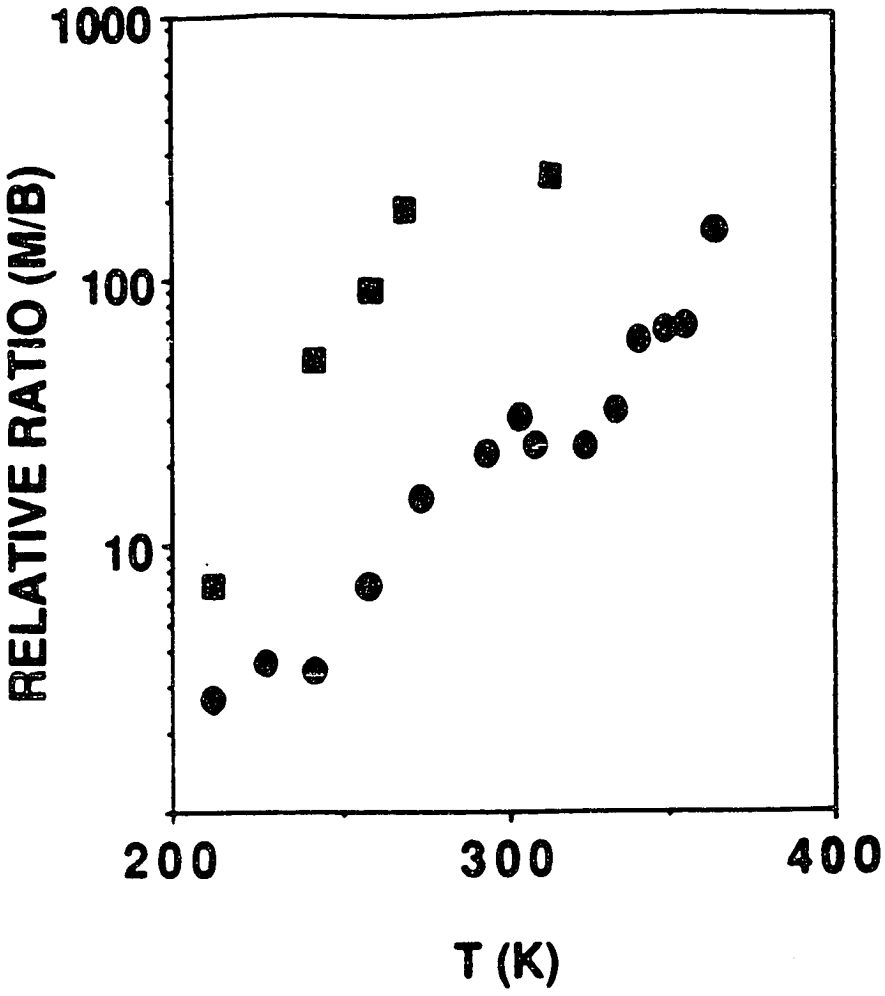

Figure 3.6 Mobile to bound (M/B) Na^+ ratios of both 12:1 (top) and 8:1 (bottom) PMPS-EO complexes as a function of temperature.

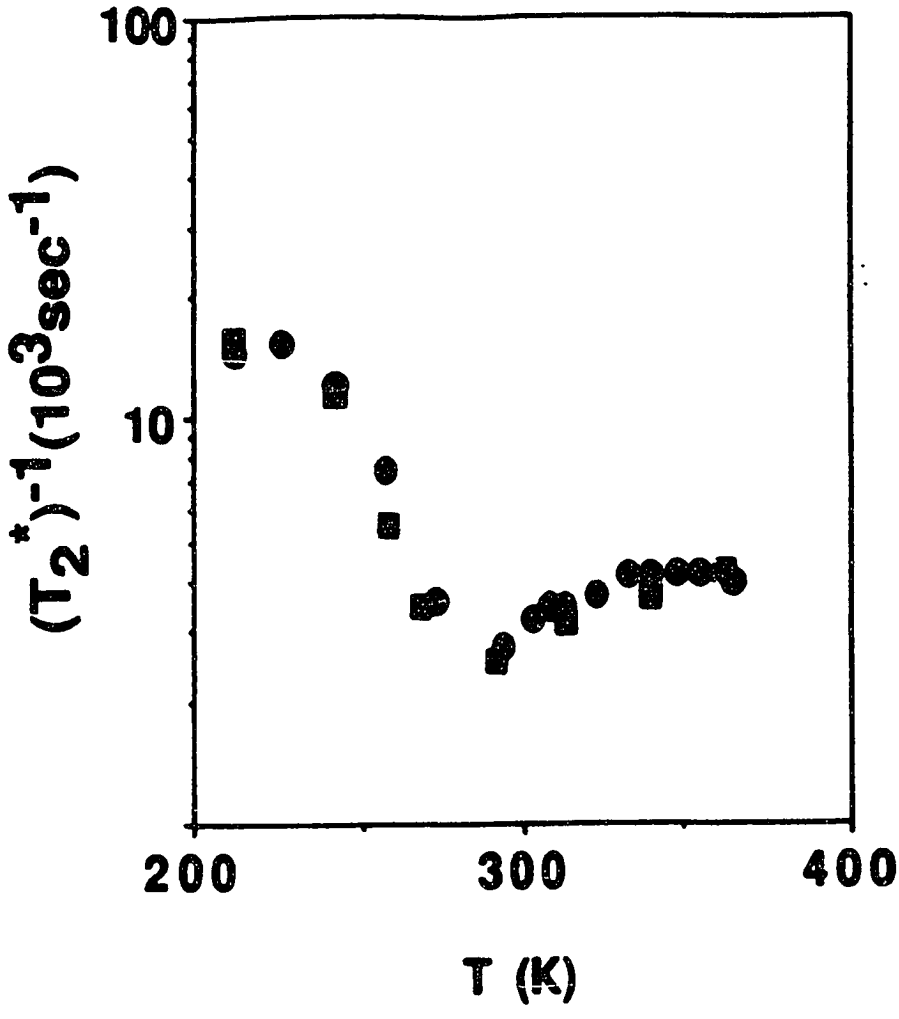

Figure 3.7 Temperature dependence of ^{23}Na linewidth $(T_2^*)^{-1}$ of mobile Na^+ in 8:1 and 12:1 PMPS-EO complexes.

short(~ 300 μs) T_1 values measured in this region. This broadening of the line is due to the finite life of a spin in any eigenstate as a result of the spin lattice relaxation. By the Heisenberg Uncertainty Principle, the order of the lifetime broadening can be estimated to be $1/T_1$. This is the major contribution to the linewidth as T_1 becomes very short.

(B) Poly(bis-methoxyethoxyethoxide) phosphazene (MEEP)

MEEP attracts attention as a candidate for solid electrolyte applications because of its rather high conductivity at room temperature [45, 46]. The sample was prepared by T. Nishikawa of Shin Nisso Kako, Tokyo, Japan. As observed for other samples, there are two Na species with T_1 being two or three orders of magnitude different from each other. Only small quantities (less than ~5%) of the nuclei giving rise to the total signal could be identified with the bound Na at any given temperature range (133-371 K). Figure 3.8 is an Arrhenius plot of T_1, for the mobile Na resonance signal. The T_1 minimum occur at 318 K and is roughly linear in the region between 213 and 306 K. A similar result was observed in the PDMS/EO-$NaCF_3COO$ complex. However, an activation energy of approximately 0.27 eV is inferred from the linear region of the plot for the MEEP complex. Figure 3.9, temperature dependence of $(T_2^*)^{-1}$, shows similar features as that of the siloxane sample, such as motional narrowing above T_g. This strongly supports the view that segmental motion of the polymer chain is a crucial factor in the ion transport process.

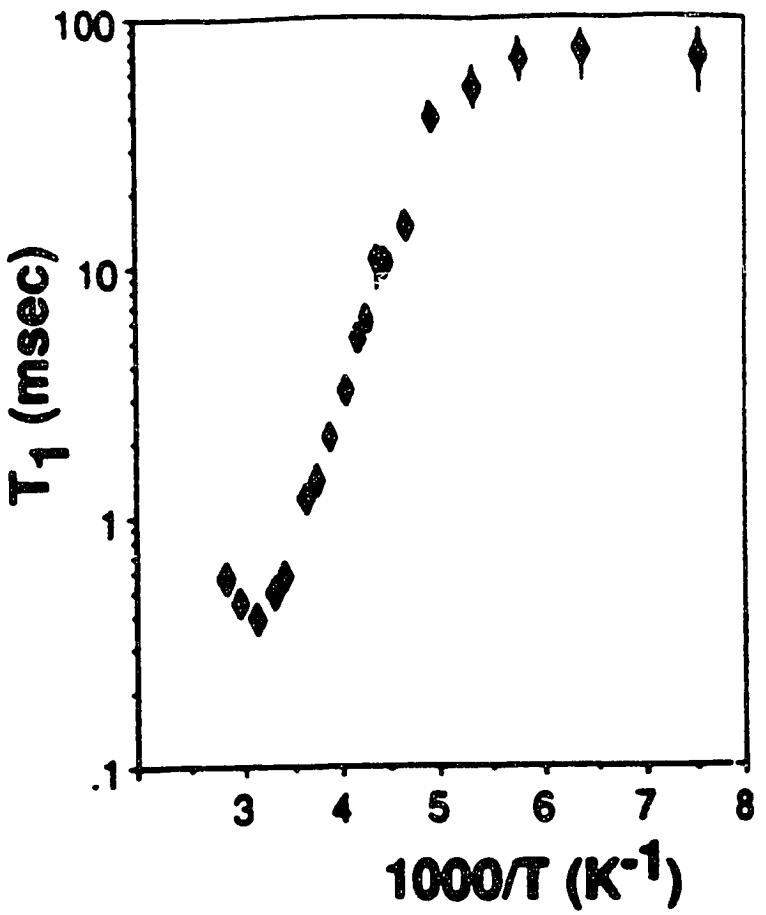

Figure 3.8 Arrhenius plot of the ^{23}Na spin-lattice relaxation time in $MEEP_4NaCF_3SO_3$. The T_1 minimum occurs at about 318 K.

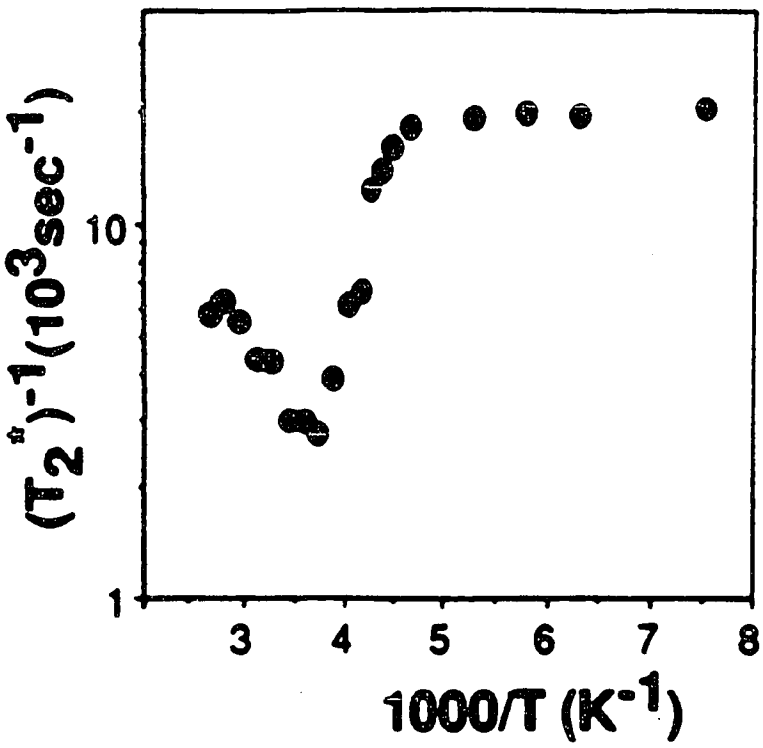

Figure 3.9 Arrhenius plot of the inverse ^{23}Na free induction decay, $(T_2^*)^{-1}$, in $MEEP_4NaCF_3SO_3$.

(C) Poly(propylene oxide) Complexes

In order to understand the ion-polymer and ion-ion interaction in the polymer electrolytes more thoroughly, several series of complexes based on PPO have been investigated. The ion-ion interaction in a salt solution depends on (a) the "polarity" of the solvent, (b) the concentration of the ions in the solvent. The macroscopic dielectric constant or relative permittivity gives a measure of the solvating ability of a solvent. The onset of significant ion-pair formation, where the energy of mutual electrostatic attraction of oppositely charged ions exceeds that of thermal motion, occurs at lower ion concentrations in solvents which have a small value of relative permittivity. In the polymer complexes in our studies, the salt concentration is very high and thus ion-pair formation is likely to occur.

PPO was chosen because of its relatively simple structure and its completely amorphous character. The first set of measurements was based on PPO-NaI complexes with different salt concentrations (O/Na denoted by n = 8:1, 12:1, 16:1 respectively), which gave us some insight into the phase separation and the salt precipitation in the complexes. The second project involved PPO complexed with different anions but of the same salt concentration. In addition, ^{13}C NMR experiments were done to study the nature of the polymer chain motion.

The PPO used in the samples was Parel 58 (Hercules, Incorporated) elastomer which is a sulfur-vulcanizable copolymer of propylene oxide and allyl glycidyl ether, containing approximately 95 % polypropylene oxide. Samples were obtained by solution casting with methanol as solvent. All preparations were done in a dry N_2

glove bag. The final drying was done in a vacuum with the initial anneal at 80 °C for 24 hours and the final anneal at 60 °C for at least 24 hours.

As in other systems, there are two ^{23}Na absorption lines superimposed on each other. The narrow component has a smaller T_1 (about 2 ms at 56 ° C) while the broad component has an almost temperature independent T_1 of about 10 s. The mobile ^{23}Na reciprocal FID time constants, $(T_2^*)^{-1}$, for all three PPO_nNaI complexes (n=8:1, 12:1 and 16:1) are plotted as a function of temperature in fig. 3.10. The universal features of the $(T_2^*)^{-1}$ plot, such as the motional narrowing above T_g, were also observed. However, all samples exhibit approximately the same linewidth at a given temperature which indicates that the nature of the mobile phase of the sodium ion in the complexes is independent of salt concentration. This interpretation is also supported by DSC results obtained in the collaborative work by Professor Fontanella et al. at the Naval Academy [47]. Figure 3.11(a) shows the low temperature DSC thermogram for the PPO samples. Two glass transitions are observed in all samples containing NaI. The lower transition occurred in the vicinity of that of uncomplexed PPO ($T_g \approx 213$ K) and the other one was in the vicinity of 270 K. The higher temperature glass transitions, corresponding to that of the salt complexes, became more pronounced as the salt concentration increased. Correspondingly, the lower glass transition exhibited decreasing strength as salt concentration increased. Consequently, there is a tendency for the ions to form an amorphous complex with a well defined stoichiometry, corresponding to that of n = 8:1. This preference for a particular stoichiometry is in contradiction to what is usually observed in polymer electrolytes which, in most cases, can assume any concentration with increasing T_g

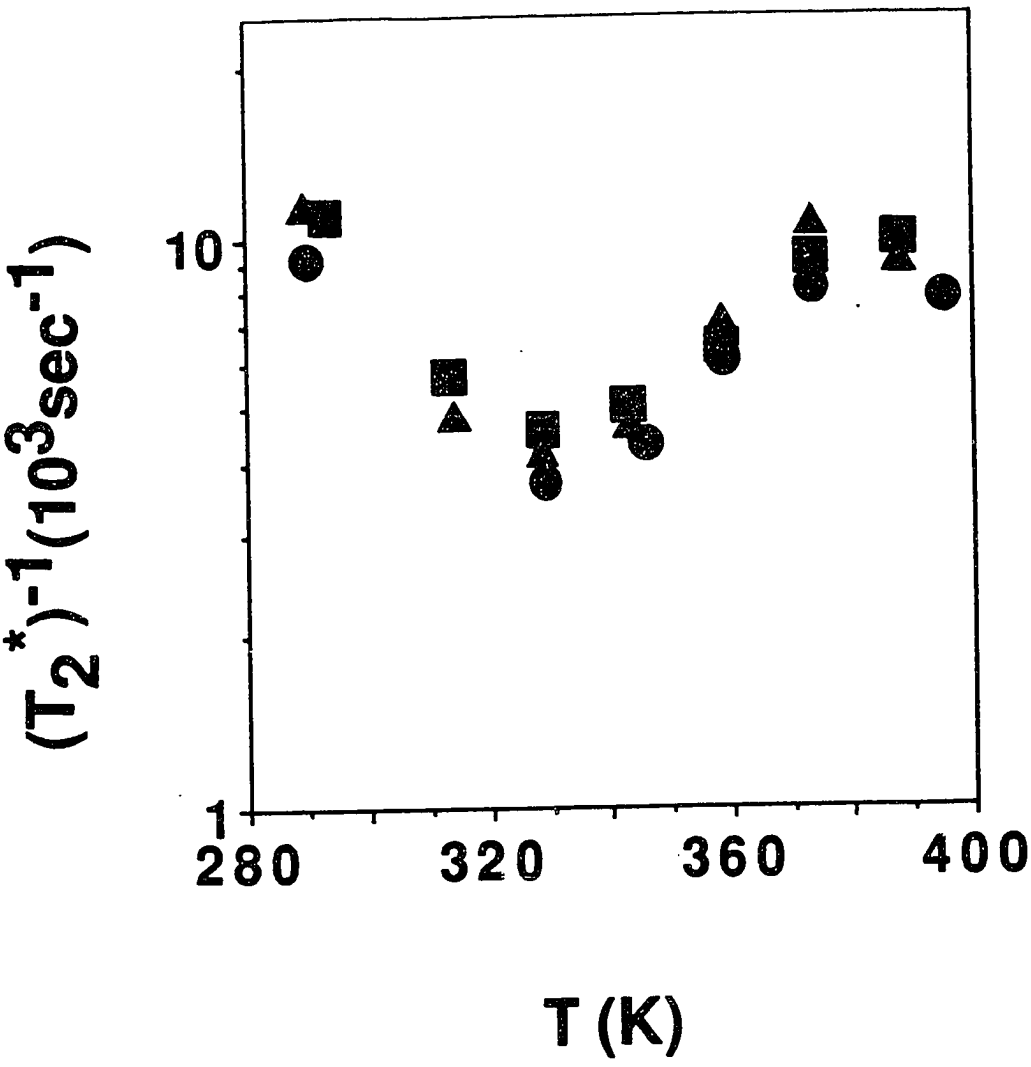

Figure 3.10 ^{23}Na reciprocal time constants $(T_2^*)^{-1}$ of the mobile Na in PPO_nNaI; n=8: circle, n=12: triangles, n=16: squares.

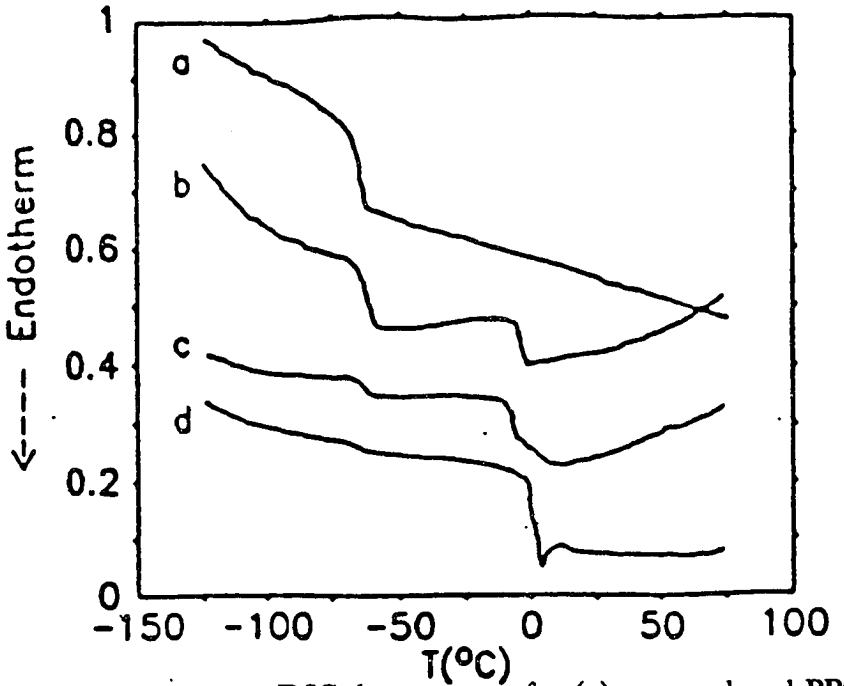

Figure 3.11a Low temperature DSC thermograms for (a) uncomplexed PPO, (b) $PPO_{16}NaI$, (c) $PPO_{12}NaI$, and (d) PPO_8NaI. The data were taken at 10 K/min.

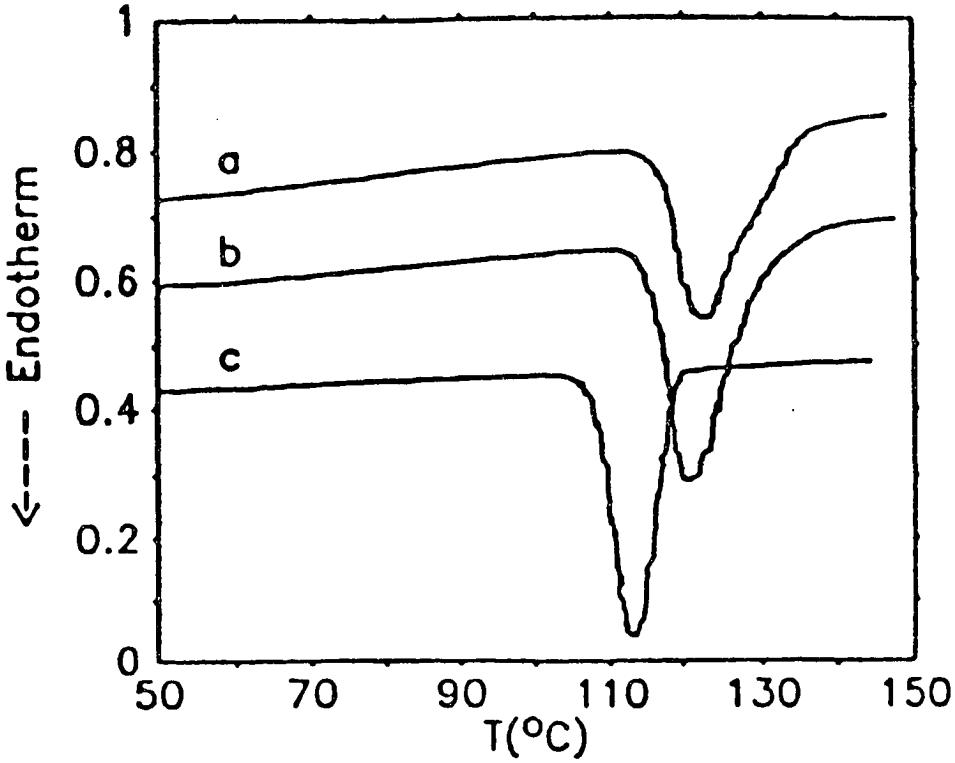

Figure 3.11b High temperature DSC thermograms for: (a) $PPO_{16}NaI$, (b) $PPO_{12}NaI$, and (c) PPO_8NaI. The data were taken at 10 K/min.

as salt concentration increases [21, 48].

The temperature dependence of the ratio of mobile to bound Na is plotted in fig. 3.12. The low temperature regions indicate that n = 8:1 has the highest M/B. This observation, in conjunction with the DSC results cited above, indicates that the 8:1 composition is the most homogeneous material. In fact, the complexes of lower salt concentration are cloudier in appearance than the 8:1 material. This suggests that the bound sodium ions in these material may exist as uncomplexed salt crystallites in the phase boundaries. The bound Na were found to be spectroscopically similar to pure NaI (both in linewidth and T_1). The 8:1 material having a large M/B is attributable to the lack of phase boundaries. As the temperature is increased, the more dilute complexes exhibit a relatively rapid increase in the mobile concentration which is attributable to the greater degree of ion solvation. Finally, it is apparent from fig. 3.13 [47] that the 8:1 sample exhibits the most rapid increase in electrical conductivity with increasing temperature while the number of mobile ions is relatively unaffected. Consequently, the NMR and the conductivity data imply that the concentrated phase is the conducting phase. This is different from the results for PEO in which dilute amorphous regions are assumed to be more highly conducting than concentrated phases.

Another issue to be addressed is the salt precipitation phenomenon at higher temperature in this kind of material. Salt precipitation (SP) effects in PPO complexes have been previously reported by other groups [41, 49]. In this work, we are going to address this problem in terms of the dielectric constant of the host

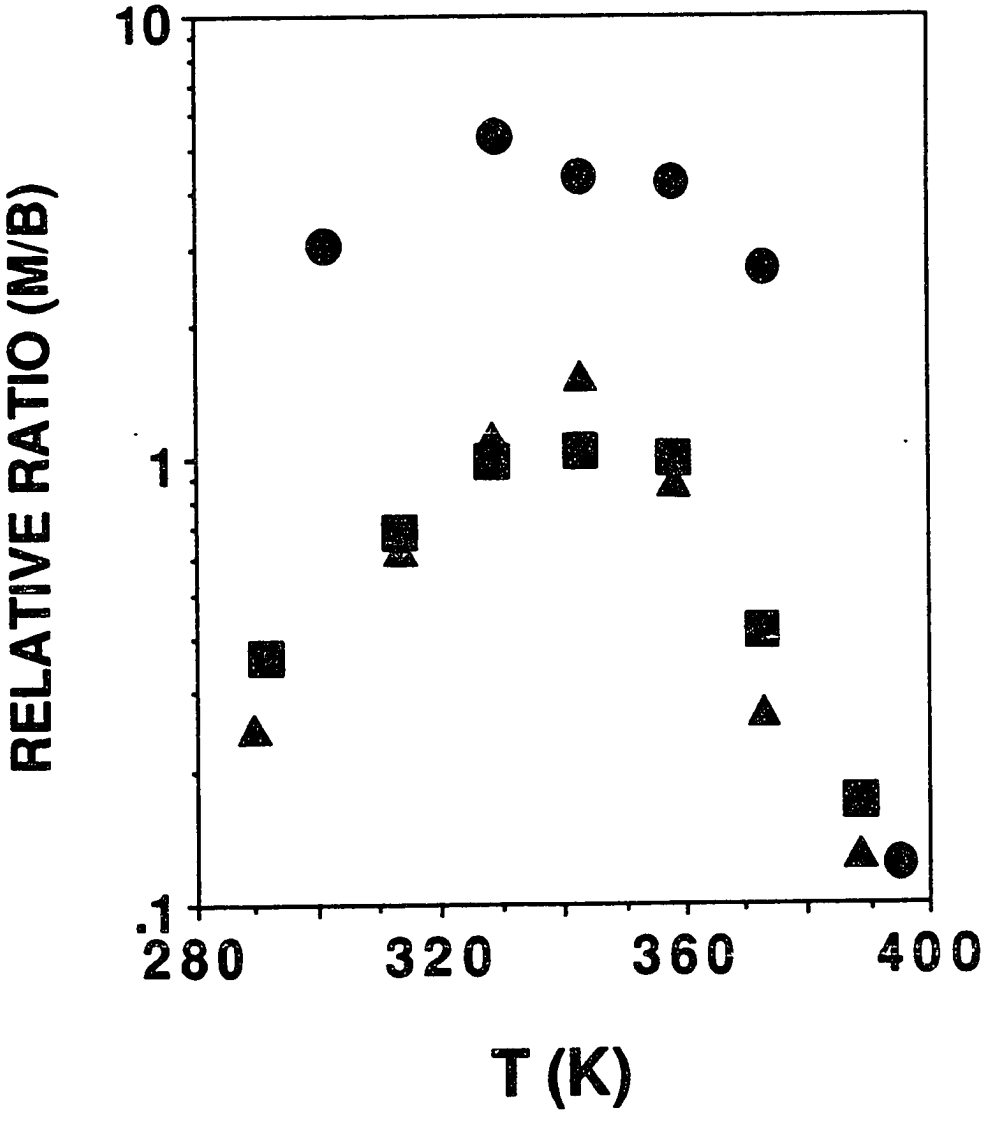

Figure 3.12 Mobile to bound Na ratios as a function of temperature, determined from FID intensities; n=8: circles, n=12: triangles, n=16: squares.

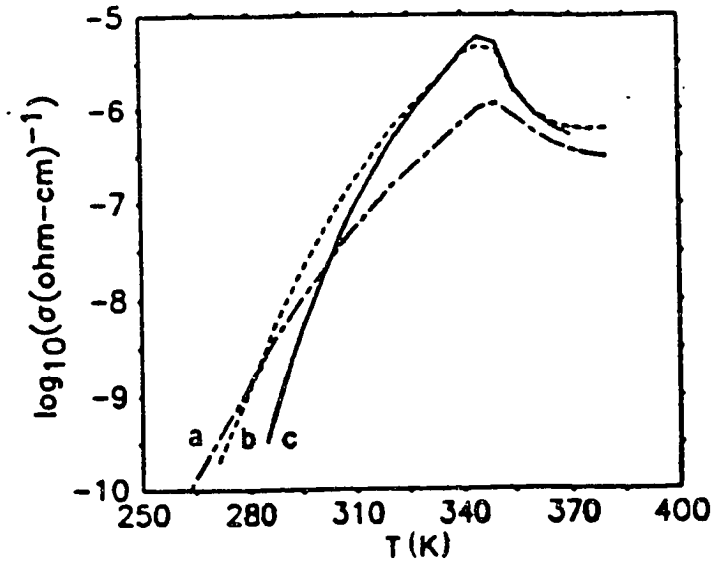

Figure 3.13 Electrical conductivity as a function of temperature. The curves are: (a) $PPO_{16}NaI$ (chain link), (b) $PPO_{12}NaI$ (dash), and (c) PPO_8NaI (solid). Straight line segments connect the datum which are about 5°C apart.

polymer and the ion-ion interaction of the various salts in terms of their melting points. In fig. 3.12, there is a sharp drop in M/B above 80 °C. This is ascribed to the salt precipitating out. This result is consistent with the DSC and conductivity data. The conductivity drop above 100 °C, as shown in fig. 3.13, indicates that fewer ions are available for transport in the polymer matrix because most of the salt has precipitated out. The only other possible factor leading to reduction in conductivity would be the suppression of polymer segmental motion which, of course, should not occur at higher temperatures. The dips in the DSC thermogram, as shown in fig. 3.11(b), demonstrate the salt precipitation. It should be noted that both NMR and conductivity measurements imply lower SP temperature than the DSC results. However, the samples were equilibrated for at least 30 minutes for NMR and conductivity, and scanned at 10 K/min. for DSC [47]. Dielectric constant measurement gives us some insight into the SP phenomenon. Figure 3.14 [47] depicts the results for the host polymer, which indicates that the real part of the dielectric constant decreases with increasing temperature above T_g. Consequently, salts precipitate out as the dielectric constant becomes too low to mediate solvation. Clearly, it also depends on the ion-ion interaction. The SP temperature increases slightly with decreasing salt concentration, as more PPO is available in the more dilute complexes. This is expected because lower concentration implies weaker ion-ion interaction in the complexes and thus higher SP temperature.

The second set of measurements was based on PPO complexes with different anions, thiocyanate (SCN^-), perchlorate (ClO_4^-), triflate ($CF_3SO_3^-$), iodide (I^-), and a 1:1 mixture of I^- and $CF_3SO_3^-$. $(T_2^*)^{-1}$ for the mobile Na^+ ions in the PPO

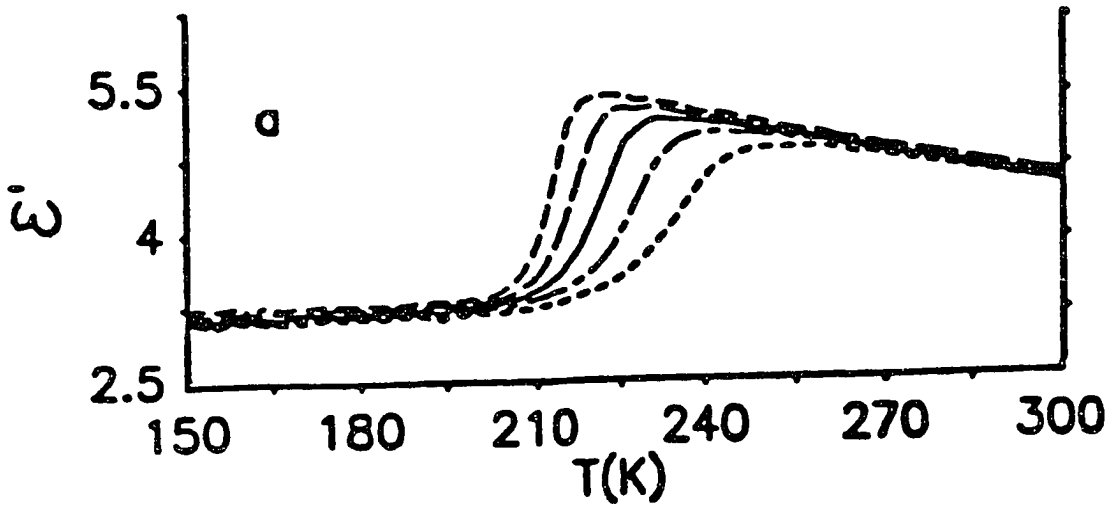

Figure 3.14 Real part of the dielectric constant at five frequencies; 10 Hz short dash, 100 Hz: long dash, 1000 Hz: solid, 10,000 Hz: chain link, and 100,000 Hz: dotted lines.

complexes are plotted as a function of temperature in fig. 3.15. All samples exhibit behavior similar to that observed in the siloxane and MEEP complexes. The temperature dependence of the ratio of mobile to bound sodium is plotted in fig. 3.16. The ClO_4 and SCN complexes (fig. 3.16(a)) show a gradual increase in mobile sodium ion followed by a decrease as ionic aggregation begins to occur. The sharp decrease in M/B in the perchlorate complex is clearly attributable to SP, although the gradual decrease of M/B prior to SP suggests that large ($\geq$10) ion aggregates are being formed. These large aggregates are expected to be spectroscopically similar to salt crystallites. The SP temperature for the thiocyanate was determined by DSC [50] to be 438 K, which is outside the range of the NMR probe. It is consistent with the NMR results as there is no sharp drop in M/B for SCN in fig. 3.16(a). There is a considerable scatter in the perchlorate data for M/B values approaching 100. However, the data is believed to reliable to be within about 25% for M/B values less than 20. Mobile/bound Na^+ data for the I, $CF_3SO_3^-$, and mixed anion samples are displayed in fig. 3.16(b). The triflate data shows a similar pattern (no SP observed within the temperature range) to that of thiocyanate, but with a higher ratio of M/B. Ionic aggregation and ultimately SP effects occur in the mixed anion complexes. There is apparently still a substantial mobile ion concentration after SP. Therefore, it is likely that only NaI is present in the precipitate. This argument is further verified by the DSC plot as shown in fig. 3.17 [50]. The mixed anion sample clearly exhibits a SP endotherm at about the same temperature as the iodide complexed material.

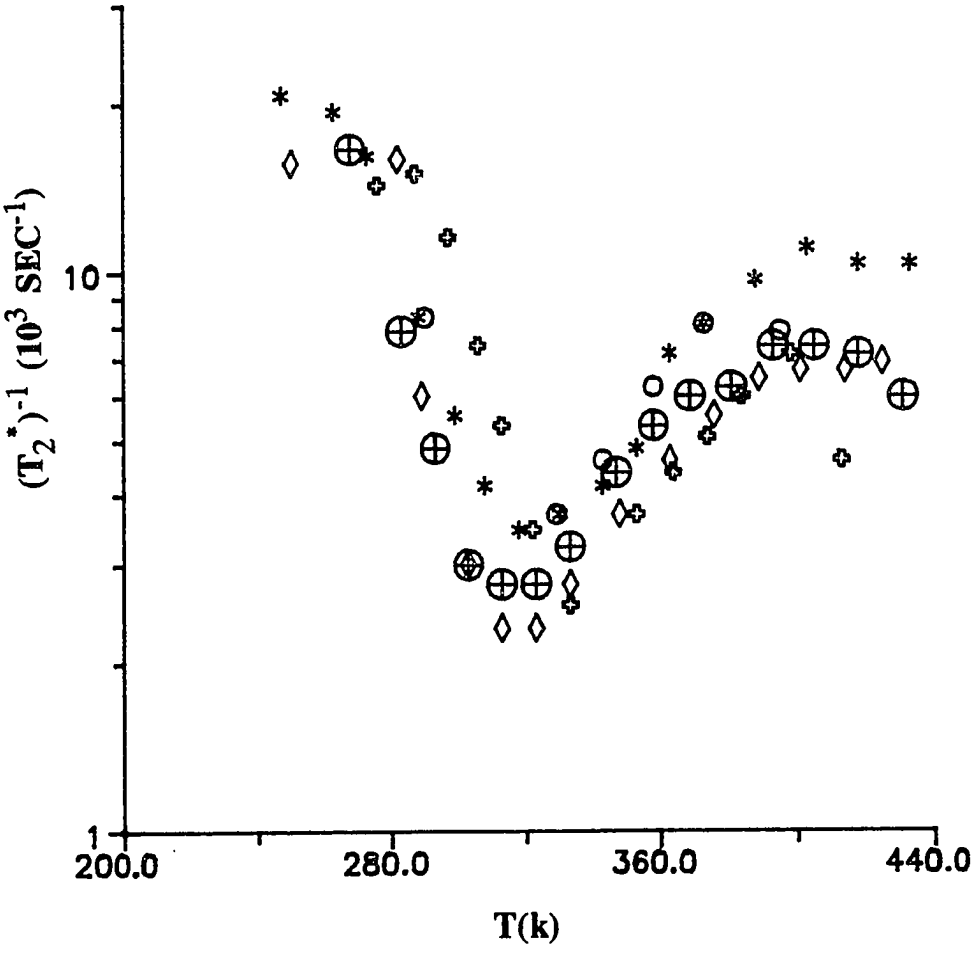

Figure 3.15 Reciprocal T_2^* (proportional to linewidth) temperature dependence of mobile Na^+ in PPO_8NaX where X = I (O); ClO_4 (+); SCN (*); CF_3SO_3 (◇); $(CF_3SO_3)_{½}(I)_{½}$ (⊕).

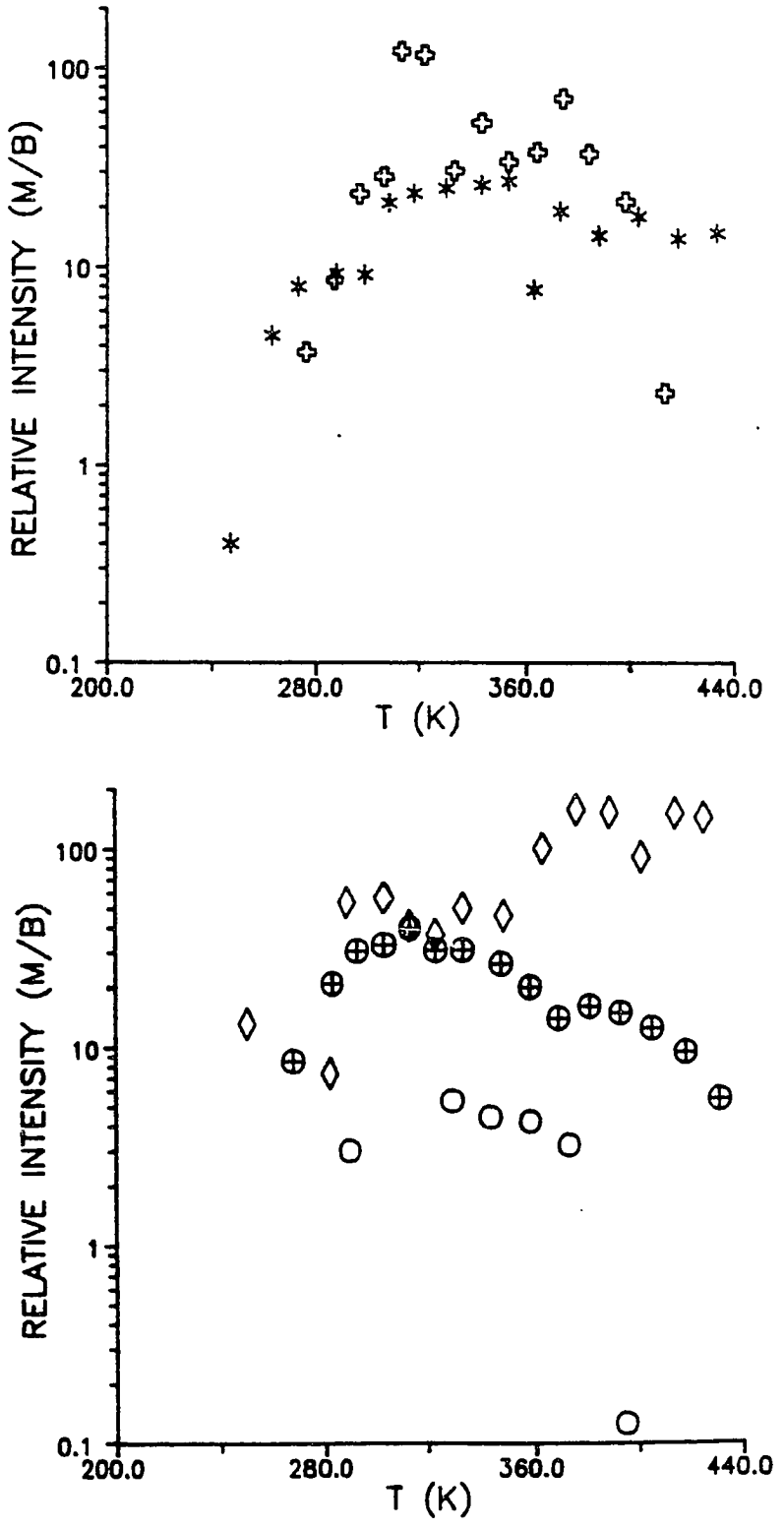

Figure 3.16 Mobile/Bound Na^+ ratios vs T in (a) PPO_8NaClO_4 (+) and PPO_8NaSCN(*); and (b) $PPO_8NaCF_3SO_3$ (◇); PPO_8NaI (O) and the mixed anion complex $PPO_8(CF_3SO_3)_{½}(I)_{½}$ (⊕).

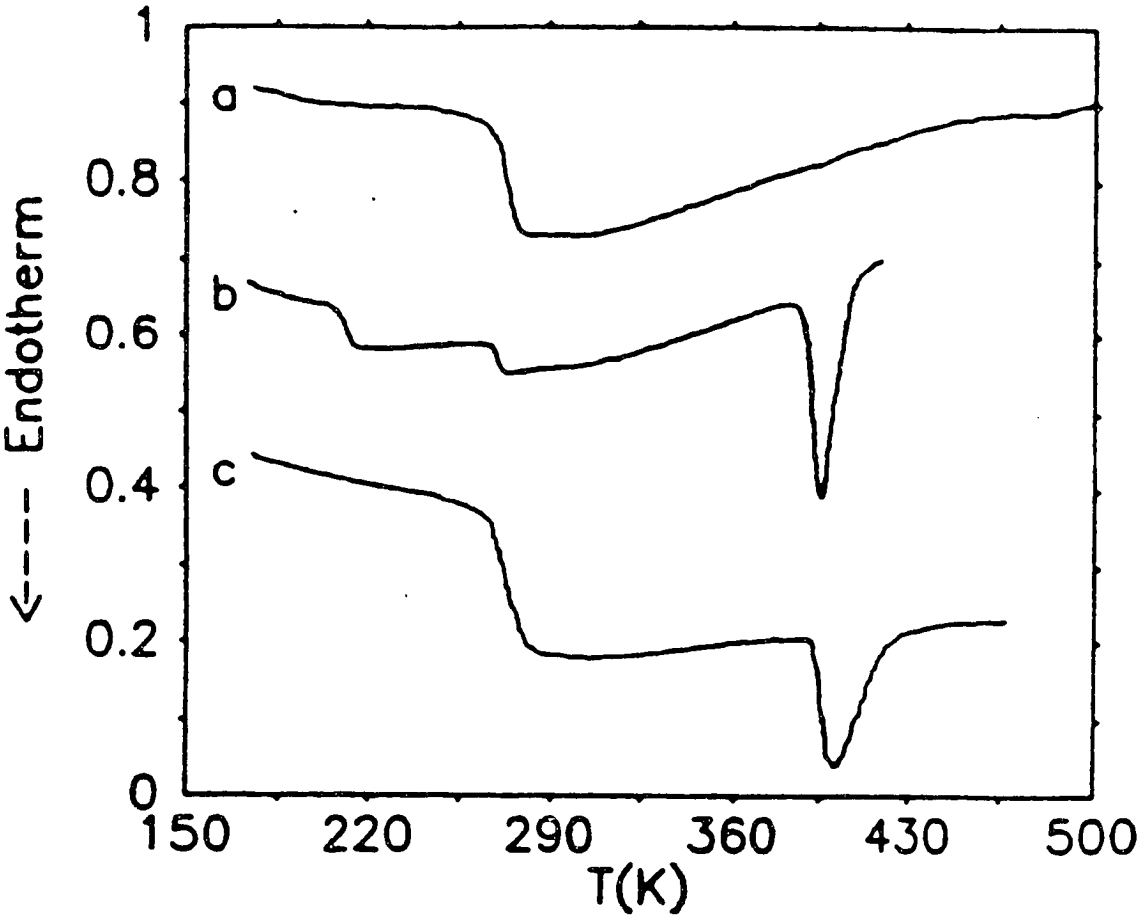

Figure 3.17 Comparison of DSC results for (a) $PPO_8NaCF_3SO_3$; (b) $PPO_{16}NaI$; (c) $PPO_8(CF_3SO_3)_{½}(I)_{½}$ (⊕).

The correlation between different strengths of ion-ion interactions of salts in the complexes (as reflected by the respective SP temperature) and the melting point of the pure salts is summarized in the following table. The SP temperatures were determined by DSC [47]. It is clear that the higher the melting point of the pure salt, the larger the ion-ion interaction. Consequently, SP occurs at lower temperature for those salts having larger ion-ion interactions (higher melting points).

	SP temperature of polymer-salt complexes (K)	Melting Point of pure salt (K)
NaI	353	933
$NaClO_4$	410	755
NaSCN	438	560
$NaCF_3SO_3$	not observed	520

The chemical shifts of the alkali ions are very sensitive to both the solvent and the salt concentration and anion present in non-aqueous solvents [51]. Therefore, analysis of chemical shifts of the alkali ion should be a useful method for studying ion-solvent and ion-ion interactions in this system. Concentration dependence of ^{23}Na chemical shifts have been studied in siloxane-based polymer electrolyte by Spindler et al. [52].

^{23}Na NMR absorption spectra for PPO_8NaClO_4 at 413 K, just above the temperature at which the salts begins to precipitate out, are shown in fig. 3.18. A repeat delay of 2 s was used to acquire the top spectrum, which consists of Na^+ in

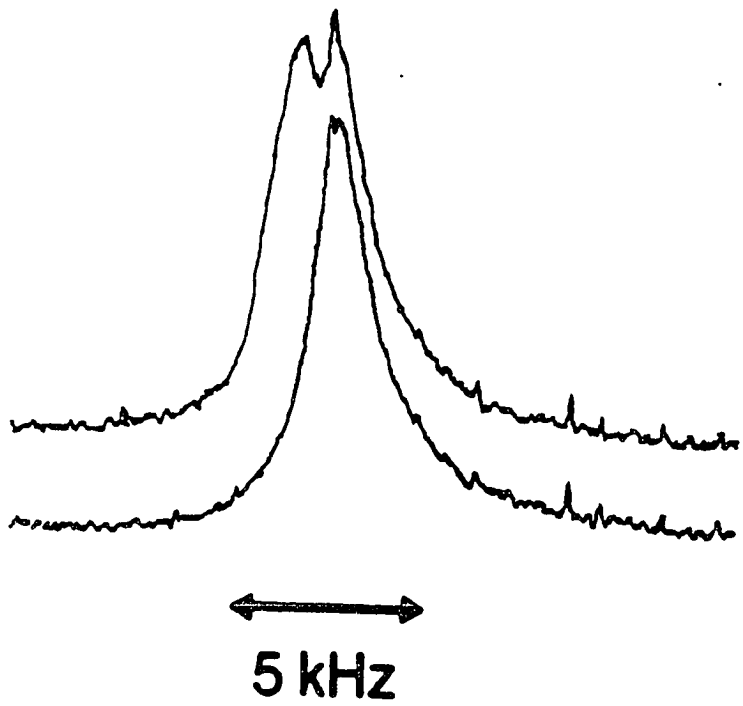

Figure 3.18 ^{23}Na NMR spectra in PPO_8NaClO_4 at 413 K. Top: Spectrum acquired with repeat delay of 2 s, left haft of the doublet is attributable to $NaClO_4$ precipitate. Bottom: Spectrum acquired with repeat delay of 10 ms, salt signal is almost completely saturated.

the complexes and Na^+ in the $NaClO_4$ precipitate. The bottom spectrum, acquired with 10 ms repeat delay, consists of only Na^+ in the complexes, as the $NaClO_4$ signal is almost completely saturated. The doublet in the top spectrum is attributable to different chemical shift interactions by Na^+ in these two different environments (complex and salts). Thus chemical shift effects are resolvable without the use of magic angle spinning (MAS) techniques, particularly in the motionally narrowed region.

For the chemical shift experiment, 1 M aqueous NaCl solution sealed inside a 3 mm quartz tube was put into a 10 mm quartz tube with the polymer sample. The chemical shift will be the frequency difference between the absorption peaks of the complex and the solution. ^{23}Na chemical shifts of the mobile Na^+ resonances for several PPO complexes are plotted as a function of temperature in fig. 3.19. The chemical shift clearly depends on the anions as well as the temperature. Except for the anomalous behavior of the perchlorate at lower temperature, all complexes exhibit a downfield shift with increasing temperature. The shift in the direction of the reference is designated as "downfield". Similar results obtained in siloxane-based polymer electrolytes have been interpreted in terms of reduced cation-anion association at higher temperatures [52]. However, this interpretation may not be applicable to the PPO system in which the the dielectric constant decreases with increasing temperature, which leads, ultimately, to SP. It should be noted that SP at high temperature is not observed in the siloxane system. The chemical shift in the PPO system thus far provides information about only average ion association effect

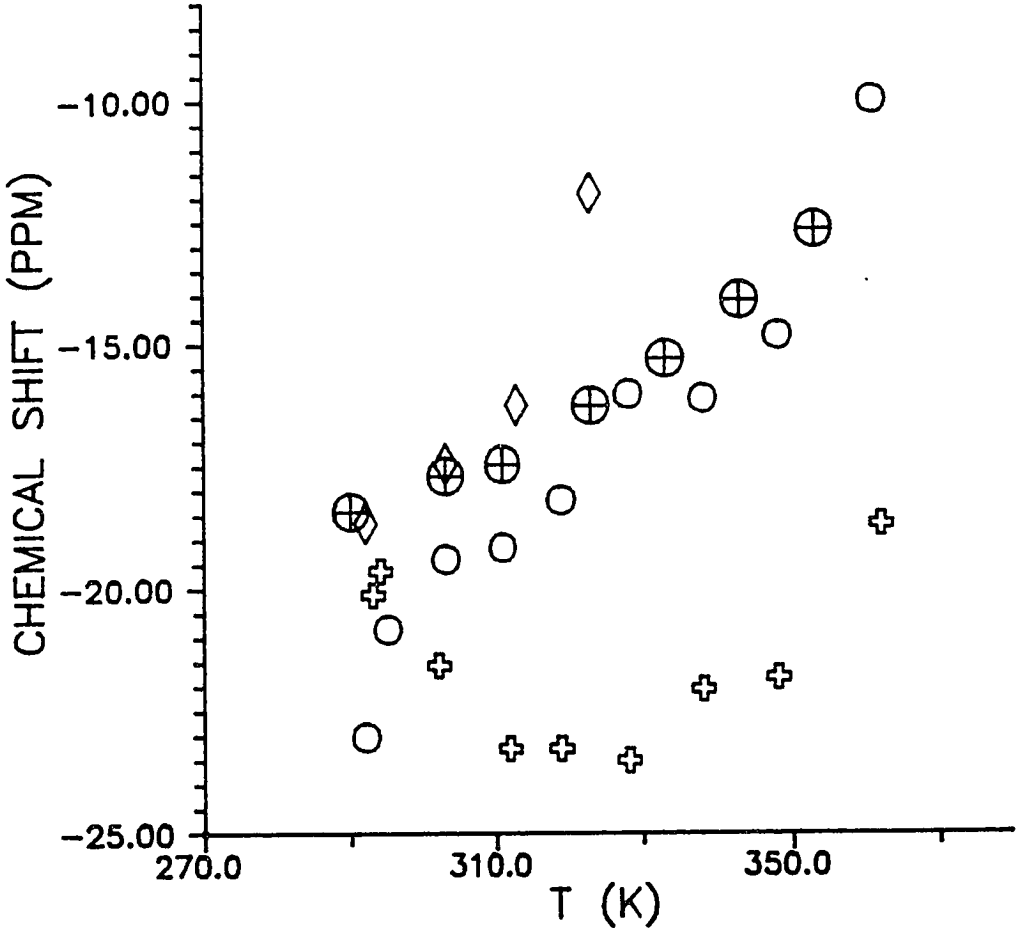

Figure 3.19 Temperature dependence of ^{23}Na chemical shifts, relative to 1 M aqueous NaCl, on PPO_8NaX where X = I (O); ClO_4 (+); CF_3SO_3 (◊); $(CF_3SO_3)_{½}(I)_{½}$ (⊕).

of respective anions. More detailed interpretation is complicated by the influence of cation-ether oxygen association on the chemical shift [53].

The results presented so far have demonstrated that the mobility of Na^+ is enhanced in the temperature region just above T_g. This is consistent with the result that the ion transport process is highly dependent on the polymer segmental motion. Thus, another technique to probe the polymer chain or segmental dynamics is essential. Solid state ^{13}C NMR is one of the powerful techniques commonly employed for this purpose. In addition, comparison of ^{13}C chemical shifts between the complexed and uncomplexed polymer electrolytes offers an opportunity to assess the degree of interaction of the polyethersegments and the solvated cations.

^{13}C NMR experiments were done in Professor R. Stark's laboratory. Details of the spectrometer and experimental procedures are described in chapter 2. Three polymer samples (PPO, PPO_8LiI, and PPO_8NaI) have been studied by solid state ^{13}C NMR techniques. Figure 3.20 shows room temperature ^{13}C CPMAS spectra obtained for PPO alone and PPO complexed to two alkali salts. The effect of complex formation on the chain mobility is evident from the spectral linewidths of PPO_8LiI and PPO_8NaI. In the presence of salts, all peaks are broadened by factors of 4-6. Line broadening is reminiscent of the effect of immobilization of the chain by the salt. This result is consistent with the fact that T_g increases upon complex formation [54]. In addition, the linewidth of the Li^+ complex is slightly larger than that of the Na^+ complex. The result reflects the observation that the Li complex has a slightly higher T_g than that of the Na complex [26, 55].

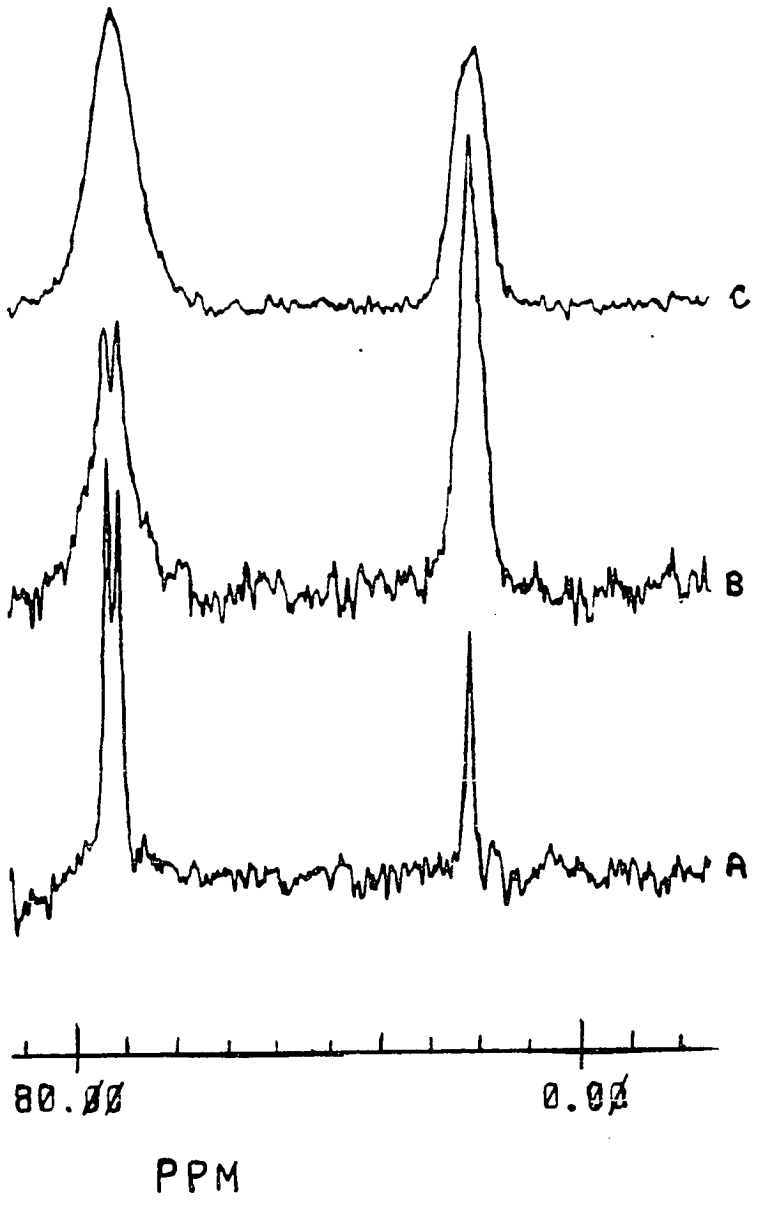

Figure 3.20 50.33 MHz ^{13}C NMR spectra of (a) PPO, (b) PPO_8NaI, and (c) PPO_8LiI. Data were obtained with cross polarization (contact time 500 μs, repeat delay 2s), magic angle spinning (2.7 or 3.0 kHz), and dipolar decoupling ($\gamma H_2/2\pi$ = 42 kHz). Spectral widths were 20 kHz, defined by 4 k data points. The NMR data were processed with a digital line broadening of 20 Hz. The chemical shifts were referenced to tetramethylsilane, via p-di-tert-butylbenzene as a secondary substitution reference.

Chemical shift assignments in the solid state, which are made with the assistance of published solution state spectra results [56], are listed in table 3.5. The methyl carbon signal shows a surprisingly large upfield shift upon salt complexation which may be due to steric interactions between the methyl group and the ions. The Li complex exhibits a larger effect than the Na complex. There are no clear cut chemical shift alterations found for the methine (CH) and methylene (CH_2) resonances in PPO. Coupled with the undesirable methyl group interaction, this may reflect the inferior solvating properties of PPO relative to PEO.

(D) Amorphous PEO Copolymers

Studies of polymer electrolytes based on linear poly(ethylene oxide), PEO, are complicated by the crystallization of the polymer. Therefore, amorphous material such as siloxane- PEO copolymers were studied. Some of the results have been presented in the previous section. Recently it has been shown that the crystallinity of PEO can be suppressed by incorporating randomly-spaced oxymethylene units into the linear PEO chain [57, 58], i.e.

$$[\text{--}(OCH_2CH_2)_mOCH_2\text{--}]_n$$

Amorphous complexes formed between oxymethylene-linked PEO and NaI or $NaCF_3SO_3$ (EO/Na = 9:1) were prepared by Professor Chadwick, UK [60]. The uncomplexed PEO is semicrystalline below room temperature but completely amorphous at higher temperature. The complexed materials are completely amorphous with the NaI complex having a higher T_g than the $NaCF_3SO_3$ complex [59].

Compound	^{13}C Chemical Shift[a] (ppm)			Linewidth[b] (Hz)		
	CH	CH_2	CH_3	CH	CH_2	CH_3
PPO	75.6	73.6 (74.6)[c]	18.0	45	31	37
PPO_8NaI	75.9	73.1 (74.5)[c]	17.3	177	212	153
PPO_8LiI	74.0[d]		16.4	414[d]		199

[a] Referenced to TMS, via p-tert--butylbenzene as a secondary substitution reference. Values for closely-spaced peaks are derived from a curve-fitting routine. Estimated error limits are 0.2 ppm.

[b] Linewidths are half-height, derived from a curve-fitting routine and quoted after subtraction of digital line broadening. The sample temperature is 296 K. Estimated error limits are 10 Hz.

[c] Average values for CH and CH_2.

[d] Methylene and methine signals are not resolved.

Table 3.5 NMR parameters for PPO-Ion complexes in ^{13}C NMR experiments

As in the case of PPO complexes, the ^{23}Na NMR absorption generally consists of two separate spectra corresponding to mobile and bound Na. Figure 3.21 displays the temperature dependence of $(T_2^*)^{-1}$ for PEO_9NaI and the corresponding triflate complex. The iodide-complex shows the onset of motional narrowing about 10 K higher than that of triflate complex. This is consistent with the DSC results in which the T_g's of PEO_9NaI (259 K) and $PEO_9NaCF_3SO_3$ (251 K) have been determined.

Figure 3.22 shows the plot of the relative intensity (M/B) as a function of temperature. The triflate complex displays a consistently higher mobile Na^+ concentration than the iodide. This result suggests that NaI has a stronger cation-anion interaction than that of $NaCF_3SO_3$. However, it has been observed that the mobile Na^+ concentration in PEO_9NaI continues to increase slowly with increasing temperature up to 130 °C. Thus there is no indication of salt precipitation (at least up to 130 °C), which has been shown to occur in the PPO-salt complexes.

(E) Cationic Conducting Copolymer

In "conventional" polymer electrolytes, both the cation and anion are mobile. In general, the cationic transference number is not unity, being typically close to 0.5 [21, 60]. Moreover, ionic aggregation effects in these high salt concentration complexes limit the number of available charge carriers . These factors have led to the investigation of various copolymers with anions attached to the polymer backbone [61].

The cation conductor in the following study consists of a nylon backbone, attached anionic groups and polyether side chains. The copolymer was synthesized

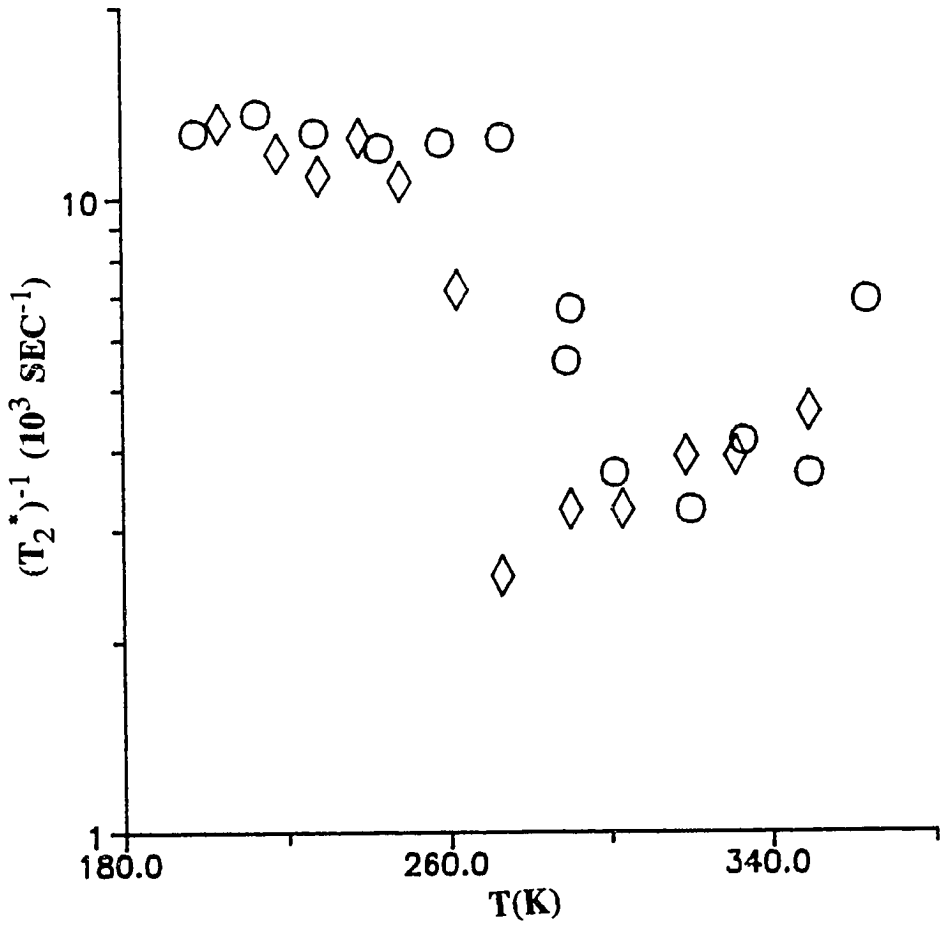

Figure 3.21 Temperature dependence of reciprocal ^{23}Na free induction decay constant $(T_2^*)^{-1}$, for $PEO_9NaCF_3SO_3$ (diamonds) and PEO_9NaI (circles).

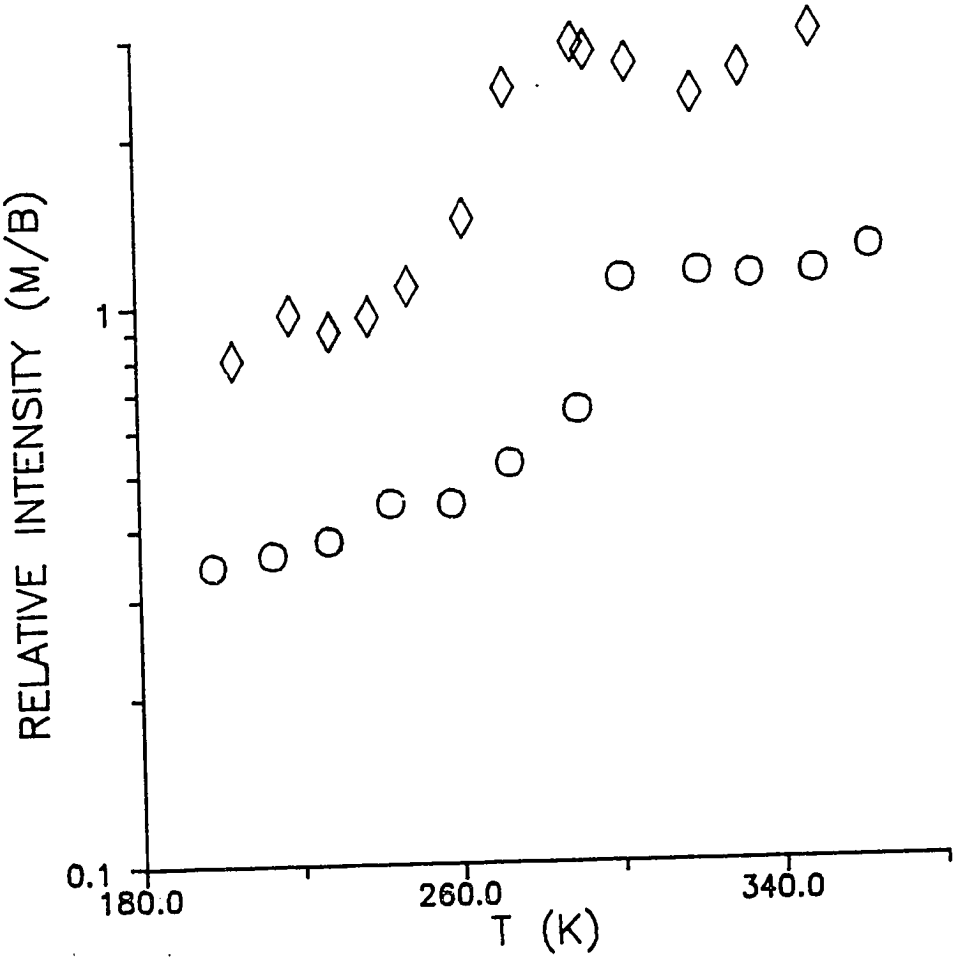

Figure 3.22 Temperature dependence of ratio of mobile/bound sodium concentration in $PEO_9NaCF_3SO_3$ (diamonds) and PEO_9NaI (circles).

by Professor Okamoto of Polytechnic University. Figure 3.23(a) shows the structure of the copolymer.

The schematic picture of the cation-anion pair is shown in fig. 3.23(b). The two important features of this anion are the delocalization of the negative charge over the ring and the steric hinderance of the butyl groups near the oxygen. ^{23}Na NMR resonance of sodium tributyl phenolate is substantially quadrupole broadened, reflecting the steric influence of the butyl groups.

As in the previous "conventional" polymer electrolyte, ^{23}Na resonance absorption consists of two components: a short T_1 resonance with strongly temperature dependent linewidth; and a long T_1 resonance of temperature independent linewidth. Figure 3.24 shows the relative intensity (M/B) as a function of temperature. There is a steady increase of mobile Na^+ concentration with increasing temperature until about 40°C, after which the concentration remains constant at approximately 75%. Thus the availability of charge carriers at or near room temperature is certainly adequate for conduction.

(F) Pressure Dependence of ^{23}Na Resonance of Polymer Electrolytes

From the previous discussions, it is apparent that segmental motion of the polymer chain plays an important role in the ionic transport processes. Large scale segmental motion, which occurs above the glass transition temperature, is usually strongly pressure dependent. There are some studies in the literature about the effect of pressure on either the conductivity or α relaxation peak in dielectric

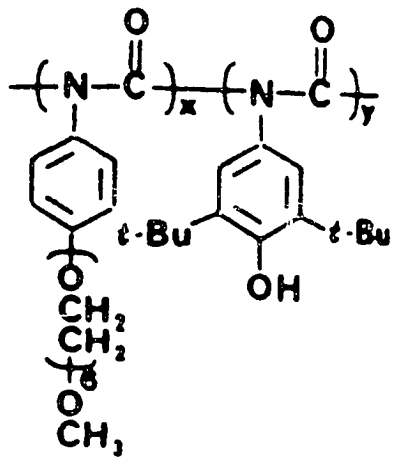

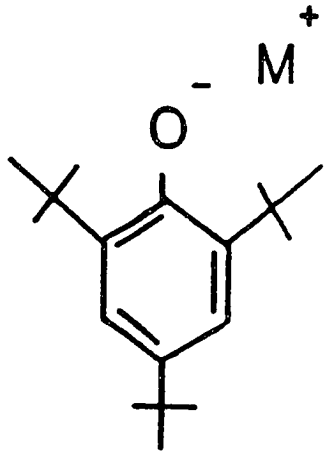

Figure 3.23 (a) Copolymer structure of the cation-conducting polymer electrolyte. (b) Schematic diagram of 2,4,6 - tributyl phenolate anion-cation pair (M=Na).

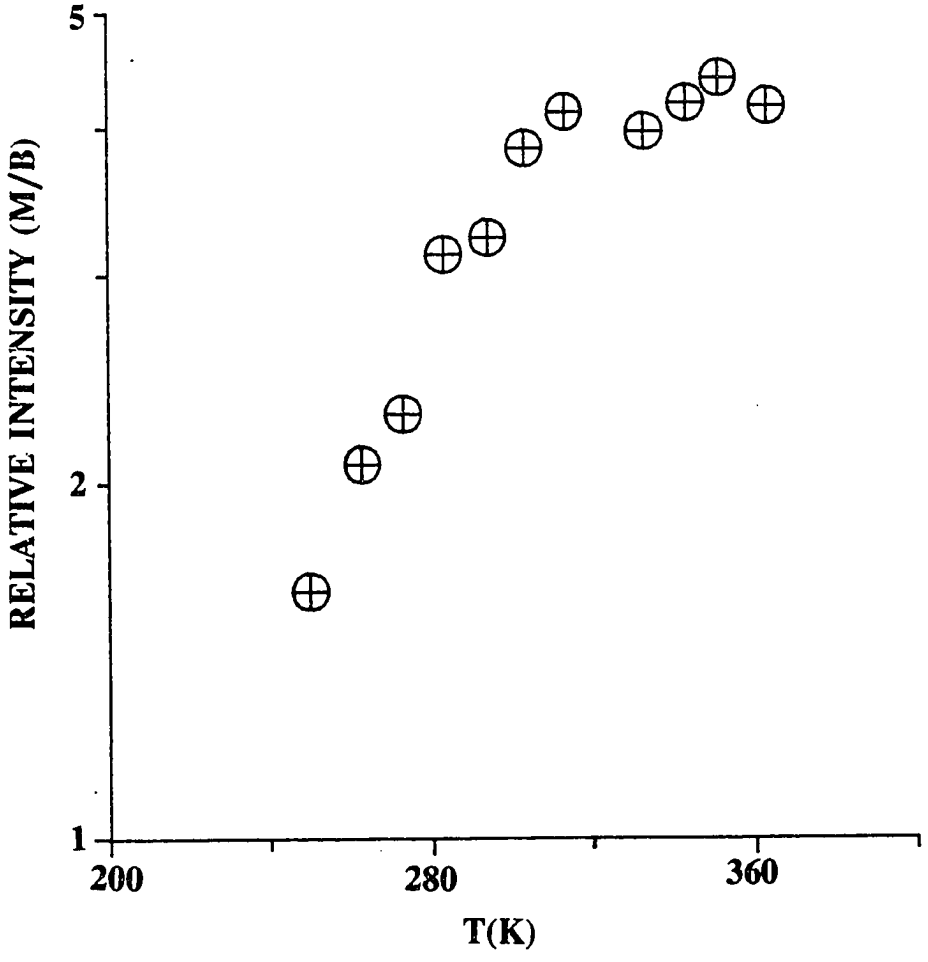

Figure 3.24 Temperature dependence of mobile to bound Na^+ ration in cation-conducting complex.

relaxation (DR) experiments [62, 63]. Pressure dependent measurement of NMR parameters should be complementary to other methods which focus on the chain mobility, such as DR. Pressure studies performed in this laboratory are described below.

Figure 3.25 shows the plot of $(T_2^*)^{-1}$ of the mobile resonance in PPO_8NaI at 45 °C as a function of pressure. It should be noted that the data was obtained at 318K which corresponds to $T - T_g \approx 45$ K. As previous linewidth results have shown, the minimum of $(T_2^*)^{-1}$ is usually about 50 K above T_g. Hence, the sample is in the motional narrowing region. The interpretation of the data is that pressure induces an increase in T_g, which pushes the ^{23}Na linewidth back out of the motional narrowing region. This result is consistent with previously observed shifts in T_g for uncomplexed PPO with pressure [64]. Interestingly, the opposite effect of pressure on the linewidth was observed in PDMS-EO copolymer complexed with $NaCF_3SO_3$. The effect of hydrostatic pressure on the linewidth $(T_2^*)^{-1}$ is shown in fig. 3.26. The two data symbols correspond to previously unpressurized and pressure cycled samples. There is a systematic decrease in linewidth with increasing pressure. The measurements were performed at 290 K, or 85 K above T_g. The linewidth at that temperature is within the motionally broadened region (as discussed on p.53, the short T_1 at higher temperatures leads to lifetime broadening). It is apparent that linewidth decreases with increasing pressure because $T-T_g(p)$ is decreasing. That is, the sample is now out of the motionally broadened region. Therefore, the principal effect of pressure appears to be an increase in T_g on the order of 10-15 K/kbar. This result is consistent with the conductivity pressure dependence which reflects a

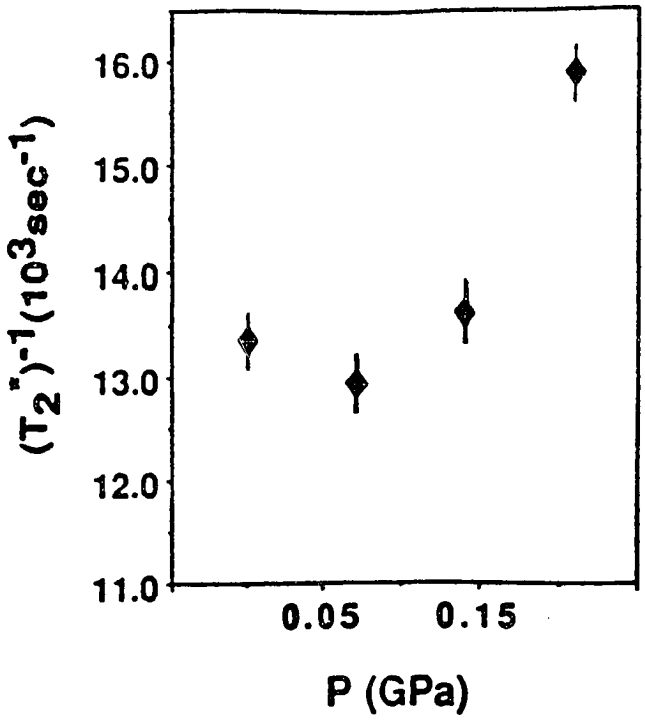

Figure 3.25 ^{23}Na reciprocal FID time constant $(T_2^*)^{-1}$ of the mobile Na in PPO_8NaI at 45°C as a function of pressure.

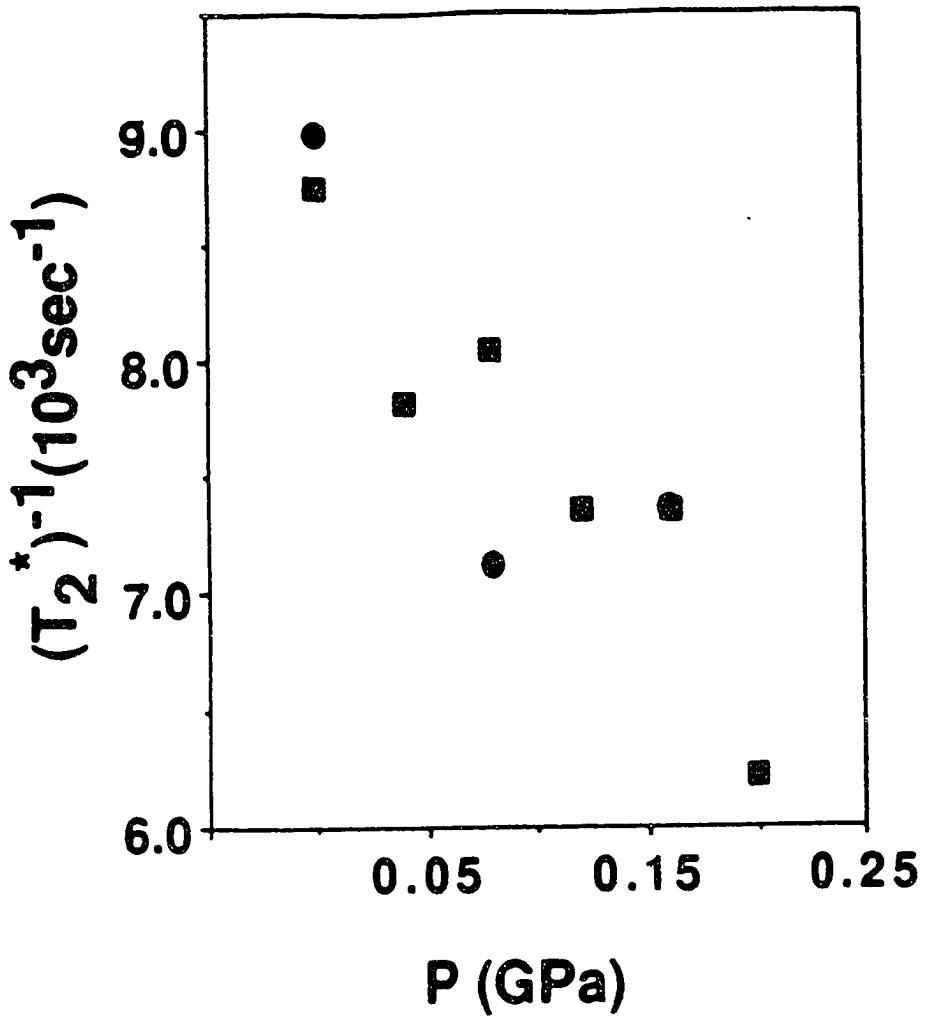

Figure 3.26 Pressure dependence of ^{23}Na linewidth $(T_2^*)^{-1}$ of mobile Na^+ in PDMS-EO triflate complex at 290 K. The squares correspond to the sample subjected to pressure for the first time; the circles represent data taken after several 0-0.2 GPa cycles.

similar increase in T_o (the fitting parameter in the VTF equation) [40,45]. It should be pointed out that the linewidth data in figures 3.25 and 3.26 do not represent the true linewidth, which is attributable partly to magnetic field inhomogeneities associated with the pressure probe. However, the above interpretation should be valid regardless of the broadening due to field inhomogeneities.

Additional evidence of pressure induced increase in T_g is observed in the M/B pressure dependence measurements. The pressure dependence (at 290 K) plot of M/B in PDMS-EO is displayed in fig. 3.27, which shows that M/B decreases with increase in pressure. This is also explainable in terms of a T_g shift. Similar results have been obtained in PPO_8NaI [47].

However, an anomalous pressure result is obtained in the single ion conductor. Figure 3.28 displays the free induction decay amplitude of the mobile Na^+ signal under varying degrees of pressure, from 1 bar to 2 kbar. The apparent pressure insensitivity of the linewidth is inconsistent with the previous results. Further studies of analogous cation conductors based on flexible siloxane rather than nylon-1 backbone are expected to give some insight into this anomalous pressure effect.

(G) Frequency variation in ^{23}Na NMR studies of Polymer Electrolytes

In order to have a better understanding of ion-ion interaction in the polymer system, the following work was carried out at different resonance frequencies. The three resonance frequencies in the following discussion are 19.0 MHz, 81.5 MHz and 105.6 MHz (done in Chemistry Department of Hunter College as mentioned in chapter 2). It should be noted that the frequency 81.5 MHz is slightly larger than the

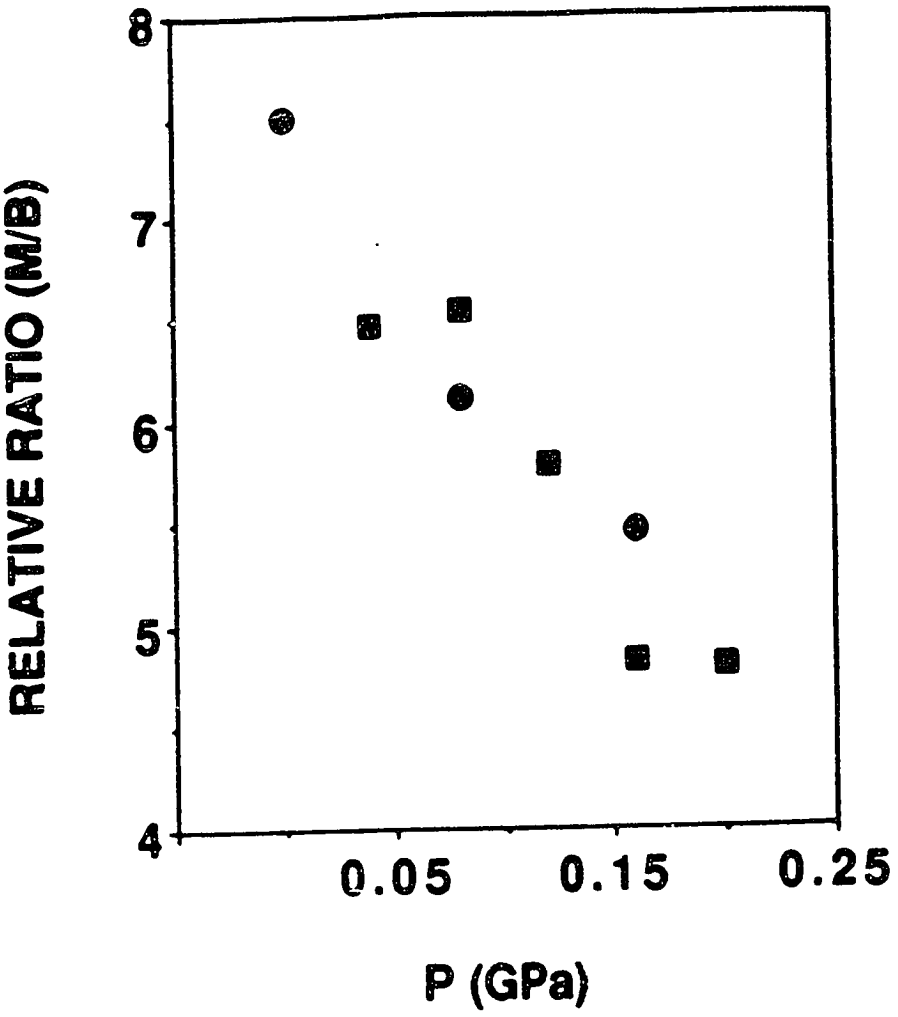

Figure 3.27 Mobile to bound (M/B) Na^+ ratio of PDMS-EO triflate complex as a function of pressure. Circles: pressure cycled sample; Squares: uncycled (first pressure run).

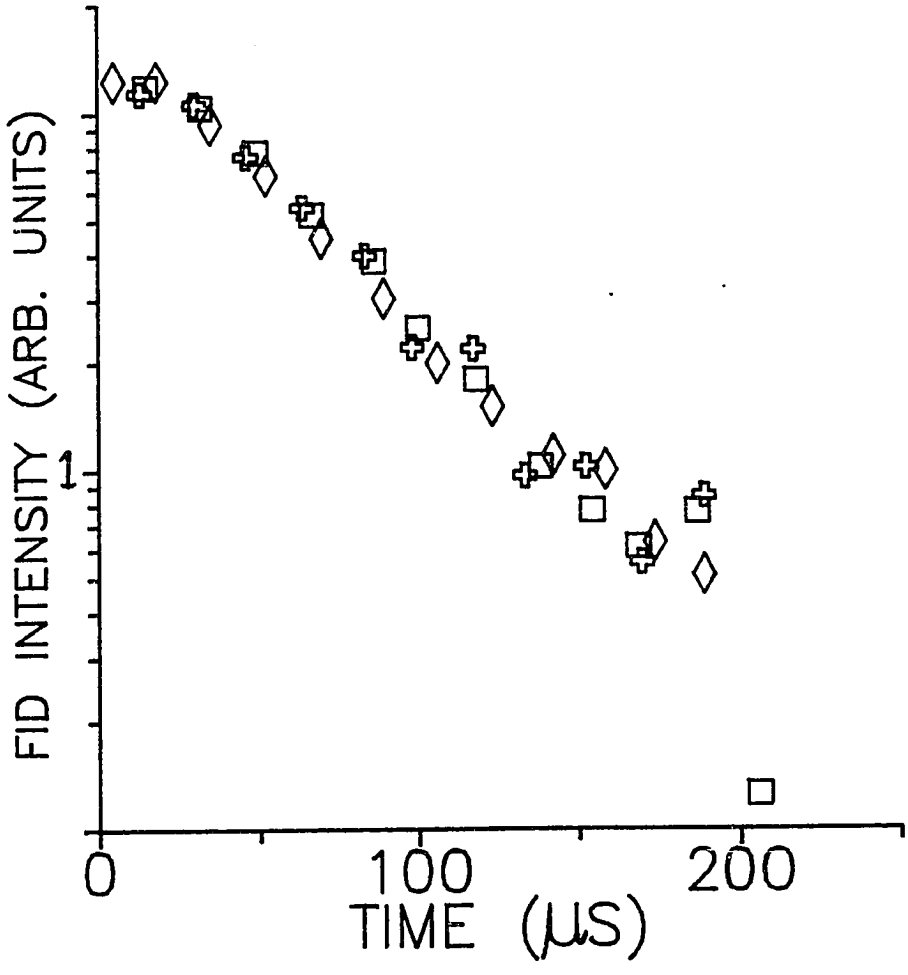

Figure 3.28 Pressure dependence of ^{23}Na FID in cation-conducting polymer complex, 1 bar (atmospheric)- diamonds; 1 kbar- squares; 2 kbar- crosses.

one (i.e. 80.6 MHz) mentioned in the experimental section because the super-conducting magnet has been energized to a slightly larger field. Three samples were studied in this work, $PPO_8NaB(C_6H_5)_4$, PPO_8NaClO_4 and (PDMS-EO) sodium triflate complex. PPO network polymer with $NaB(C_6H_5)_4$ has been previously studied by others [21, 62]. This complex attracts relatively little attention because of its low conductivity, $\sigma \approx 2.7x10^{-9}Scm^{-1}$ at 30 °C [21]. However, $PPO_8NaB(C_6H_5)_4$ is of interest to us because of the bulky anion which may provide more information about the cation-anion interaction in the complexes.

Figure 3.29 shows a T_1 plot of the ^{23}Na resonance at 81.5 MHz in $PPO_8NaB(C_6H_5)_4$ as a function of temperature. In this complex, it is not easy to distinguish between the two Na components as their T_1 values are different by only a factor of 5 to 10. This conclusion follows the observation that the data from inversion recovery experiment shows two null points in the vicinity of each other. If there is a single T_1, a single null point is expected. The T_1 shown in fig. 3.29 is that of the faster relaxation (smaller T_1). T_1 decreases from 55 ms to about 70 μs as temperature increases from 218 to 393 K. From the Arrhenius plot of T_1 (not shown), the linear region between 250 to 350 K gives an activation energy of about 0.3 eV. In fig. 3.29, additional T_1 values for different resonance frequencies are plotted. It is obvious that T_1 increases with resonance frequency. However, a simple relationship between T_1 and resonance frequency (e.g. power law) cannot be deduced from the data at the present time.

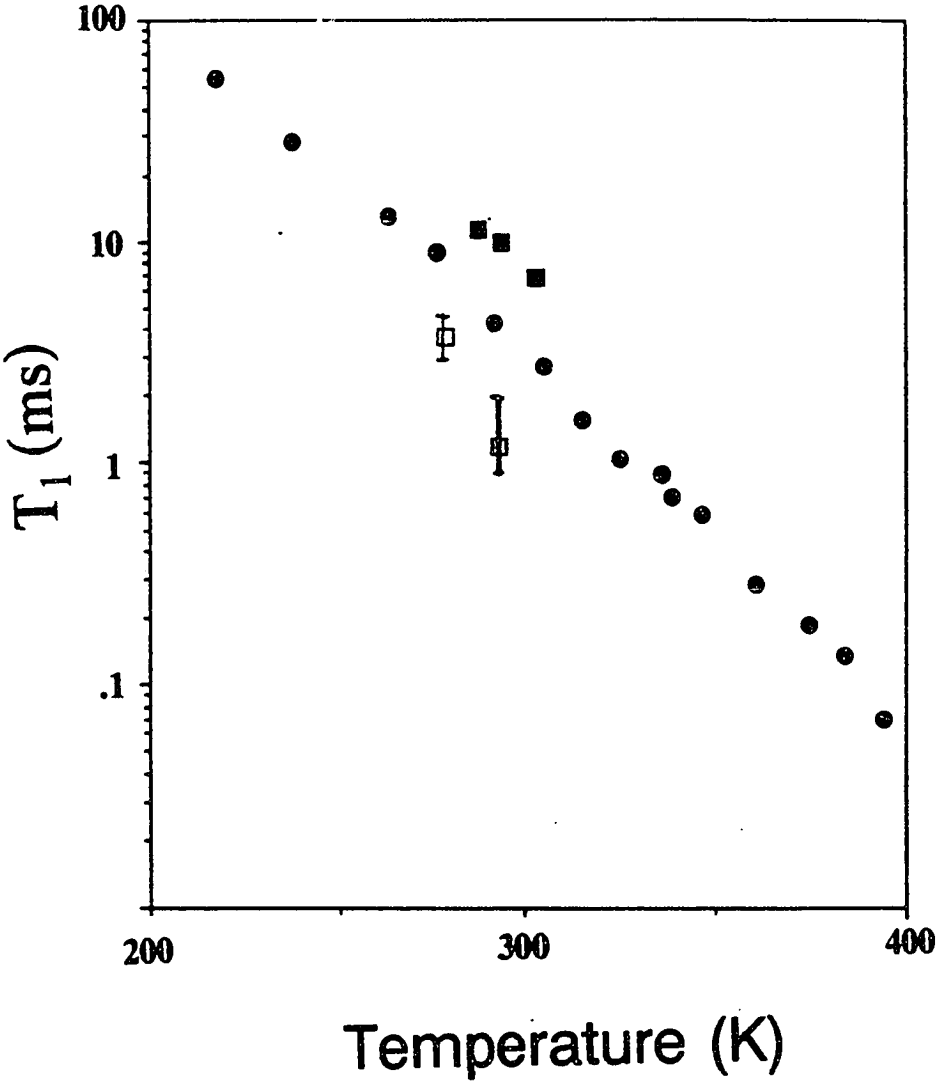

Figure 3.29 Temperature dependence of T_1 of ^{23}Na resonance in $PPO_8NaB(C_6H_5)_4$ at frequencies (a) 19.0 MHz (□); (b) 81.5 MHz (●); (c) 105.6 MHz (■).

Figure 3.30 shows the temperature dependence of the linewidths in $PPO_8NaB(C_6H_5)_4$ at three different resonance frequencies. For resonance frequency of 81.5 MHz, it shows similar patterns to the previous samples, i.e. motional narrowing above T_g (306 K), a minimum, and then the broadening as a result of the short T_1 in the higher temperature region. Although there are not many data points shown in the 105.6 MHz plot, it is obvious that the temperature at which motionally narrowing begins (hereafter, this temperature is called the "onset" temperature) is just above T_g. However, there is a tremendous drop in the "onset" temperature, to about 50 K below T_g, in the 19.0 MHz plot. This low resonance frequency feature, lower "onset" temperature, is not observed in PPO_8NaClO_4. A plot of $(T_2^*)^{-1}$ of the Na resonance in PPO_8NaClO_4 as a function of temperature is shown in fig. 3.31. In the figure, the motional narrowing occurs at the same temperature irrespective of resonance frequency. In both samples, the linewidth increases as the resonance frequency decreases. As will be discussed in the following paragraph, the increase in linewidth is due to second order quadrupole broadening, which is inversely proportional to the resonance frequency. Thus, we propose the following explanation for the low temperature narrowing region in $NaB(C_6H_5)_4$. The contribution to the linewidth from the quadrupole interaction is significantly greater at low frequency than at high frequency, while the dipolar contribution is frequency independent. In the motionally narrowing region above T_g, decrease in linewidth is due to large scale segmental motion at those temperatures. For the 19.0 MHz resonance, the linewidth decreases within the temperature range from 50 K below T_g to T_g because of the quadrupole interaction between the Na^+ ion and its local environment. It is

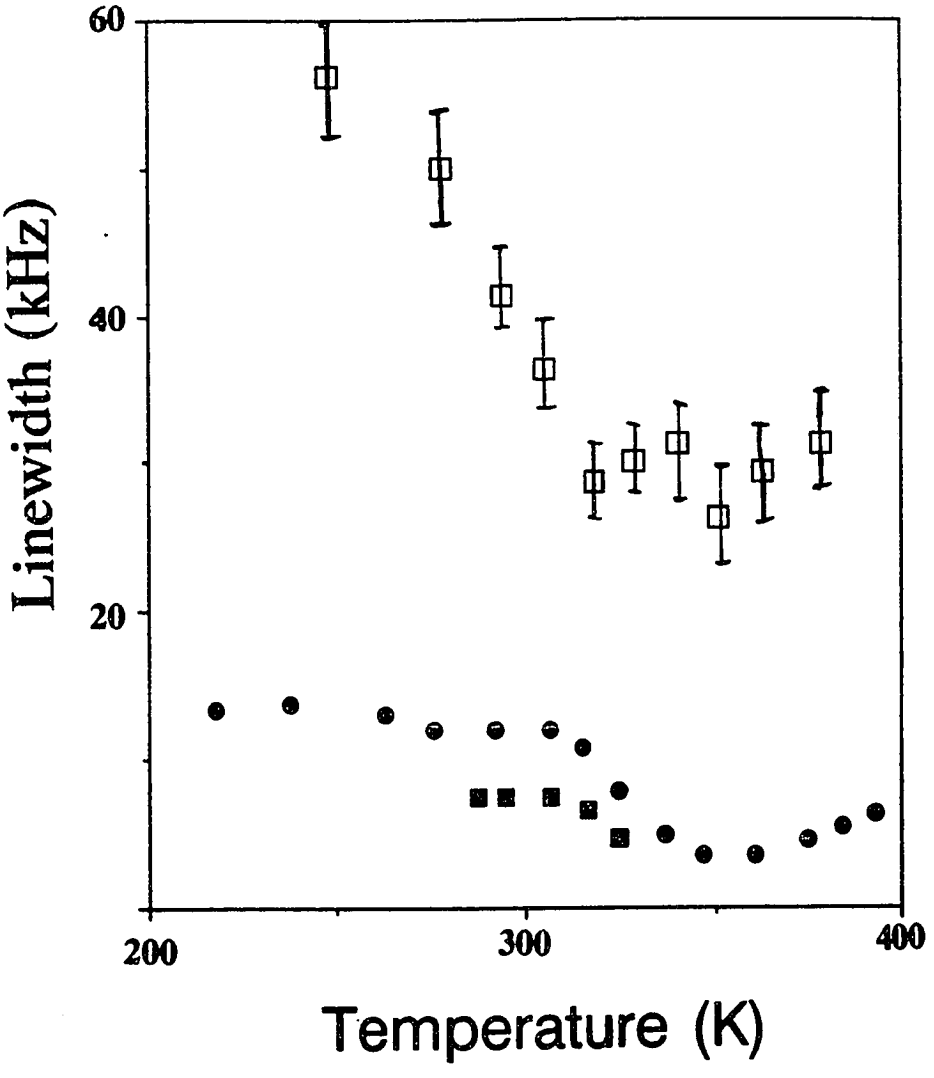

Figure 3.30 Temperature dependence of ^{23}Na linewidth in $PPO_8NaB(C_6H_5)_4$ at resonance frequencies (a) 19.0 MHz (□); (b) 81.5 MHz (●); (c) 105.6 MHz (■).

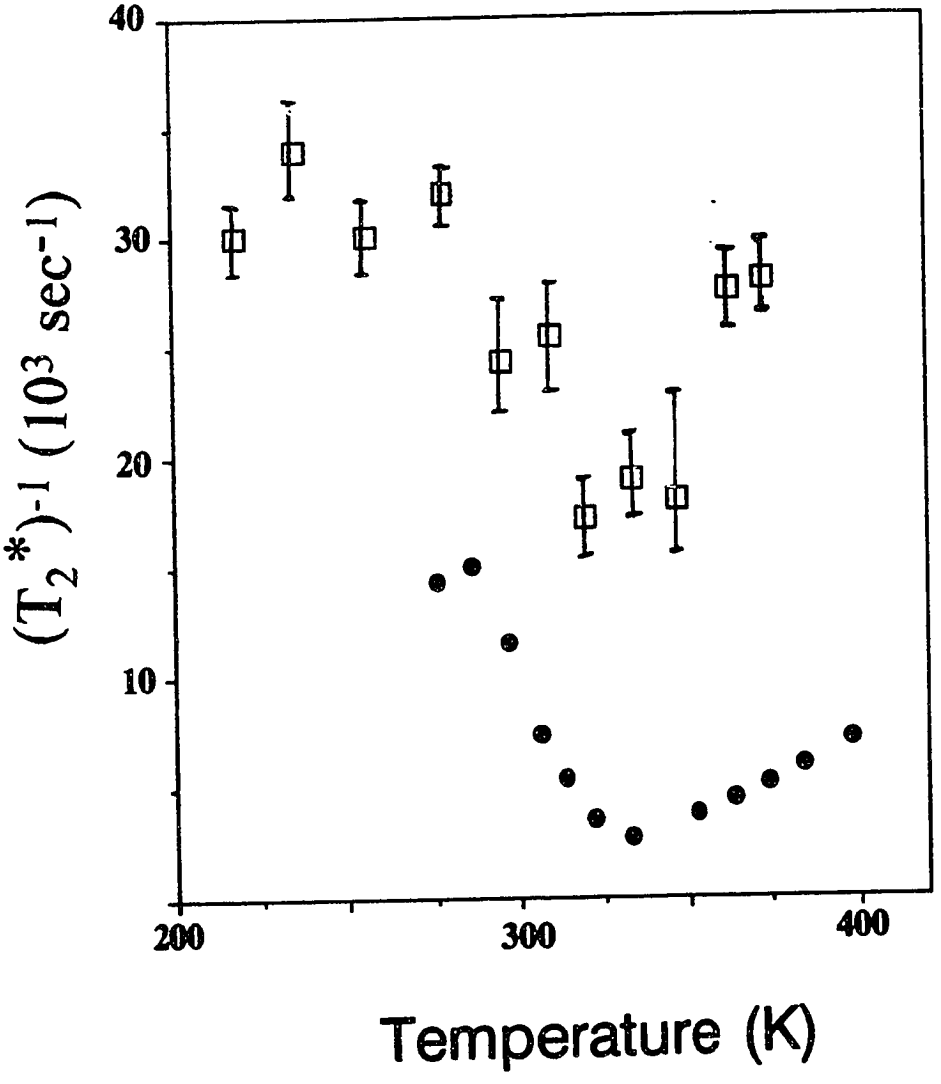

Figure 3.31 Temperature dependence of ^{23}Na linewidth $(T_2^*)^{-1}$ in PPO_8NaClO_4 at resonance frequencies (a) 19.0 MHz (□); (b) 80.6 MHz (●).

probable that there are anions present in the vicinity of the cation. Cation-anion interactions and torsional or reorientational motions associated with the large $B(C_6H_5)_4^-$ anion may give rise to motional narrowing of the quadrupole inter-action-determined lineshape and thus the linewidth decreases as temperature increases up to T_g. Further narrowing above T_g is due to the segmental motion of the polymer chain. Question may arise because there is no appreciable change in linewidth below T_g in PPO_8NaClO_4 at either high or low frequency. The probable answer is that the ClO_4^- anion does not produce as large an efg at the Na as does the $B(C_6H_5)_4^-$ anion (as evidenced by the larger "rigid" linewidth of the latter complex), and that the ClO_4^- does not execute large enough amplitude vibrations to relax the nuclei. In fact, the relatively small T_1 of the "second" component of the $PPO_8NaB(C_6H_5)_4$ signal may reflect the presence of ion aggregates in which anionic motions of the type described above can even relax the Na nuclei in the aggregate (as opposed to the complex).

As mentioned above, linewidth increases as the resonance frequency decreases. Comparing the 19.0 MHz and 81.5 MHz plots in both samples, there is an increase of the linewidth by a factor of about 4 (at most temperature) at 19.0 MHz resonance frequency. As is discussed in chapter 1 (section 1.2), the resonance frequency shift of the central transition ($\frac{1}{2} \leftrightarrow -\frac{1}{2}$) is inversely proportional to resonance frequency ω_o if there is a second order quadrupole interaction. The results thus show that the quadrupole interaction of ^{23}Na in the complexes is of second order. Similar results are observed in another polymer system, (PDMS-EO)-$NaCF_3SO_3$ complex. Figure 3.32 shows the plot of $(T_2^*)^{-1}$ vs temperature in (PDMS-EO)-$NaCF_3SO_3$ complex.

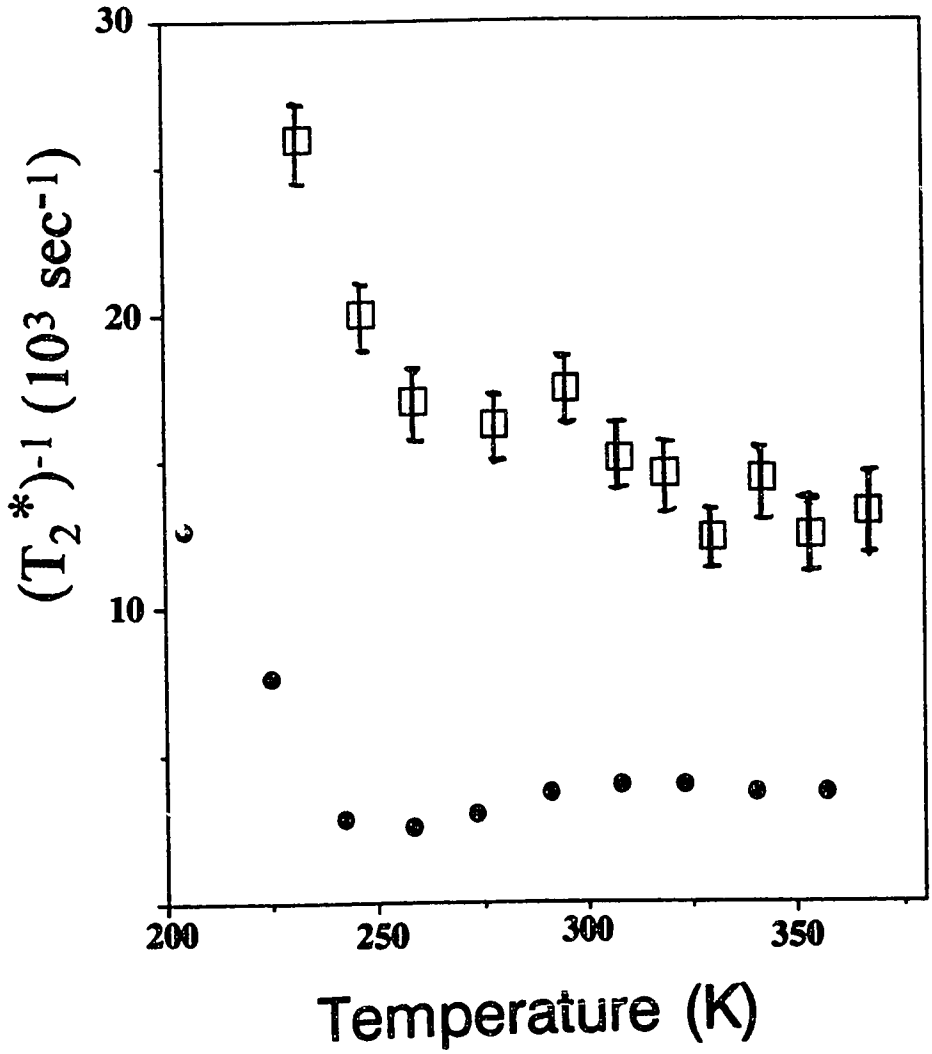

Figure 3.32 Temperature dependence of ^{23}Na linewidth $(T_2^*)^{-1}$ in (PDMS-EO)-$NaCF_3SO_3$ complex at resonance frequencies (a) 19.0 MHz (□); (b) 80.6 MHz (●).

There is again a factor of 4 increase in the resonance linewidth in going from 81.5 to 19.0 MHz. It should be noted that the samples used for the 19.0 MHz and 80.6 MHz resonance data are from different batches. However, this is not expected to change our interpretation of the results. Figure 3.33 shows the FID of (PDMS-EO)-$NaCF_3SO_3$ complex at 19.0 MHz resonance frequency and a corresponding exponential best fit. The two peaks in the first 20 μs are due to the influence of magneto-acoustic noise which is inevitable at low resonance frequency. However, the accuracy of the fit is within 10% for our better FID signals. No detailed measurement on the bound Na in siloxane complexes were carried out. Figure 3.34 shows the spectra of bound Na (obtained by selective subtraction) at two different resonance frequencies. The resonance line is broadened roughly by a factor of 4 in lower field, and this broadening is also second order. The bound signal in the siloxane therefore is probably not attributable to simple ion aggregrates, which would be primarily dipole rather than quadrupole broadened.

Finally, our results seem to support the model that cations form transient crosslinks between polymer chains, possibly involving anions in the vicinity. $PPO_8NaB(C_6H_5)_4$ has an anomalously high T_g (306 K, as determined by DSC), compared to other Na-salt complexes, which may be due to the "stiffening" effect of the $B(C_6H_5)_4^-$ ion on the polymer chain . Previous work by Sandahl's group [66] shows that the transient crosslink is independent of cation. On the other hand, our results show that the polymer network can, indeed be affected by the anion.

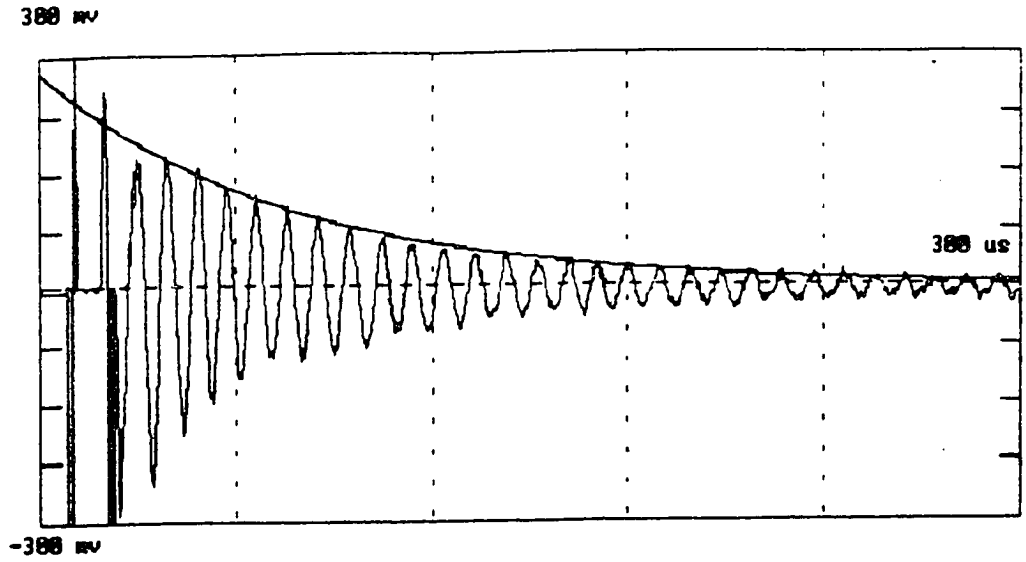

Figure 3.33 FID of (PDMS-EO)-$NaCF_3SO_3$ complex at 19.0 MHz and an exponential best fit.

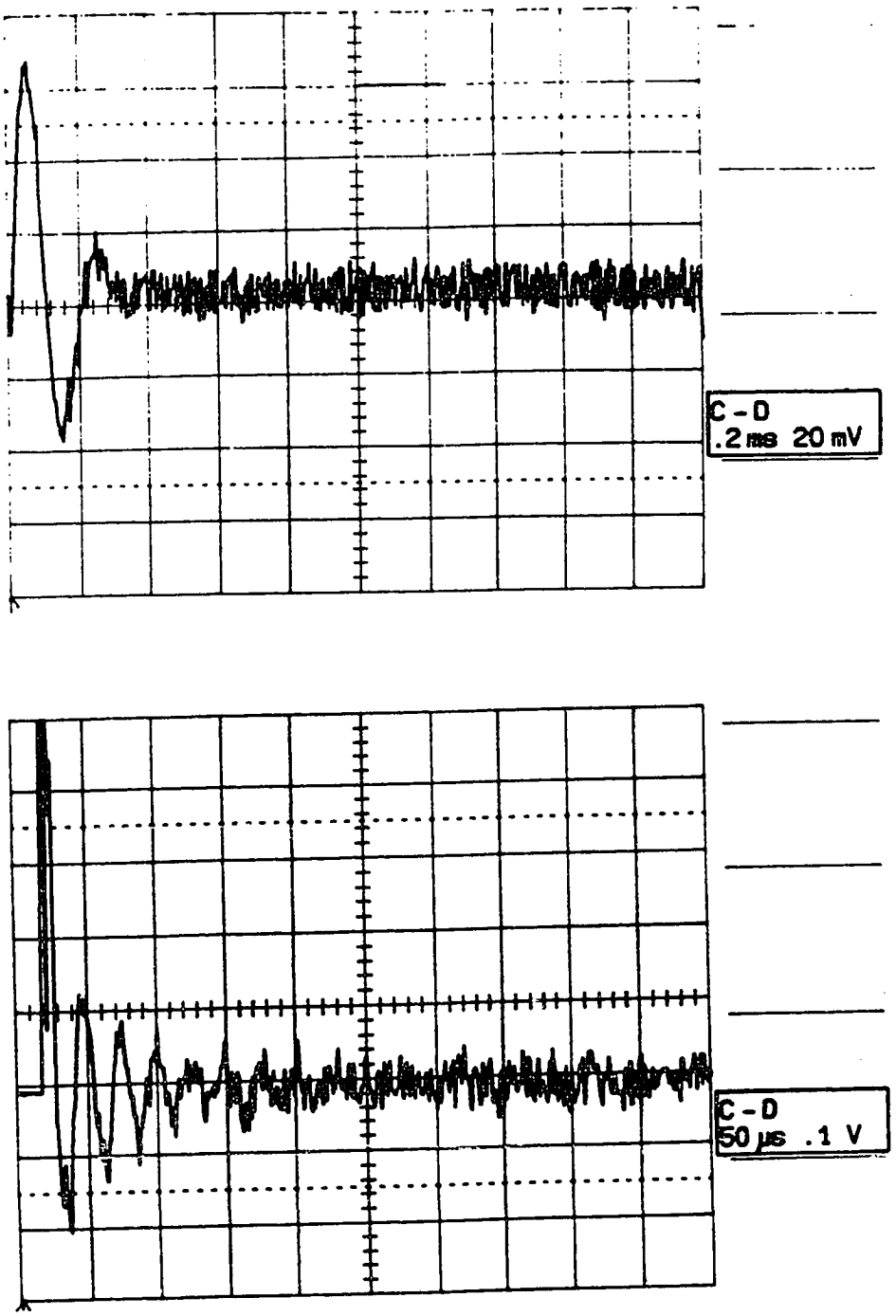

Figure 3.34 The spectra of bound Na (obtained by selective subtraction) in (PDMS-EO)-$NaCF_3SO_3$ complex at two different resonance frequencies, 81.5 MHz (top), 19.0 MHz (bottom).

(H) Summary

A variety of Na salt-polymer complexes (including PPO, amorphous PEO, MEEP, exclusively cation conducting and siloxane-based complexes) have been investigated in this thesis work. In all of them, two different Na species exist in the material. With the exception of $PPO_8Na(C_6H_5)_4$, spin-lattice relaxation times T_1's of the components differ by 2-3 orders of magnitude (milliseconds and seconds respectively). The short and long T_1 components are identified as mobile and bound (or ion aggregates of 10 or more ions) Na^+ ions respectively. As both T_1's (on the order of ms) of $PPO_8Na(C_6H_5)_4$ are only different by a factor of 5 to 10, only the short T_1 resonance is studied. Linewidth (about 5 kHz) of the bound Na is relatively insensitive to temperature, while that of mobile Na shows a universal dependence on temperature. Linewidth of the mobile Na begins to decrease at about T_g, reaches a minimum at around 45-55 K above T_g and then broadens again. The typical linewidth of the mobile Na is approximately 5 kHz at about T_g and the minimum value (at about T_g + 50 K) is about 0.5 kHz. The motional narrowing reflects the large scale motion of the polymer chain, and the higher temperature broadening is a result of the short T_1 at those temperatures.

Quantitative measurement of the ratio of mobile and bound Na (M/B) shows an increase with temperature. This increase reflects the ion dissociation process of the salt in the complex. In PPO complexes, salt precipitation (SP) occurs at high temperature, indicated by a tremendous drop in M/B as well as a sharp endotherm in DSC measurement. SP is attributable to the strong ion-ion interaction and the

decreasing solvation power of the host polymer at higher temperature (shown by the drop in the real part of dielectric constant at that temperature). SP temperatures of the salts in the complexes correlate well with the melting point of the pure salt. The higher the melting point of the pure salt, implying stronger ion-ion interaction, the lower the corresponding SP temperature in the complex. ^{23}Na chemical shift results also demonstrate the anion effect on the material. ^{13}C NMR results show that Li^+ and Na^+ ions have different ion-polymer interaction. There is no observable effect of SP in the a-PEO or siloxane-based complexes. M/B increases by a factor of 10 to 100 in the temperature range from 180 to 380 K. However, ionic conductivity increases by 5 - 6 orders of magnitude in the same temperature range. This result combined with the motional narrowing studies demonstrates that the "carrier" generation process plays only a minor role in the ionic conductivity, i.e. segmental motion of the host polymer is the primary driving mechanism for ion transport. Measurements of linewidth and M/B as a function of pressure are consistent with an increase of T_g of about 10-15 K/kbar.

Multi-frequency NMR results show that the Na^+ ion is second order quadrupole broadened in the complexes. The quadrupole interaction is thus not as significant in the high field measurement as it is at low fields. In $PPO_8Na(C_6H_5)_4$ measurements at low field, linewidth narrowing occurs below T_g and is explained in terms of the averaging of the electric field gradient by torsional or reorientational motion of the large anions.

APPENDIX

The following document is for the program 9400.bas. The program, to interface LeCroy 9400 with IBM PC, is written in Microsoft QuickBasic version 4.5. There are several things to be noted for the program:

(1) RS 232C is required for the interface.

(2) Data must be stored/restored in Memory C or D of the LeCroy 9400.

(3) The filename of the data file always has with an extension "LCY" , i.e. "********.LCY". No extension is required when you type the filename.

(4) It is possible to store data by using different skip point factors (1, 5 or 10). For example, "1" means that there are 25000 data points in your data file. However, a reasonable number of data points is 2500, i.e. skip point factor "10".

A typical format of the data file is shown as follows:

```
RD=.01 -14 DEG C 2000 Scans
.*,10,2550,0
#L,150,28,120,.....
.....
#L,1363,37082,35736,.....
.....
.....
.
.
#L,8192
#I
```

The first line is the comment typed in by the operator when the data is stored. The second line is the reminder of the skip point factor used. For example, ".*,10,2550,0" means that the skip factor 10 has been chosen. The third set of the

data beginning with the format as "#L,150,....." is the parameter data for the LeCroy 9400, e.g. time per division, volt per div. etc.. A detailed description of the parameter file can be found in the LeCroy user Manual. The data of the signal start from the fourth section with "#L,1336,.....". It should be noted that the number following "#L" is the number of data points in that set of data. The end of the data file is marked by the parameter "#I". Finally, the program is attached as a reference.

```
DECLARE SUB MENU () : DECLARE MESS2 () : DECLARE MESS1 ()
' PROGRAM FOR LINKING THE LECROY 9400 TO AN IBM-PC VIA RS 232C
'AUTHOR : STEVE PAK      FEB,1989.      HUNTER COLLEGE : modified MAY, 89
'
     CLS : ON ERROR GOTO Handler        'ACTIVATE ERROR TRAPPING
     TRUE = -1: FALSE = 0: MLOOP = TRUE: EX = FALSE: ECHO = TRUE:
STORE = FALSE
     CPRM$ = "%"
     CLOSE #1
     OPEN "COM1:9600,N,8,1,RB10000" FOR RANDOM AS #1 LEN = 10000
     PRINT #1, CHR$(27) + "["          'Tell LECROY not send any extraneus nonsense
     PRINT #1, "CHLP PPO"
     PRINT #1, "CTRL OFF"
     PRINT #1, "CFMT,L,WORD,UNSIGNED_SHORT"
     PRINT #1, "CBLS 8192"
     PRINT #1, "MASK 6,1"
     PRINT #1, "RS_CONF 6,13,0,0,0" '<ACK>, <CR>
     PRINT #1, "CPRM " + CHR$(34) + CPRM$ + CHR$(34)
     CALL MESS1
     LOCATE 8, 1
     PRINT STRING$(80, "-")
     CALL MENU
     LOCATE 22, 1
     PRINT STRING$(80, "-")
50    ON KEY(1) GOSUB FILESTORE
     ON KEY(2) GOSUB FILECALL
     ON KEY(3) GOSUB REMOTE
     ON KEY(4) GOSUB TOQUIT
     KEY(1) ON: KEY(2) ON: KEY(3) ON: KEY(4) ON
     GOTO 50
100   CLOSE
     CLS
     END

FILESTORE:          'Store data to IBM PC
     STORE = TRUE
     VIEW PRINT 10 TO 20
     CALL MESS2
     CLS 2
200   INPUT "SPECIFY SOURCE MEMORY ( C OR D ) :  "; M$
     IF M$ = "c" THEN M$ = "C"
     IF M$ = "d" THEN M$ = "D"
400   INPUT "ENTER SKIP POINT FACTOR (1, 5 OR 10 ):  "; SP$
     IF SP$ = "5" THEN
       G$ = ".*," + SP$ + ",5100,0"
     ELSEIF SP$ = "10" THEN
       G$ = ".*," + SP$ + ",2550,0"
     ELSEIF SP$ = "1" THEN
       G$ = ".*"
     ELSE
```

```
        GOTO 400
    END IF
    LINE INPUT "SPECIFY DIR. AND FILENAME (no extension): "; MYFILE$
    LINE INPUT "COMMENT : "; COM$
    F$ = MYFILE$ + ".LCY"
    RD$ = "RD M" + M$ + G$
    PRINT #1, RD$
    CLOSE #2
    OPEN F$ FOR OUTPUT AS #2
    PRINT #2, COM$
    PRINT #2, G$
    LINE INPUT "ECHO DATA TO SCREEN (Y/N) :  ", Y$
    IF Y$ = "n" THEN Y$ = "N"
    IF Y$ = "N" THEN ECHO = FALSE: PRINT "UPLOADING....." ELSE
    ECHO = TRUE
    GOSUB GETSTRING
    STORE = FALSE: ECHO = TRUE: CLOSE #2
    CLS 2
    RETURN
    '
FILECALL:          ' restore file to the LECROY 9400
    VIEW PRINT 10 TO 20
    CALL MESS2
    CLS 2
    A$ = CHR$(27) + "R": PRINT #1, A$
    LINE INPUT "SPECIFY TARGET MEMORY (C OR D) :  "; B$
    IF B$ = "c" THEN B$ = "C"
    IF B$ = "d" THEN B$ = "D"
    PRINT : LINE INPUT "SPECIFY DIR. AND DISK FILE (no extension):  "; MFJ$
    CLOSE #3
    FJ$ = MFJ$ + ".LCY"
    OPEN FJ$ FOR INPUT AS #3
    LINE INPUT #3, C$
    PRINT " COMMENT : "; C$
    LINE INPUT #3, G$
    WT$ = "WT M" + B$ + G$ + CHR$(13)
    PRINT #1, WT$;
    PRINT #1, CHR$(6);
    LINE INPUT "ECHO DATA TO SCREEN (Y/N)  :  ", Y$
    IF Y$ = "n" THEN Y$ = "N"
    IF Y$ = "N" THEN ECHO = FALSE: PRINT "DOWNLOADING....." ELSE ECHO
    = TRUE
    WHILE NOT EOF(3)
        D$ = INPUT$(1, #3)
        IF ECHO THEN PRINT D$;
        PRINT #1, D$;
    WEND
    CLOSE #3
    GOSUB GETSTRING
    A$ = CHR$(27) + "L": PRINT #1, A$: GOSUB GETSTRING
```

```
    ECHO = TRUE
    CLS 2
    RETURN
    '
REMOTE:              ' remote control of the LECROY 9400
    VIEW PRINT 10 TO 20
    CLS 2
    A$ = CHR$(27) + "R"
    PRINT #1, A$
    MLOOP = TRUE
    LOCATE 11, 10
    PRINT " *****          REMOTE CONTROL OF LECROY 9400          ***** "
    LOCATE 12, 10
    PRINT " *****  ANY VALID COMMAND DESCRIBED IN THE User's Manual
    ***** "
    LOCATE 13, 10
    PRINT " *****          TURN <CAPS LOCK> ON                    ***** "
2100  WHILE MLOOP
    PRINT
2200  LINE INPUT "  Enter  Command ( EX---> to exit ):  "; P$
    IF LEN(P$) < 2 THEN 2200
    IF P$ = "EX" THEN MLOOP = FALSE: GOTO 2300
    PRINT #1, P$: GOSUB GETSTRING
2300  WEND
    Q$ = CHR$(27) + "L"
    PRINT #1, Q$: GOTO 100
    RETURN
    '
GETSTRING:          '
    ON TIMER(2) GOSUB 3000: TIMER ON
    CYCLE = TRUE
    WHILE CYCLE
    PRINT #1, CHR$(6);
2600  IF EOF(1) THEN 2600
    TIMER STOP
    R1$ = INPUT$(LOC(1), #1): R2$ = MID$(R1$, 1, LEN(R1$))
    ' to test end of data
    L = INSTR(R2$, CPRM$): IF L > 0 THEN L = L - 1: R2$ = MID$(R1$, 1, L):
    CYCLE = FALSE
    IF ECHO THEN PRINT R2$
    IF STORE THEN FOR I = 1 TO LEN(R2$): PRINT #2, MID$(R2$, I, 1);
    NEXT I
    WEND
    TIMER OFF
2800  RETURN

TOQUIT:          ' quit the program
    GOTO 100
    RETURN
    '
```

```
Handler:            ' error handling routine
     CLS 2
     BEEP
     PRINT "ERROR NO.  "; ERR
     GOSUB TOQUIT
     RETURN
     '
3000   PRINT " TIME OUT ": TIMER OFF: GOTO 2100

SUB MENU
     LOCATE 2, 20
     PRINT " F1--- STORE          F2--- RECALL   "
     LOCATE 5, 20
     PRINT " F3--- REMOTE          F4--- QUIT     "
END SUB

SUB MESS1
     LOCATE 5, 1
     PRINT STRING$(70, "#")
     PRINT "#" + SPACE$(68) + "#"
     PRINT "#" + SPACE$(68) + "#"
     PRINT "#" + SPACE$(10) + "INTERACTIVE PROGRAM FOR LINKING THE
LECROY 9400" + SPACE$(11) + "#"
     PRINT "#" + SPACE$(15) + " TO AN IBM PC VIA RS 232C " + SPACE$(27) +
     "#"
     PRINT "#" + SPACE$(68) + "#"
     PRINT "#" + SPACE$(68) + "#"
     PRINT "#" + SPACE$(68) + "#"
     PRINT "#" + " SETTINGS : 9600BD,NO PARITY,8 BITS,1 STOP BIT " +
     SPACE$(21) + "#"
     PRINT "#" + SPACE$(68) + "#"
     PRINT "#" + SPACE$(68) + "#"
     PRINT "#" + SPACE$(68) + "#"
     PRINT "#" + SPACE$(10) + "HIT ANY KEY TO CONTINUE"+SPACE$(35)+"#"
     PRINT "#" + SPACE$(68) + "#"
     PRINT "#" + SPACE$(68) + "#"
     PRINT STRING$(70, "#")
WAITFORKEY2: IF INKEY$ = "" THEN GOTO WAITFORKEY2
     CLS
END SUB

SUB MESS2
     LOCATE 13, 15
     PRINT "*****     STOP ACQUIRING DATA    ******* "
     LOCATE 14, 15
     PRINT "*****    HIT ANY KEY TO CONTINUE    ***** "
WAITFORKEY: IF INKEY$ = "" THEN GOTO WAITFORKEY
     CLS
END SUB
```

REFERENCES

(1) a) C. P. Slichter, Principles of Magnetic Resonance, Springer-Verlag (1978).
b) A. Abragam, The Principles of Nuclear Magnetism, Oxford University Press, London (1978).

(2) E. L. Hahn, Phys. Rev., 80, 580 (1950).

(3) H. Y. Carr and E. M. Purcell, Phys. Rev., 94, 630 (1954).

(4) S. Meiboom and D. Gill, Rev. Sci. Instrum., 29, 688 (1958).

(5) N. Bloembergen, E. M. Purcell, and R. V. Pound, Phys. Rev., 73,7, 679 (1948).

(6) a) T. P. Das, E. L. Hahn, Nuclear Quadrupole Resonance Spectroscope, Academic Press, New York (1958).
b) M. H. Cohen, and F. Reif, Solid State Physics, vol 5, 321 (1957).

c) W.H. Jones, Jr., T. P. Graham, and R. G. Barnes, Phys. Rev., 132, 5 (Dec. 1963).

d) Nuclear Magnetic Resonance in Solids, ed. by Lieven Van Gerven, NATO Advanced Study Institute Series, series B: Physics, Plenum Publishing Co., New York (1977).

(7) C. Cohen-Tannoudji, B. Diu, F. Laloe, Quantum Mechanics, vol. 1, Hermann, Paris (1977).

(8) Costantino S. Yannoni, ACC. Chem. Res., 15, 201 (1982).

(9) C. A. Fyfe, Solid State NMR for Chemists, CFC Press, Guelph, Ontario, 1983.

(10) Novex NMR Software, User Manual, Novex INC. (1985).

(11) Handbook of Electronics Calculations, ed. by M. Kaufman, A. H. Seidman, McGraw-Hill Book Company, 1988.

(12) W. G. Clark and J. A. McNeil, Rev. Sci. Instrum., 44(7), 844 (1973).

(13) E. Fukushima, S. B. W. Roeder, Experimental Pulse NMR- A Nuts and Bolts Approach, Addison-Wesley, Reading, MA (1981).

(14) NMR tables, fifth edition, Varian Associates.

(15) M. L Buess and G. L. Petersen, Rev.Sci. Instrum., 49(8), 1151 (1978).

(16) E. Fukushima and S. B. W. Roeder, J. Magn. Res., 33, 199 (1979).

(17) P. V. Wright, Br. Polym. J., 7, 319 (1975).

(18) M. B. Armand, J. M. Chabagno and M. J. Duclot in Fast Ion Transport in Solids, ed. P. Vashishta, J. N. Mundy and G. K. Shenoy, North-Holland, Amsterdam, 1979, p.131.

(19) Polymer Electrolyte Reviews, vol.1 and 2, ed. by J. R. MacCallum and C. A. Vincent Elsevier Applied Science, London 1987 and 1989 respectively.

(20) Polymers for Electronic Applications, p.1-157, ed. by J. H. Lai, CRC press, 1989.

(21) Polymer Electrolyte Reviews, vol.1 , chapter 3, ed. by J. R. MacCallum and C. A. Vincent, Elsevier Applied Science, London 1987.

(22) Polymer Electrolyte Reviews, vol.1, chapter 4, ed. by J. R. MacCallum and C. A. Vincent, Elsevier Applied Science, London 1987.

(23) P. M. Blonsky, D. F. Shriver, P. E. Austin and H. R. Allock, J. Amer. Chem. Soc., 106, 6854 (1984).

(24) M. Armand, Solid State Ionics, 9&10, 745 (1983).

(25) Polymer Electrolyte Reviews, vol.1, chapter 8, ed. by J. R. MacCallum and C. A. Vincent, Elsevier Applied Science, London 1987.

(26) J. J. Fontanella, M. C. Wintersgill, M. K. Smith, J. Semancik and C. G. Andeen, J. Appl. Phys., 60, 2665 (1986).

(27) M. H. Cohen and D. Turnbull, J. Chem. Phys., 31, 1164 (1959).

(28) C. A. Angell, Solid State Ionics, 9&10, 3, (1983); 18&19, 72, (1986).

(29) C. Berthier, W. Gorecki, M. Minier, M. B. Armand, J. M. Chabagno and P. Rigaud, Solid State Ionics, 11, 91 (1983).

(30) W. Gorecki, R. Andreani, C. Berthier, M. B. Armand, M. Mali, J. Roos and D. Brinkmann, Solid State Ionics, 18&19, 295 (1986).

(31) (a) E. O. Stejskal and J. E. Tanner, J. Chem. Phys., 42, 288 (1965).
(b) R. E. Gordon and J. H. Strange, J. Phys. C., 11, 3213 (1978).

(32) (a) Polymer Electrolyte Reviews, vol.1, chapter 7, ed. by J. R. MacCallum and C. A. Vincent, Elsevier Applied Science, London 1987.
(b) M. A. Ratner, S. D. Druger and A. Nitzan, Mat. Res. Soc. Symp. Proc., 135, 13 (1989).

(33) (a) J. H. Gibbs and E. A. Dimarzio, J. Chem. Phys., 28, 373 (1958).
(b) G. Adam and J. H. Gibbs, J. Chem. Phys., 43, 139 (1965).

(34) Polymer Electrolyte Reviews, vol.2, chapter 9, ed. by J. R. MacCallum and C. A. Vincent, Elsevier Applied Science, London 1989.

(35) S. SKaarup and K. West, Solid State Sodium Cells, the Technical University of Denmark, DK-2800 LYNGBY 1989.

(36) R. Splindler and D. F Shriver, J. Electrochem. Soc., 134, 270 (1987).

(37) A. Bouridah, F. Dalard, D. Deroo, H. Cheradame, and J. F. Lenest, Solid State Ionics, 15, 233 (1985).

(38) K. J. Adamic, S. G. Greenbaum, M. C. Wintersgill and J.J. Fontanella, J. Appl. Phys.,60, 1342 (1986).

(39) H. L. Mei, Y. Okamoto, T. Skotheim and C. Harris, Mol. Cryst. Liq. Cryst., 160, 321 (1988).

(40) Lakshman Pandey, S. Towta and D. G. Hughes, J. Chem. Phys., 85(12), 6923 (1986).

(41) D. Teeters and R. Frech, Solid State Ionics, 18&19, 271 (1986).

(42) R. Dupon, B. L. Papke, M. A. Ratner, D. H. Whitmore and D. F. Shriver, J. Amer. Chem. Soc., 104, 6247 (1982).

(43) M. C. Wintersgill, J. J. Fontanella, M. K. Smith, S. G. Greenbaum, K. J. Adamic and C. G. Andeen, Polymer, 28, 633 (1987).

(44) C. P. Slichter, Principles of Magnetic Resonance, ch. 5, Springer-Verlag (1978).

(45) J. S. Tonge and D. F. Shriver, J. Electrochem. Soc., 134, 269 (1987).

(46) P. M. Blonsky, D. F. Shriver, P. Austin and H. R. Allock, Solid State Ionics, 18&19, 258 (1986).

(47) S. G. Greenbaum, K. J. Adamic, Y. S. Pak, M. C. Wintersgill, J. J. Fontanella, D. A. Beam and C. G. Andeen, Proceedings of Electrochem. Soc. Symp. on Electro-Ceramics and Solid State Ionics, 88-3, 211 (1988).

(48) C. K. Chiang, G. T. Davis and C. A. Harding, Solid State Ionics, 18&19, 300 (1986).

(49) C. Bridges, A. V. Chadwick and M. R. Worboys, Br. Polymer. J., 20, 213 (1988).

(50) S. G. Greenbaum, Y. S. Pak, M. C. Wintersgill and J. J. Fontanella, Solid State Ionics, 31, 241 (1988).

(51) NMR and the Periodic Table, ed. by R. K. Harris and B. E. Mann, Academic Press p. 152 (1978).

(52) R. Spindler and D. F. Shriver, J. Am. Chem. Soc., 110, 3036 (1988).

(53) A. Ricard, Eur. Poly. J., 15, 1 (1979).

(54) Proceedings of the First International Conference on Polymer Electrolytes, Br. Polym. J., 20(3) (1988).

(55) M. C. Wintersgill, J. J. Fontanella, S. G. Greenbaum and K. J. Adamic, Br. Poly. J., 20, 195 (1988).

(56) (a) F. C. Schilling and A. E. Tonelli, Macromolecules, 19, 1337 (1986).
(b) N. Oguni, S. Shinohara and K. Lee, Polym. J. (Tokyo), 11, 755 (1979).

(57) E. Linden and J. R. Owen, Solid State Ionics, 28&30, 994 (1988).

(58) C. V. Nicholas, D. J Wilson, C. Booth and J. R. M. Giles, Br. Polym. J., 20, 289 (1988).

(59) M. C. Wintersgill, J. J. Fontanella, Y. S. Pak, S. G. Greenbaum, A. Al-Mudaris and A. V. Chadwick, Polymer, 30, 1123 (1989).

(60) S. Bhattacharja, S. W. Smoot and D. H. Whitmore, Solid State Ionics, 18&19, 306 (1986).

(61) H. Liu, Y. Okamoto, T. Skotheim, Y. S. Pak, S. G. Greenbaum and K. J. Adamic, Mat. Res. Symo. Proc., 135, 337 (1989).

(62) Polymer Electrolyte Reviews, vol. 2, chapter 2, ed. by J. R. MacCallum and C. A. Vincent, Elseview Applied Science, London 1989.

(63) S. G. Greenbaum, J. J. Wilson, M. C. Wintersgill and J. J. Fontanella, Proceedings of 2nd Int'l Symposium on Polymer Electrolytes, Siena, Italy, June 1989, p.35, Elsevier Applied Science.

(64) J. J. Fontanella, M. C. Wintersgill, J. P. Calame, M. K. Smith and C. G. Andeen, Solid State Ionics, 18&19, 253 (1986).

(65) J. Sandahl, S. Schantz, L. M. Torell and R. Frech, Solid State Ionics, 28&30, 958 (1988).